An Investigation into the Frequency Stability of Non-oven Controlled Crystal Oscillators

Thesis

Christopher Charles Brighty BSc

An Investigation into the Frequency Stability of Non-oven Controlled Crystal Oscillators

For the degree of
Doctor of Philosophy

Electronics Discipline

Submitted
January 1992

Date of submission: 13 January 1992
Date of award: 12 May 1992

ProQuest LLC
789 East Eisenhower Parkway
P.O. Box 1346
Ann Arbor, MI 48106 - 1346

CONTENTS

FIGURES

PREFACE

The work in this thesis is all my own work except when stated otherwise. The early research was carried out by myself while working as a Teaching Company Associate on the Teaching Company Scheme between The Open University and Cathodeon Crystals Ltd which later became a division of Newmarket Microsystems Ltd. Later theoretical work carried out as part of the investigation I funded privately. Some of the experimental work for the digital compensation was undertaken by myself whilst I was acting as a consultant to the Teaching Company Scheme.

The research presented in chapters 5 and 6 is being prepared for publication.

I would like to thank Dr Michael Payne, Dr Ed da Silva and my wife Cheryl for their patient reading of the manuscript.

ABSTRACT

Temperature induced frequency deviation of quartz crystal oscillators can be reduced by tuning the oscillator to compensate for the thermal effects. A varactor tuned AT cut resonator is typically used to make a voltage controlled crystal oscillator. Compensation is then achieved by applying a "compensation voltage" to the varactor. The earliest compensation circuits comprised resistors and thermistors. Over the temperature range -40°C to +85°C resistive compensation circuits have achieved frequency stabilities of approximately $\pm$1ppm. Alternative analogue circuits have achieved frequency stability of $< \pm$0.5ppm.

The research described in this thesis is an investigation of resistive networks in order to improve the levels of stability that can be achieved by this method of temperature compensation for crystal oscillators. The objective was to achieve a stability of $< \pm$0.5ppm over the temperature range -40°C to +85°C.

Optimisation techniques have been employed to identify a new temperature compensation circuit. This new circuit uses an amplifier with temperature sensitive gain to modify thermistor characteristics and improve the compensation over the high part of the temperature range. Two forms of this circuit are presented. Computer simulation of this circuit has shown that it is capable of achieving frequency stability of $< \pm$0.3ppm in an oscillator operating from a 4.5V supply over the temperature range -40°C to +85°C.

1. HISTORICAL REVIEW

1.1. Piezoelectricity

The piezoelectric effect was discovered by Pierre and Jacques Curie in 1880, although the name piezoelectricity was not applied immediately. The piezoelectric effect manifests itself in two forms, the direct piezoelectric effect and the converse piezoelectric effect. These names are merely reflections on the order of discovery because the effects are related. The direct piezoelectric effect is the name given to the phenomenon whereby a mechanical stress on the material gives rise to an electrical potential across the material. This was the Curies' original discovery in 1880 and it is from this that the name is derived, piezo being the Greek for to press. The converse piezoelectric effect was predicted by Lippmann and was confirmed by the Curies in 1881 and is the phenomenon whereby an applied electrical field will give rise to mechanical strain [1].

In their work the Curie brothers found many crystals that exhibited piezoelectricity, one of them being quartz. Quartz is one of the naturally occurring forms of silicon dioxide (SiO_2) and today is the most widely used piezoelectric material because its mechanical and chemical properties make it ideally suited for frequency control.

In 1910 Voigt [2] published a detailed mathematical explanation of the properties of crystals, including the piezoelectric effect and this book became the standard text on the subject.

As with many discoveries, piezoelectricity first found practical application with the military. In the first world war submarines were an undetectable menace and the French authorities requested Professor Langevin to investigate methods of

submarine detection. Langevin's solution was to use quartz as a transducer to send out an acoustic pulse and subsequently receive the echo. This was the first sonar. The system, however was not completed until after the end of the war and this device did not see active service. By the time of the second world war sonar was in widespread use with the navies of both sides.

1.2. Crystal oscillators

Early experimenters who worked on the application of piezoelectric materials for frequency control were Nicholson, Cady and Pierce. Texts differ as to who was the first of these to produce the first working crystal controlled oscillator. Heising and Mason give the credit to Nicholson who used a Rochelle salt crystal to control the frequency of an oscillator [3], whereas the majority of authors give the credit to Cady [4][5] who initially used Rochelle salt crystals and who, later, was the first to use quartz crystals in an oscillator. Pierce followed a little later and built on the work of Cady and Nicholson, using quartz instead of Rochelle salt [6].

Two avenues of research were pursued; Nicolson used the crystal in association with other frequency selective components to add stability to the existing oscillator; Cady used the crystal as the only frequency selective element of the circuit. The main advantage of the crystal tuned oscillator over the conventional oscillator tuned by capacitive and inductive elements is improved stability and low noise. The resonant frequency of the quartz crystal resonator is stable because its resonant properties are determined purely by the mechanical dimensions and elasticity of the device which have very low coefficients with temperature especially when compared to the physical properties which determine the resonance of practical capacitor and inductor circuits.

Much of the early work used bars of piezoelectric material, usually quartz or Rochelle salt. As time went on quartz was predominantly used, usually in the form of a bar in which the largest dimension determined the resonant frequency. Hence the frequencies of the oscillators were relatively low, in the range of 1kHz to 100kHz. For higher frequencies, crystal resonators employing the smallest dimension of the geometry were developed. The first of these higher frequency resonators to be developed was the X cut of quartz in which the electric field and the mechanical strains occur in the same direction. Next to be developed was the Y cut quartz resonator in which the electric field causes thickness shear strain in the crystal. The Y cut became the more popular because it was less susceptible to vibrating at spurious modes and was easier to provide mechanical mounting for [5]. However the Y cut resonator had a greater coefficient of temperature than the X cut.

1.3. High stability resonators

Lack, Willard and Fair, and independently, Bechmann, and others found that the orientation of the atomic lattice with respect to the physical boundaries of the crystal resonator gave rise to different characteristics with temperature. They showed that some of the problems inherent in the Y cut crystal could be eradicated by changing the lattice orientation relative to the physical boundaries of the device during the fabrication process. Instead of cutting the crystal into slices with the saw parallel to the Y axes the saw was presented at an angle so changing the orientation of the atomic lattice within the resonator. Two cuts, the AT cut and BT cut [7] have the linear term for temperature sensitivity equal to zero which meant that compared to the other crystals in use at that time they were insensitive to temperature change. However, higher order coefficients are non zero so the cuts are prone to small changes in resonant frequency with changes in temperature.

Bechmann showed that the crystal characteristic could be fitted accurately to a cubic polynomial of the form given in (1.1) over the temperature range -200°C to +250°C and that over this range higher order coefficients were not needed to describe the behaviour.

$$\frac{\Delta f}{f} = a(T - T_0) + b(T - T_0)^2 + c(T - T_0)^3 \qquad (1.1)$$

where Δf is the difference between the frequency at temperature T and the frequency at T_0 and f is the frequency at T_0.

A major change in crystal resonator and crystal oscillator research was caused in America between 1939 and 1941 by the impending war. Before this time crystal resonators were made by small companies, usually one or two men, working to supply the local amateur radio enthusiasts and research institutions working in the field of precision time measurement, although some commercial radio stations used crystal oscillators in their transmitters to improve the quality of their broadcasts. The importance of radio communications in wartime meant that the demand for reliable equipment, with war on the horizon, became very great. The newest and most reliable and versatile communications equipment used crystal controlled oscillators. In these pieces of equipment changing channel meant changing crystal, either by physically swapping crystals or electrically switching between crystals. The result was that the demand for crystals increased dramatically and the quartz crystal resonator research and development was undertaken with top priority. The major problem lay in availability of the raw material. The electrical grade quartz used at that time was mined in Brazil, a problem that was not solved until after the war. Two avenues were pursued to reduce the demand for quartz; the quartz resonators were made smaller and the number needed for each communications set was reduced [8]. When the war ended the US army contracted research

institutions to build on the work performed in wartime. It was found both convenient and useful to bring all the groups together once a year so that the results of research could be shared and commented on. This was the beginning of the Annual Frequency Symposium which is still the major forum for precision frequency control research.[9][10]

1.4. Temperature compensated crystal oscillators

After the war, development of the crystal oscillator was influenced by the new technology of semiconductor components, which resulted in smaller oscillator units. The use of handheld portable radio communications equipment meant that the equipment had to be light, which required that the batteries used to provide power for the equipment had to be small. This precluded the use of ovens to improve the thermal stability of the resonator when the crystal characteristic was not stable enough for a particular application. The solution adopted was to tune the oscillator to compensate for the frequency deviation of the crystal resonator brought about by the change of ambient temperature. The techniques originally tried included applying stress to the crystal, creating temperature sensitive reactances using thermistors with capacitors, and a varactor diode which had a temperature sensitive bias voltage. The varactor diode arrangement was taken up by many researchers and manufacturers. The most common means of generating the temperature sensitive bias voltage was to use a temperature sensitive resistive network using thermistors as the temperature sensitive elements. The level of stability that was obtained was ± 0.3ppm (parts per million) over the temperature range -40°C to +60°C but as the upper temperature increased, the level of frequency stability decreased so that over the temperature range -40°C to +85°C this method of compensation has achieved compensation to approximately ± 1ppm. Alternative arrangements for generating the compensation voltage include

segmenting the temperature range so that the elements of the compensation scheme only act over a small part of the temperature range and the use of alternative temperature sensitive components.

With the development of the integrated circuit and digital electronics the compensation voltage can now be generated by converting the temperature into a digital representation and performing the transformation to the required compensation voltage, which is then converted to an actual voltage to tune the crystal. Modern techniques use addition and subtraction of pulses instead of tuning the crystal.

The objective of the research described in this thesis was to investigate networks of resistors and thermistors in order to improve the levels of stability that could be achieved by this method of temperature compensation for crystal oscillators over the temperature range -40°C to +85°C, the objective being to achieve a stability of $< \pm 0.5$ppm. This level of stability has been claimed by alternative analogue temperature compensation techniques [11]. During the course of the research aspects of digital temperature compensation have also been investigated.

1.5. References

[1] Cady, W. G. (1946, 1st ed.). Piezoelectricity, *McGraw-Hill, New York.* pp. 1-8.

[2] Voigt, W. (1910, 1st ed.). Lehrbuch der Kristallphysik, *B. G. Teubner, Leipzig.*

[3] Heising, R. A.. Mason, W. P. (1946). Quartz Crystals for Electrical Circuits, *Van Nostrand Company Inc., New York.* pp. 11-56.

[4] Cady, W. G. (1946, 1st ed.). Piezoelectricity, *McGraw-Hill, New York.* pp. 489-509.

[5] Bechmann, R. (1964). Piezoelectricity - frequency control. *Proc 18th Annu. Freq. Control Symp.*, pp. 43-92.

[6] Pierce, G. W. (1923). Piezoelectric crystal resonators and crystal oscillators applied to the precision calibration of wavemeters. *Amer. Acad. of Arts and Sciences, Oct.*, pp. 81-106.

[7] Lack, F. R., Willard, G. W. and Fair, I. E. (1934). Some improvements in quartz crystal circuit elements. *Bell System Technical Journal, vol.13*, pp. 453-463.

[8] Doxey, W. L. (1986). Quartz crystals paved the way. *Proc 40th Annu. Freq. Control Symp.*, pp. 9-14.

[9] Gerber, E. A. (1986). Reminiscences of early frequency control activities in honour of the 40th anniversary of the frequency control symposium. *Proc 40th Annu. Freq. Control Symp.*, pp. 8.

[10] Bottom, V. E. (1986). Origin and influence of the AFCS. *Proc 40th Annu. Freq. Control Symp.*, pp. 15.

[11] Wilson J. S. (1983). An improved method of temperature compensation of crystal oscillators. *Proc 37th Annu. Freq. Control Symp.*, pp. 442-447.

2. HIGH STABILITY CRYSTAL OSCILLAOTRS

2.1. Introduction

Frequency stability with temperature of an oscillator depends principally on the thermal frequency stability of the frequency selective part of the circuit. In the case of a crystal oscillator this is the thermal stability of the crystal resonator. A crystal resonator is selected to ensure that the minimum frequency deviation occurs over the required operating temperature range of the oscillator. Using an AT cut crystal resonator the best that can be achieved over the temperature range -40°C to +85°C is approximately ±10ppm (parts per million), as in figure 3.14. To achieve greater stabilities two techniques are available; either the oscillator can be isolated from changes in ambient temperature by maintaining it at a constant temperature within an oven, or the oscillator experiences changes in ambient temperature and the temperature induced frequency deviations are compensated for by applying a correction to the oscillator.

In this chapter literature covering temperature compensated crystal oscillators is reviewed. A short section is presented on ovened oscillators in order to show the relative limits of the two methods of overcoming thermal instabilities. Most of the chapter considers the various techniques used for temperature compensation with emphasis on indirect tuning temperature compensation, where the compensation circuit generates a compensation voltage or current which controls a reactance in the crystal circuit.

2.2. Oven controlled crystal oscillators

Very high frequency stabilities are obtainable with the oven controlled crystal oscillator (OCXO) approach but at the cost of relatively high power consumption and large size; the crystal and oscillator drive circuit are built into the oven and power has to be supplied to heat both the oven and the oscillator unit. When the ambient temperature is low more power has to be supplied to maintain the oven temperature than when the ambient temperature is high because at low temperatures the loss of heat energy is greater. Usually there is no controlled means of cooling the oven; the system is dependant on losing heat to the environment so the control parameters of the oven change with temperature also. The frequency stability limit is set by how well the oven temperature can be controlled and the dynamic temperature characteristic of the crystal which determines how the crystal responds to the rate of change of temperature. The stabilities of this approach start in the region of ± 0.2ppm and go through to 10^{-6}ppm over the temperature range -20°C to 50°C [1]. Thermal stabilities, equivalent to a frequency stability of 10^{-7}ppm are achieved using multiple, computer controlled ovens [2].

2.3. Temperature compensated crystal oscillators

The frequency stability that can be achieved by a temperature compensated crystal oscillator (TCXO) depends on the temperature range it is expected to operate over and the method of compensation being used. In general there is a compromise between stability and temperature range. Techniques that have been applied for temperature compensating crystal oscillators are described under four headings; Resonator stress, Direct tuning, Indirect tuning and Pulse train. The first three methods were initially investigated about the same time, and operate by changing

the frequency of the resonator. Of these indirect tuning has become the most widely used technique. The fourth method is relatively new and modifies the output of the oscillator.

2.3.1. Resonator stress

It had previously been shown that stress applied to different parts of a resonator would alter its frequency of vibration. The magnitude and direction of the frequency change was a function of where the stress was applied, both positive and negative changes of frequency were obtainable for force directed towards the centre of the resonator. For temperature compensation Gerber and Miles [3] applied stress in two places on the circumference of a resonator by means of bimetallic probes. These made the applied stress temperature dependent. Over the temperature range -30°C to +80°C this arrangement achieved a stability level of ±2.5ppm. Newell, Hinnah and Bangert [4] report applying stress to the face of the resonator which gives lower sensitivity. They report that the best that they were able to achieve was ±3ppm over the temperature range -30°C to +55°C due to poor repeatablility of the method. This form of temperature compensation has not been widely investigated.

2.3.2. Direct tuning

Direct tuning temperature compensation is implemented by using a temperature dependant capacitance in the crystal circuit. The temperature dependant capacitance is realised by connecting a thermistor and resistors in parallel with a capacitor. This may be regarded as an apparent series combination of a capacitor and a resistor because the impedance of the parallel combination is given by

$$Z_{C//R} = \frac{R}{1+\omega^2C^2R^2} - \frac{j\omega CR^2}{1+\omega^2C^2R^2} \qquad (2.1)$$

where $Z_{C//R}$ is the impedance of the parallel circuit, $\frac{1}{j\omega C}$ is the reactance of the capacitor and R is the resistance of the thermistor and associated resistors. As R forms part of the apparent capacitance, this capacitance is temperature dependant. The fixed resistors are selected to make the capacitance offset the frequency variations of the crystal. The apparent resistance in series with the capacitor degrades the performance of the oscillator, making it unsuitable for certain applications. Okano, Mitsuoka and Ohshima [5] review the literature covering direct tuning temperature compensation and conclude that this method has application where small physical volume, low power and low cost are important considerations. They present the design of a compensation circuit which is capable of $\pm$2ppm over the temperature range -30°C to +60°C. Ikeda [6] describes the development of the technique over a wider temperature range for providing stability of $\pm$2.5ppm over the temperature range -30°C to +75°C.

2.3.3. Indirect tuning

Indirect tuning temperature compensation is implemented by using a voltage or current controlled capacitance in the crystal circuit. Temperature compensation is achieved by applying an appropriate control to the capacitance. In the majority of oscillators where this method of compensation is employed a varactor diode is used as the controlled capacitance. The generation of the required varactor diode bias voltage, called *compensation voltage*, is described in section 2.4 under three headings: Analogue compensation, Segmented compensation and Digital compensation.

2.3.4. Pulse train

The temperature compensation methods discussed above alter the effective resonant frequency of the crystal in a controlled manner. Pulse train compensation is

different because the correction is not applied to the resonator. Instead cycles are either inserted or deleted from the output of the oscillator under the control of a microprocessor. The output of this form of compensation is typically a square wave with a period of 1 second. Where it is required that the compensation be applied to an oscillator with a frequency typically associated with crystal oscillators a voltage controlled oscillator is used in a phase locked loop. This method of temperature compensation has been investigated using an SC cut resonator which is driven by two oscillator circuits. Hence the crystal gives two outputs at different frequencies. From these the temperature of the resonator can be determined without the use of an external temperature transducer. Frequency stabilities between ± 0.02ppm and ± 0.05ppm over the temperature range -55°C to +85°C have been published for time keeping and frequency control [7] to [11]. This method of temperature compensation could be applied to an oscillator based on an AT cut resonator with an external temperature transducer. However, the advantages of using an SC cut crystal are the superior representation of resonator temperature, due to dual mode operation, and lower thermal hysteresis which is a feature of the SC cut.

2.4. Indirect tuning compensation voltage generation

In this section the techniques for generating the compensation voltage for varactor tuned oscillators are reviewed. Analogue compensation is discussed first and considered in greatest detail because the major part of the research presented in this thesis sought to improve the level of temperature compensation that the resistive circuits, which are included in this category, were able to achieve. The components used for the oscillator and the compensation network are subject to manufacturing tolerances. Hence to make a TCXO the compensation circuit has to be individually made to suit a particular oscillator.

2.4.1. Analogue compensation

This class of compensation covers methods where the compensation voltage is generated by a single electronic circuit which operates over the whole temperature range and provides a continuous function of voltage with temperature. Typically this takes the form of a resistive network comprising thermistors and fixed resistors and these are considered first. The compensation voltage is derived from a constant voltage reference by the temperature dependant transfer function of the resistive network.

Newell and co-authors published three papers which are representative of the early research into resistive temperature compensation networks and methods for calculating values for the fixed resistors [4][12][13]. They present results showing that over the temperature range -35°C to +65°C they had achieved ±0.25ppm frequency stability and over the temperature range -40°C to +75°C they had achieved ±0.35ppm. As a possible mark of the difficulty or time consuming nature of achieving this level of frequency stability they conclude that over the temperature range -40°C to +70°C the method provides compensation to ±0.5ppm or better and that at that time the likely limit was ±0.25ppm. An upper temperature limit was convenient because crystal angles could be selected which had only one turning point in the characteristic, that being the lower turning point.

Swanson and McVey [14] published theoretical results showing that using a resistive network comprising two thermistors and three resistors, which had been presented by Newell, the optimum stability was ±0.3ppm over the temperature range -40°C to +60°C. The supply voltage to the compensation voltage for this work was 5V which the authors recognised at that time was low, the typical voltage used was 8V, but they stated that some oscillators used this lower value. Hence their work represented the worst case at the time.

Buroker and Frerking [15][16] introduced a hybrid temperature compensation circuit comprising analogue and digital compensation at a time when digital electronics was new. The analogue section was termed the coarse compensation and the digital section was termed the fine compensation. Their intention was to compensate an oscillator to ± 0.05ppm over the temperature range -40°C to +80°C. For this TCXO the analogue compensation was applied then the digital compensation was used to increase the level of compensation by a factor 10. The results of the coarse compensation are of interest here. The compensation circuit operated from a 9V regulator and comprised three thermistors and three resistors. The results presented show that this coarse compensation achieved just under ± 0.4ppm over the whole range. However, over the lower half of the temperature range, -40°C to +20°C, the frequency stability is $< \pm 0.1$ppm, indicating that over the top half of the temperature range compensation is significantly more demanding.

Thomann, [17] using a similar resistive compensation circuit to that of Buroker and Frerking, presents results which indicate that over the same temperature range, compensation to ± 2ppm has a predominantly linear characteristic which shows that the compensation is capable of higher levels of stability which is confirmed in the paper as he states that some oscillators had achieved frequency stability to $< \pm 1$ppm over the temperature -40°C to +80°C. An important feature of the paper is the way the compensation circuit is assembled, the characteristics of the thermistor are matched to the requirements of the oscillator by computer. This is a departure from the standard approach where only the fixed resistors are selected to suit the oscillator.

Mroch and Hykes [18] developed the work of Buroker and Frerking and claim to have achieved coarse compensation of ± 0.5ppm over the temperature range -46°C to +85°C but they have not published their results. Their results were based on a

crystal that had a particularly large range between the turning points, 50ppm, with upper turning point at 80°C. The varactor tuning sensitivity was 10ppm/V making the range of the compensation voltage 5V. The compensation circuit comprised three thermistors and six resistors and operated from a 9V reference. No other details were given concerning the coarse compensation. These results would indicate that resistive compensation had achieved compensation of ± 0.5ppm over an extended temperature range, however this may not be supported by subsequent literature. Rosati and Thompson evaluated many TXCO's and conclude that over a wide temperature range frequency stability of ± 1ppm represents the state of the art and that TCXO's with frequency stability of $\leq \pm 0.6$ are not available. These frequency tolerances include age adjustment considerations but the suggestion made in the paper is that the compensation limit for the compensation circuits used at that time, which were predominantly resistive, was $> \pm 0.6$ppm. Harrison, Dowsett and Sharpe [19] suggest that when manufacturing tolerances are taken into account the frequency stability of resistive networks is approximately ± 3ppm but this figure seems excessive when compared with the results obtained by Thomann discussed earlier.

Wilson [20] and Harrison, Dowsett and Sharpe [19] describe an alternative analogue compensation circuit which does not use thermistors. The reason given by the authors for investigating this alternative method was that resistive temperature compensation circuits appear to have reached their limit of stability. This alternative method of compensation uses a new integrated circuit (IC) which generates Chebyshev polynomials. These are weighted and summed to derive the required compensation voltage. The degree of weighting applied to each Chebyshev polynomial is determined to suit each oscillator. Two versions of this IC are used: the first forms cubic polynomial functions of voltage against temperature and the second forms fifth order polynomials. The second form of

this IC has achieved frequency stabilities of $< \pm 0.5$ppm over the temperature range -40°C to +85°C.

Keller, Marvin and Steele [21][22] describe an integrated circuit for temperature compensation which they describe as a segmented compensation method but according to the definition given above this temperature compensation circuit is qualified here as analogue compensation because the circuit generates a continuous function of voltage with temperature. The circuit has three temperature dependant current sources, one for each gradient region of the required characteristic. These currents are summed to form the single output current which is converted to the compensation voltage. Results published for this compensation circuit show frequency stability of $< \pm 1$ppm over the temperature range -40°C to +95°C.

2.4.2. Segmented compensation

The use of two or more sub-circuits which are selected to only operate over part of the temperature range is referred to as segmented compensation. Segmented compensation can be regarded as the transition between analogue compensation and digital compensation. This method of generating the compensation voltage was first investigated when thermistor networks appeared to have reached the limit of frequency stability that they could achieve and at a time when the methods used to determine the fixed resistor values was tedious. The application of high stability segmented compensation has been superseded by digital compensation.

Newell and Hinnah [23] describe a segmented compensation circuit in which the required compensation voltage is approximated be a series of exponential voltage against temperature functions. They describe how the circuit can be compensated automatically but do not present results showing frequency stability. Vovelle [24] describes a similar circuit which approximates the compensation voltage to a series

of linear voltage against temperature functions. Results presented for this circuit show compensation to ± 0.3ppm over the range -40°C to 70°C which is similar to analogue compensation circuits. A problem with these circuits was that the active segment was not truly independent of the other segments.

Sarkar [25] presents a segmented temperature compensation circuit which comprises three resistive circuits which are matched to the required compensation voltage over part of the temperature range. The paper presents the analysis used to determine the fixed resistors and claims compensation to ± 0.25ppm over a wide, but otherwise unspecified, temperature range.

2.4.3. Digital compensation

The term digital temperature compensation refers to a circuit which uses a digital representation of the ambient temperature to identify the required compensation voltage in digital form. The digital representation of compensation voltage is converted to a real voltage which is applied to the varactor diode. Two forms of digital circuit are widely used to derive the required compensation voltage. Either read only memory is used to store the required compensation voltage in digital form and the digitised temperature is used to address the required data or a microprocessor is used to calculate the required compensation voltage using the temperature information. Scott [26]; Hara, Kudo, Uriya, Saiti, Ogou and Katsuta [27] and Miyayama, Ikeda and Okano [28] together form a good review of the literature for the implimentation of read only memory based temperature to compensation voltage transformation and Frerking [29][30] and Onoe, Yamagishi and Nariai [31] form a similar review for microprocessor compensation. Consideration of this literature leads to the conclusion that the memory based circuit provides the more favourable arrangement on the grounds of ease of

implementation and relatively lower power consumption. In terms of frequency stability the results obtained are equal.

Digital temperature compensation is capable of achieving stability of $< \pm 0.1$ppm over a wide temperature range. At this level of stability the crystal hysteresis starts to become significant and sets the limit that can be achieved. Digital temperature compensation is often applied where the required stability is well below the limit where hysteresis becomes a problem as an alternative to analogue compensation because it is easier to implement with modern integrated fabrication techniques [27].

2.5. Conclusions

Temperature compensation for crystal oscillators using established resistive networks appears to have reached a limit of obtainable frequency stability at approximately ± 1ppm over the temperature range -40°C to +85°C. There is a strong likelihood that the difficulty is with the higher temperatures in the specified range due to effects of the high temperature turning point in the cubic characteristic of AT cut resonators. Alternative analogue methods and digital methods of temperature compensation have overcome these difficulties, showing that higher levels of compensation are possible. It was considered appropriate to investigate resistive circuits with the objective of achieving temperature compensation to stability levels similar to those reported for the alternative analogue techniques, typically $< \pm 0.5$ppm. Resistive compensation circuits which are reported to have achieved the best frequency stability operate from a relatively high reference voltage. It was considered appropriate that the research should use a relatively low reference voltage.

2.6. Description of the Temperature Compensated Crystal Oscillator

In this section the block level description of the Temperature Compensated Crystal Oscillator (TCXO) used during the research is presented. The general form of the oscillator was the indirect type. An indirect TCXO comprises a voltage controlled crystal oscillator, a stable voltage reference and a compensation circuit as in figure 2.1.

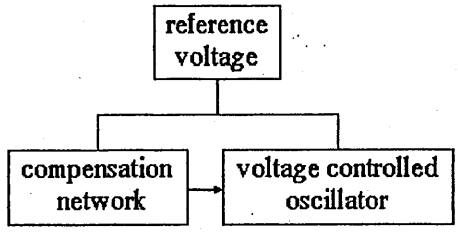

Figure 2.1. General arrangement of the temperature compensated oscillator.

Voltage controlled crystal oscillator comprises a resonator driving circuit, a crystal resonator and a varactor diode which provides voltage tuning of the oscillator frequency.

Voltage reference is used to provide a voltage which is insensitive to the changes in the ambient temperature for the compensation circuit. The output of the voltage reference is used to supply the oscillator and the compensation circuit.*

---

* The voltage reference used for the experiments was a new integrated circuit voltage regulator, the ZNREF040. This integrated circuit offered superior voltage stability with temperature over the regulator used by the company at that time. The company's regulator used a zener diode to provide the internal reference. A zener diode needs typically 5mA to bias it to a stable voltage and as the experimental temperature compensated oscillator's maximum supply current was 1.5mA a zener diode would not be capable of providing a stable reference voltage. A ZNREF040 voltage regulator requires only 0.15mA to ensure a stable output voltage of 4 volts.

Compensation circuit provides the required compensation voltage that has to be applied to the varactor diode to offset the temperature induced frequency deviations of the crystal resonator. Two types of compensation circuit are considered in this thesis; resistive networks and digital circuits.

2.7. References

[1] Garvey, R. M., Emmons, D. A. and Beaubien, A. F. (1984). Space qualified high performance digitally tuned quartz crystal oscillator. *Proc Annu. Freq. Control Symp.*, pp. 374-379.

[2] Marianneau, G. and Gagnepain, J. J. (1980). Digital temperature control for ultrastable quartz oscillators. *Proc 34th Annu. Freq. Control Symp.*, pp. 52-57.

[3] Gerber, E. A. and Miles, M. H. (1961). Temperature compensation of piezoelectric resonators by mechanical stress. *Proc 15th Annu. Freq. Control Symp.*, pp. 49-65.

[4] Newell, D. E., Hinnah, R. and Bangert, R. (1964). Advances in crystal oscillator and resonator compensation. *Proc 18th Annu. Freq. Control Symp.*, pp. 487-534.

[5] Okano, S., Mitsuoka, T. and Ohshima, T. (1980). Direct-temperature compensated crystal oscillator for advanced VHF/UHF radio communication systems. *Proc 34th Annu. Freq. Control Symp.*, pp. 488-497.

[6] Ikeda, Y. (1985). Crystal reliability aids growth of mobile cellular phone service. *J. E. E. (October)*, pp.42-46.

[7] Schodowski, S. S. (1989). Resonator self-temperature-sensing using a dual-harmonic-mode crystal oscillator. *Proc 43rd Annu. Freq. Control Symp.*, pp. 2-7.

[8] Filler, R. L. and Vig, J. R. (1989). Resonators for the microcomputer compensated crystal oscillator. *Proc 43rd Annu. Freq. Control Symp.*, pp. 8-15.

[9] Bloch, M., Meirs, M and Ho, J. (1989). The microcomputer compensated crystal oscillator (MCXO). *Proc 43rd Annu. Freq. Control Symp.*, pp. 16-19.

[10] Benjaminson, A. and Stallings, S. C. (1989). A microcomputer-compensated crystal oscillator using a dual-mode resonator. *Proc 43rd Annu. Freq. Control Symp.*, pp. 20-26.

[11] Filler, R. L., Messina, J. A. and Rosati, V. J. (1989). Frequency-temperature and ageing performance of microcomputer compensated crystal oscillators. *Proc 43rd Annu. Freq. Control Symp.*, pp. 27-33.

[12] Hykes, G. R. and Newwell, D. E. (1961). A temperature-compensated frequency standard. *Proc 15th Annu. Freq. Control Symp.*, pp. 297-317.

[13] Newell, D. E. and Bangert, R. H. (1963). Temperature compensation of quartz crystal oscillators. *Proc 17th Annu. Freq. Control Symp.*, pp. 491-507.

[14] Swanson, C. T. and McVey, E. S. (1979). A non-iterative solution for a two-thermistor TCXO. *Proc 33rd Annu. Freq. Control Symp.*, pp. 425-430.

[15] Buroker, G. E. and Frerking, M. E. (1973). A digitally temperature compensated TCXO. *Proc 27th Annu. Freq. Control Symp.*, pp. 191-198.

[16] Frerking, M. E. (1978). Crystal Oscillator Design and Temperature Compensation, *Van Nostrand Reinhold Company Inc., New York*, pp. 146-157

[17] Thomann, D. L. (1974). A microcircuit temperature compensated crystal oscillator (MTCXO). *Proc 28th Annu. Freq. Control Symp.*, pp. 214-220.

[18] Mroch, A. B. and Hykes, G. R. (1976). A miniature high stability TCXO using digital compensation. *Proc 30th Annu. Freq. Control Symp.*, pp. 292-300.

[19] Harrison, A., Dowsett, J. and Sharpe, D. (1987). High frequency stable frequency sources for advanced systems. *Proc 41st Annu. Freq. Control Symp.*, pp. 539-543.

[20] Wilson J. S. (1983). An improved method of temperature compensation of crystal oscillators. *Proc 37th Annu. Freq. Control Symp.*, pp. 442-447.

[21] Keller, T., Marvin, D. and Steele, R. (1980). Integrated circuit compensation of AT cut crystal oscillators. *Proc 34th Annu. Freq. Control Symp.*, pp. 498-503.

[22] Marvin, D. (1985). Frequency-temperature performance determination in high stability TCXO's. *R. F. Design (USA) vol. 8, pt. 3*, pp. 53-59.

[23] Newell, D. E. and Hinnah, H. (1968). Automatic compensation equipment for TCXO's. *Proc Annu. Freq. Control Symp.*, pp. 298-310.

[24] Vovelle, P. G. (1968). Recent improvements to TCXO. *Proc 22nd Annu. Freq. Control Symp.*, pp. 311-324.

[25] Sarkar, S. K. (1974). Explicit expressions for TCXO design. *Proc 28th Annu. Freq. Control Symp.*, pp. 232-236.

[26] Scott, P. J. (1977). Design considerations for a digitally temperature compensated crystal oscillator. *Proc 31st Annu. Freq. Control Symp.*, pp. 407-411.

[27] Hara, T., Kudo, T., Uriya, S., Saita, H., Ogou, S. and Katsuta, Y. (1987). A digitally compensated TCXO using a single chip LSI. *Proc 41st Annu. Freq. Control Symp.*, pp. 435-438.

[28] Miyayama, T., Ikeda, Y. and Okano, S. (1988). A new digitally temperature compensated crystal oscillator for a mobile telephone system. *Proc 42nd Annu. Freq. Control Symp.*, pp. 327-333.

[29] Frerking, M. E. (1978). Crystal Oscillator Design and Temperature Compensation, *Van Nostrand Reinhold Company Inc., New York*, pp. 157-176.

[30] Frerking, M. E., (1979). The application of microprocessors to communications equipment design. *Proc 33rd Annu. Freq. Control Symp.*, pp. 431-435.

[31] Onoe, M., Yamagishi, I. and Nariai H. (1978). Temperature compensation of crystal oscillator by microprocessor. *Proc Annu. Freq. Control Symp.*, pp. 398-402.

3. CRYSTAL RESONATOR THEORY

3.1. Crystal resonators

Crystal resonators are electronic components that are used as the frequency control elements in a wide variety of applications. At one extreme they are used as simple oscillators in microprocessor circuits because they are cheap and reliable. At the other extreme they are used as part of very stable frequency standards in laboratories. In this section the properties that are exploited to make the crystal resonators, their fabrication, electrical model, and temperature characteristics are explained with particular emphasis on the resonators used in the research described in this thesis.

3.2. Crystallography

3.2.1. Introduction

The properties of a material are determined in part by its constituent elements and in part by the crystalline structure the atoms adopt in forming the solid. During the formation of the crystal the atoms arrange themselves in the form that requires the lowest energy so, simplistically, different conditions, such as temperature and pressure, will give rise to the different crystalline forms. As an example of different properties consider carbon. Two forms are graphite and diamond. Graphite is opaque, soft and an electrical conductor; diamond is transparent, hard and an electrical insulator. For silicon dioxide (SiO_2) there are many crystalline forms; cristobalite, quartz, tridymite, coesite, keatite and stishovite. However, of these only quartz exhibits piezoelectric properties that have found widespread application. Quartz has two crystalline forms, a low temperature and high

temperature form; α quartz, otherwise known as low quartz, is stable below 573°C and β quatrz, otherwise known as high quartz, is stable above 573°C. In this section an overview of the crystallography of the piezoelectric properties of α quartz is presented.

3.2.2. Lattice

A lattice is defined as a regular array of points in space. Hence the view from any one lattice point is identical to that from all the other lattice points and it is not the same as the view from a position not on a lattice point, although the view is the same from equivalent off lattice points. By definition, a lattice is infinite [1].

3.2.3. Unit Cell

When considering the lattice, it is possible to identify groups of points which can be stacked to form the lattice. For any lattice, there are many arrangements that can achieve this, see figure 3.1. If, when the outline of the unit cell is moved slightly so as to be off the lattice points, only one lattice point is contained within the frame, the unit cell is labelled *primary unit cell.*

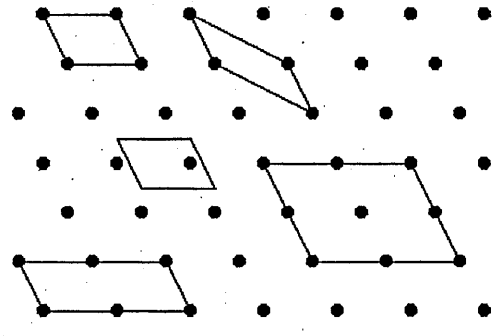

Figure 3.1. Lattice with some possible unit cells

3.2.4. Mathematical description of lattice

A coordinate system is used to describe the unit cell as shown in figure 3.2. Table 3.1 shows the seven types of unit cell that can exist and which give rise to the basic crystal groups.

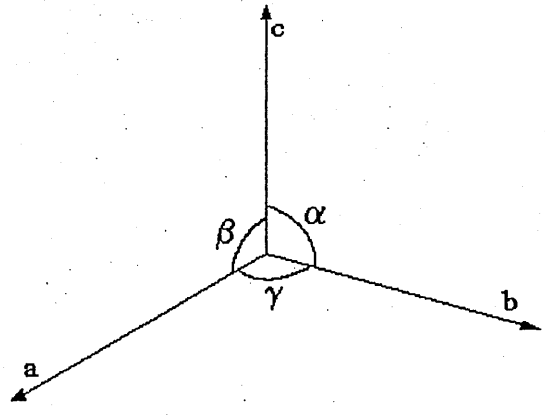

Figure 3.2. General axes for describing the unit cell.

Table 3.1
The seven crystal axis arrangements.

Triclinic	
Monoclinic	$\alpha=\beta=90°$
Orthorhombic	$\alpha=\beta=\gamma=90°$
Tetragonal	$a=b$, $\alpha=\beta=\gamma=90°$
Trigonal	$a=b\neq c$, $\alpha=\beta=90°$ $\gamma=120°$
Hexagonal	$a=b\neq c$, $\alpha=\beta=90°$ $\gamma=120°$
Cubic	$a=b=c$, $\alpha=\beta=\gamma=90°$

The a,b,c directions form the axes for the coordinate system within the lattice based on the unit cell.. The unit cell does not have to be primary. For reasons of clarity it is sometimes more convenient to use non-primary cells. This gives rise to the Bravais system which extends the generalised basic classification of table 3.2 to include 7 further forms [2].

The crystal is formed by placing an arrangement of atoms at each lattice point. This can be a single atom or a group of atoms. The arrangement of atoms placed at each lattice point is called the basis. If the basis consists of more than one atom, the relative positions of the atoms are usually given in fractional coordinates of the distance between neighbouring lattice points in the a,b,c, directions. When a basis consisting of a group of atoms is added to the unit cell the number of symmetries in the crystal may be changed, either increasing or decreasing the number of symmetries of the crystal structure. In the case of quartz the number of symmetries is increased. The basic trigonal lattice has a single axis of threefold symmetry whereas quartz also has three lines of twofold symmetry.

3.2.5. Point group of quartz

On the macroscopic scale the symmetries of the crystal structure are described by point groups. There are 32 forms of point group symmetry [3]. In the point group system, α quartz is in class 32. This means that it has one three-fold axis of symmetry (triad), which is represented by a triangle, and three two-fold axes of symmetry (diads), which are represented by paired ovals. Quartz is represented in the sterogram in figure 3.3.

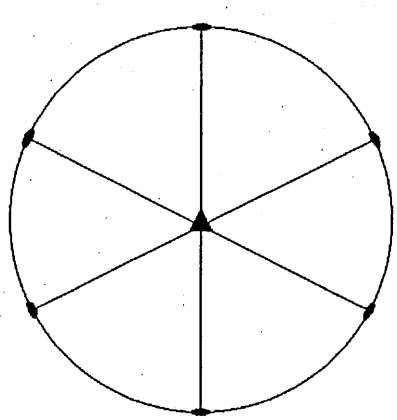

Figure 3.3. The point group symmetry of α quartz

The piezoelectric effect occurs in α quartz along the diad axes. Hence these axes are often termed the electrical axes. Class 32 of the point group system has no mirror plane of symmetry and thus α quartz has two forms, one the mirror image of the other. These are referred to as right-handed α quartz and left-handed α quartz. For the two handed forms to exist in the same piece of material there must be a grain boundary separating the two forms in the material. The two versions of quartz, α and β, have two different symmetries. α quartz is trigonal and β quartz is hexagonal. From table 3.1 it is clear that the two forms are closely related. The difference lies in the fact that the trigonal form has an axis of three-fold symmetry and the hexagonal form has an axis of six-fold symmetry. When β quartz is cooled below the transition temperature to form α quartz both right handed and left handed α quartz crystal structures are formed within the same piece of material. This means that for a piece of quartz to maintain its particular handedness it must never go above the transition temperature of 573°C. Quartz is manufactured by growing it from seed crystals in autoclaves.

3.2.6. Cartesian axes

Quartz has no naturally mutually perpendicular directions on which to base a set of cartesian axes. However, a convenient set is readily defined. The system that has been adopted makes the axis of the three fold rotation symmetry parallel to the z axis, one of the diads is made parallel to the x axis and the y axis is perpendicular to the x and the z axes. Positive directions are defined thus, z is chosen arbitrarily, x is defined so that compression gives negative polarity of voltage, y is then chosen so as to complete the right hand cartesian system regardless of the handedness of the crystal [4].

3.3. Brief review of piezoelectricity

The quartz crystal is electrically neutral when there is no stress applied to the crystal. This implies that on the atomic scale, the centres of gravity for the positive and negative charges fall at the same point in space. However, when stress is applied which is in the appropriate plane, the atoms move slightly so that the centres of gravity of the positive and negative charges are displaced, thus forming an electrical dipole. This occurs across the whole crystal. Therefore the dipole is repeated many many times through the crystal. The dipole produces an electrical potential change across the physical boundaries of the crystal as an electrical potential, or an electric field, like tiny torch cells being stacked in series. The piezoelectric effect relies on the asymmetry of the crystal structure, in particular the lack of inversion symmetry.

3.4. Review of the mathematics of crystallography

The aim of this section is to give an overview of the mathematics used in the crystallography texts, which are many and varied, and not to give a rigourous treatment of the subject. The mathematical treatment was developed in the latter part of the 19th century. The first thorough mathematical treatment of crystallography was published by Voigt [5] in 1910. The major developments since in the treatment cover notation. Modern notation will be used in this thesis although some of the texts referenced use the older styles of notation.

The mathematics of crystallography is based on the use of tensors. Tensors come in ranks, the lower ranks being familiar to many people. A tensor of rank zero is a scalar, of rank one is a vector, the higher ranks are tensors of rank n. Tensors are similar to fractals. In a three dimensional space described by three orthogonal

axes, a scalar has magnitude but no direction, a vector has magnitude in three directions, a rank 2 tensor has three directions superimposed on three directions see figure 3.4. In the standard notation the directions for tensors are denoted by the use of subscript characters e.g. x1, x2, x3.

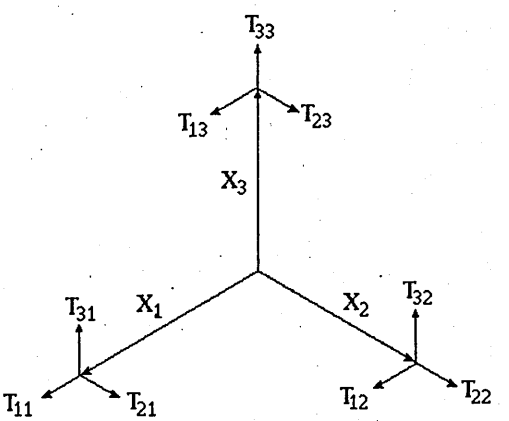

Figure 3.4. Rank 2 tensor.

For piezoelectricity the quantities of interest are stress, strain and electric field. When we come to consider the piezoelectric resonator the elasticity of the material will also have to be considered. Electric field is a vector, stress and strain are tensors of rank 2, piezoelectricity is a tensor of rank 3, elasticity is a tensor of rank 4.

3.5. Stress within a solid

Force is a vector, stress is force per unit area. When an external force is applied to an object, in this case a cube, Newton's second law tells us that it will accelerate unless a force equal in magnitude and in the reverse direction is applied. If the two forces are in line the object will experience a tensional stress (or compressive if the directions of the forces are reversed) as in Figure 3.5 (a). If the forces are not in line the object will experience a shearing stress provided further external

forces are applied to cancel the torque set up by the moment of the first two forces as in Figure 3.5 (b).

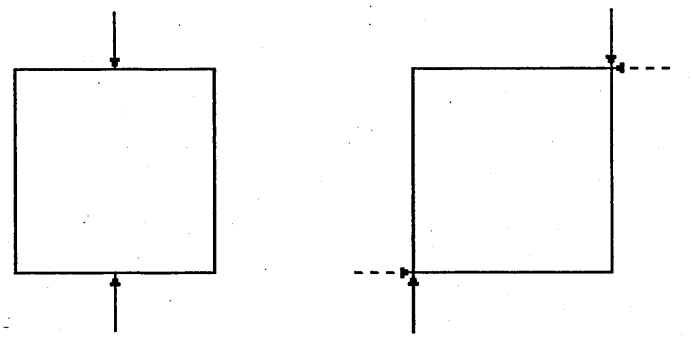

Figure 3.5. Forces on a body giving rise to (a) compression stress and (b) shear stress

If the origin of the system is placed at the centre of the cube then the stresses acting on the cube can be represented by the stress tensor in figure 3.4. The mathematical representation of this is

$$\begin{matrix} T_{11} & T_{12} & T_{13} \\ T_{21} & T_{22} & T_{23} \\ T_{31} & T_{32} & T_{33} \end{matrix} \qquad (3.1)$$

Alternatively a convenient shorthand to this tensor is

$$T_{ij} \qquad (3.2)$$

$$(i=1,2,3.\ j=1,2,3)$$

In this form when the opposing forces are in line the two subscripts are the same. Hence matching subscripts represent tensional stress. When the opposing forces are not in line the subscripts are different. Hence differing subscripts represent

shear stress. There is a reduction in the number of distinct terms in the case of the stress tensor. In the example it was stated that there had to be forces present to prevent the applied forces simply resulting in a turning moment. In figure 3.5 (b) this means that $T_{12} = T_{21}$. This is extended to form a general relationship which states that $T_{ij} = T_{ji}$. So the tensor can be represented by a row matrix comprising the 6 independent elements

$$T_1 \; T_2 \; T_3 \; T_4 \; T_5 \; T_6 \tag{3.3}$$

or in general terms as

$$T_p \tag{3.4}$$

Where the relationship between the p and the ij indices is as follows

ij	11	22	33	12,21	13,31	23,32
p	1	2	3	4	5	6

The 9 original components of the stress tensor are thus reduced to only 6 independent terms. T_1 T_2 and T_3 are tensional stresses and T_4 T_5 and T_6 are shear stresses. This symmetry or inseparability within tensors means that such a reduction of elements is possible for rank 2 tensors and above. For the piezoelectric effect the tensor consists of 27 elements but this can be reduced to a matrix of 3×6 independent elements. The tensor form is particularly convenient for changing from one sort of axes to another. The matrix form is easier to work with because of the reduced number of elements but it is not possible to change axes without reverting back to the tensor form. The relationship of rotating the axes has been calculated so for the matrix form it is a matter of reference rather than recalculation [6].

3.6. Description of the piezoelectric effect

If a compressive stress T is applied parallel to the x axis of a piece of α quartz, the resultant polarisation per unit area P is given by the following expression

$$P = dT \tag{3.5}$$

where d is the piezoelectric strain coefficient.

In the general form, (3.5) is expressed as a polarisation vector P_i, a stress tensor T_{jk} and piezoelectric strain tensor d_{ijk}

$$P_i = \sum_{\substack{j=1 \\ k=1}}^{3} \sum^{3} d_{ijk}T_{jk} \tag{3.6}$$

The standard form of presentation is to use Einstein notation where summation can be implied simply by the repetition of the subscripts. Using this notation (3.6) is written as

$$P_i = d_{ijk}T_{jk} \tag{3.7}$$

The direct piezoelectric effect can also be expressed as a relationship between polarisation P and strain S

$$P_i = e_{ijk}S_{jk} \tag{3.8}$$

The converse Piezoelectric effect can be expressed in terms of a stress tensor

$$S_{jk} = d_{ijk}E_i \tag{3.9}$$

or a strain tensor

$$T_{jk}=e_{ijk}E_i \tag{3.10}$$

where E_i represents the applied electric field.

The number of elements can be reduced as discussed above to give the matrix form

$$P_i=d_{ip}T_p \tag{3.11}$$

where the relationship between the p index and the jk indices is as follows

jk	11	22	33	12,21	13,31	23,32
p	1	2	3	4	5	6

3.7. Elasticity

Hooke's law expresses the relationship between stress and strain in the linear region. When the stress is removed the material will return to its original, unstressed, form. Hooke's law is expressed mathematically as

$$S_{ij} = s_{ijkl}T_{kl} \tag{3.12}$$

where s_{ijkl} are the elastic compliance coefficients.

In the reciprocal form

$$T_{ij} = c_{ijkl}S_{kl} \tag{3.13}$$

where c_{ijkl} are the elastic stiffness coefficients.

Elastic compliance and elastic stiffness are tensors of rank 4 so the number of coefficients for each is $3^4=81$. The pairing of elements of the tensor reduces the number of elements to 36 in the matrix form. The stiffness of the material has a

bearing on the vibrational characteristics of the material and thus plays an important role in determining the resonant frequency of resonators.

Each of the 32 point groups give rise to their own form of matrix which represents each tensor. Each crystalline form has conditions on the number of independent non-zero coefficients brought about by the symmetry of the point group structure [6]. When the symmetry of the crystalline structure is considered some of the coefficients are forced to be zero, and other coefficients are forced to be equal. The matrix of piezoelectric strain coefficients for quartz is

$$\begin{matrix} e_{11} & e_{12} & 0 & e_{14} & 0 & 0 \\ 0 & 0 & 0 & 0 & e_{25} & e_{26} \\ 0 & 0 & 0 & 0 & 0 & 0 \end{matrix} \tag{3.14}$$

with the values for the coefficients given by

$$\begin{matrix} e_{11} & -e_{11} & 0 & e_{14} & 0 & 0 \\ 0 & 0 & 0 & 0 & -e_{14} & -e_{11} \\ 0 & 0 & 0 & 0 & 0 & 0 \end{matrix} \tag{3.15}$$

The matrix of elastic stiffness coefficients for quartz is

$$\begin{matrix} c_{11} & c_{12} & c_{13} & c_{14} & 0 & 0 \\ c_{21} & c_{22} & c_{23} & c_{24} & 0 & 0 \\ c_{31} & c_{32} & c_{33} & 0 & 0 & 0 \\ c_{41} & c_{42} & 0 & c_{44} & 0 & 0 \\ 0 & 0 & 0 & 0 & c_{55} & c_{56} \\ 0 & 0 & 0 & 0 & c_{65} & c_{66} \end{matrix} \tag{3.16}$$

with the values for the coefficients given by

$$\begin{matrix} c_{11} & c_{12} & c_{13} & c_{14} & 0 & 0 \\ c_{12} & c_{11} & c_{13} & -c_{14} & 0 & 0 \\ c_{13} & c_{13} & c_{33} & 0 & 0 & 0 \\ c_{14} & -c_{14} & 0 & c_{44} & 0 & 0 \\ 0 & 0 & 0 & 0 & c_{44} & c_{14} \\ 0 & 0 & 0 & 0 & c_{14} & c_{66} \end{matrix} \qquad (3.17)$$

$$c_{66} = \frac{(c_{11} - c_{12})}{2}$$

Studying the matrix of piezoelectric strain coefficients shows that there are no conditions of stress that will result in electrical polarisation in the z direction because the bottom row of the matrix has only zeros. The e_{26} coefficient shows that a voltage applied in the y direction will give a shear stress. Conversely a shear strain will give rise to a polarisation in the y direction. Hence, e_{26} is the piezoelectric coefficient that is important for the Y cut crystals which operate in thickness shear mode.

The c_{66} coefficient in the elastic stiffness matrix is the coefficient that relates shear stress in the y direction and shear strain in the y direction. This is the coefficient that has bearing on the resonance of thickness shear vibrations of Y cut plates which is approximated by

$$f = \frac{m}{2t}\sqrt{\frac{c_{66}}{\rho}} \qquad (3.18)$$

where m is odd and represents the mode of vibration and is the number of half-wavelengths across the thickness of the resonator, t is the thickness of the resonator and ρ is the density of the material. [7][8][9] The square rooted part of (3.18) is the expression for velocity of an acoustic wave through the crystal in the direction of the subscript.

3.8. Electrical Resonators

A system that exhibits simple harmonic motion is one that gives a sinusoidal response when disturbed from its equilibrium position by an impulse. In the system, energy is being transformed from one state to another and back again. In the electrical circuits that are to be considered here the two components that store energy are capacitors and inductors.

	Capacitor	Inductor	
Energy	$\frac{1}{2}CV^2$	$\frac{1}{2}LI^2$	(3.19)
Voltage	$V = \frac{1}{C}\int i\,dt$	$V = -L\frac{di}{dt}$	(3.20)
or	$V = \frac{Q}{C}$	$V = -L\frac{d^2Q}{dt^2}$	(3.21)

In the case of a capacitor, energy is stored as an electric field set up by stationary charge, and in the case of the inductor, energy is stored as a magnetic field set up by flowing charge.

The circuit which is equivalent to equating the voltage expressions is shown in figure 3.6.

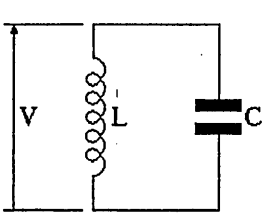

Figure 3.6. Parallel combination of a capacitor and inductor

The behaviour of this circuit is discribed mathematically by the second order differential equation

$$V = \frac{Q}{C} = -L\frac{d^2Q}{dt^2} \tag{3.22}$$

This equation has the general solution

$$Q = A\exp\left[\frac{jt}{\sqrt{LC}}\right] + B\exp\left[\frac{-jt}{\sqrt{LC}}\right] \tag{3.23}$$

where A and B are complex arbitrary constants. This can be written in the more usual oscillatory form

$$Q = C\cos\left[\frac{t}{\sqrt{LC}}\right] + D\sin\left[\frac{t}{\sqrt{LC}}\right] \tag{3.24}$$

where C and D are real constants. The waveform of Q against time is a sinusoid of frequency $\frac{1}{2\pi\sqrt{LC}}$ and the relative values of C and D determine its magnitude and phase.

In a real circuit or mechanical system there will be losses which means that the sine wave will decay. The circuit diagram of figure 3.6 is modified to that of figure 3.7, where the resistance R represents the losses in the system.

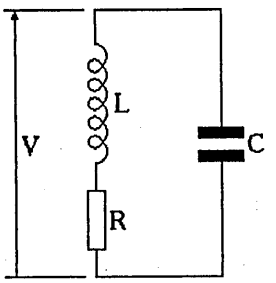

Figure 3.7. Modified circuit showing a resistor which represents loss of energy

Hence (3.22) above is modified to

$$L\frac{d^2Q}{dt^2} + R\frac{dQ}{dt} + \frac{Q}{C} = 0 \qquad (3.25)$$

Substituting $Q = Q_0e^{mt}$ into (3.25) gives

$$Q_0e^{mt}\left[Lm^2 + Rm + \frac{1}{C}\right] = 0 \qquad (3.26)$$

A non-trivial solution exists only if the bracket of (3.26) equals 0, which requires that

$$m = \frac{-R}{2L} \pm \sqrt{\frac{R^2}{4L^2} - \frac{1}{LC}} \qquad (3.27)$$

Which gives

$$Q = \exp\left[\frac{-Rt}{2L}\right]\left[A\cos\left[\sqrt{\frac{1}{LC} - \frac{R^2}{4L^2}}\right]t + B\sin\left[\sqrt{\frac{1}{LC} - \frac{R^2}{4L^2}}\right]t\right] \qquad (3.28)$$

When $\frac{1}{LC} \gg \frac{R^2}{4L^2}$ (3.28) may be approximated by

$$Q \approx \exp\left[\frac{-Rt}{2L}\right]\left[A\cos\left[\frac{t}{\sqrt{LC}}\right] + B\sin\left[\frac{t}{\sqrt{LC}}\right]\right] \qquad (3.29)$$

This represents oscillation at the original undamped frequency but modulated by a slowly decaying function. Note that rate of decay increases as R is increased as expected.

A plot of the impulse response is shown in figure 3.8 with L=1H , C=1F and R=1Ω.

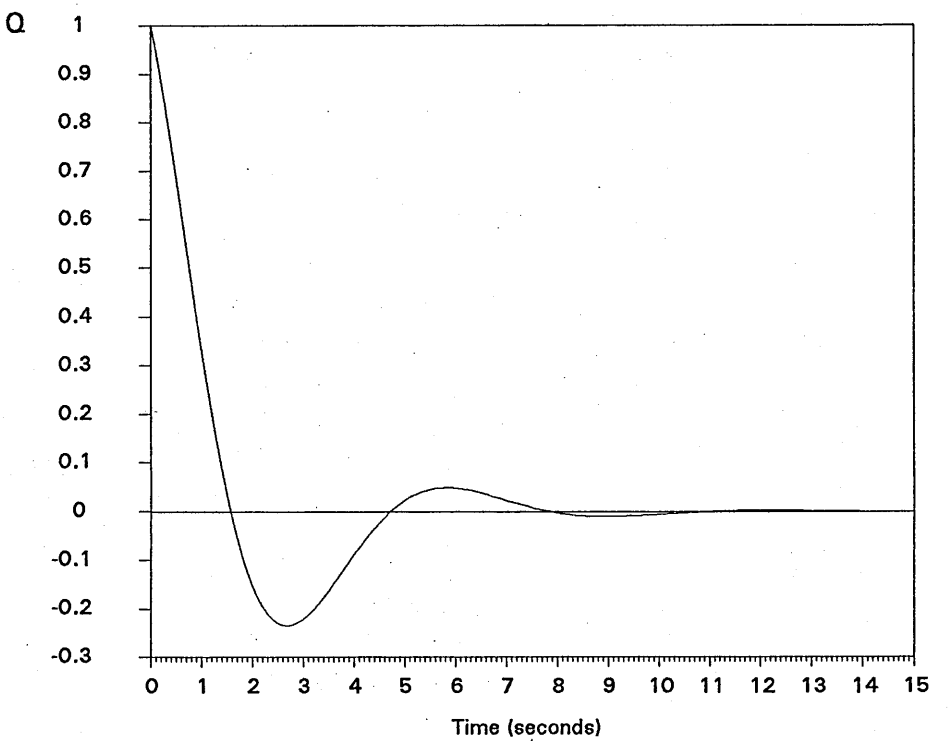

Figure 3.8. Plot of Q against time.

3.9. History and development of the AT cut quartz resonator

In the section on piezoelectricity it was explained that polarisation can occur parallel to the x direction and the y direction when appropriate stresses are applied to an α quartz crystal. When making resonators for high frequency oscillators,

crystals are cut into thin slices, with the thickness of the slice determining the resonant frequency. Originally rectangular crystal blanks were used that had all edges parallel to the cartesian axes described in section 3.2. The different arrangements of the crystal lattice with respect to the physical boundaries were named according to the thinnest plane so there were X cut, Y cut and Z cut crystals. Both Y cut and X cut crystals were used for frequency control applications; X cut resonators have the applied electric field parallel to the resultant stress, hence the vibrations are extensional; Y cut resonators have the applied electric field perpendicular to the resultant stress, hence the vibrations are shear and are usually referred to as *thickness shear.* Both cuts suffered from many spurious modes of vibration, which were dependent upon the geometry of the blank piece of quartz, and a high temperature coefficient of frequency of 85ppm/°C (parts per million per degree centigrade) for the Y cut. For some applications this was quite adequate but where the sensitivity to temperature was a problem the crystals were operated in ovens to maintain a stable thermal environment. Unfortunately this was both bulky and power consuming.

Lack, Willard and Fair [10] discovered that rotation of the crystal cut about the x axis altered the coupling to the unwanted modes of vibration within the crystal, which was brought about by mechanical coupling through the stiffness coefficient c_{56}. (See section 3.7). The mathematics indicated that there were 2 angles for which the coupling to unwanted modes was zero. These were approximately +31° and -60° and they were designated the AC cut and BC cut respectively.

Experimentally, the temperature coefficient for the AC cut is found to be 20ppm/°C and for the BC cut is -20ppm/°C. Angles for which the temperature coefficient is zero were sought. Two angles were found which were called the AT cut at +35° 15' and the BT cut at -49°. These angles are close enough to the AC cut and BC cut for their susceptibility to spurious frequency activity to be very

low. However, spurious frequency activity does occur with these cuts and occurrences are referred to as *activity dips* or *bandbreaks.* For many applications of crystal oscillators at the time of their discovery the new cuts removed the need of a oven because of their thermal insensitivity. The lattice orientation of many types of crystal is shown in figure 3.9. Worthy of note is the GT cut which is a low frequency resonator which has exceptional frequency stability with temperature. The AT cut became the more popular cut because of its higher coupling to the piezoelectric effect. In the remainder of this section the emphasis will be on the AT cut because that was the one used for the investigation.

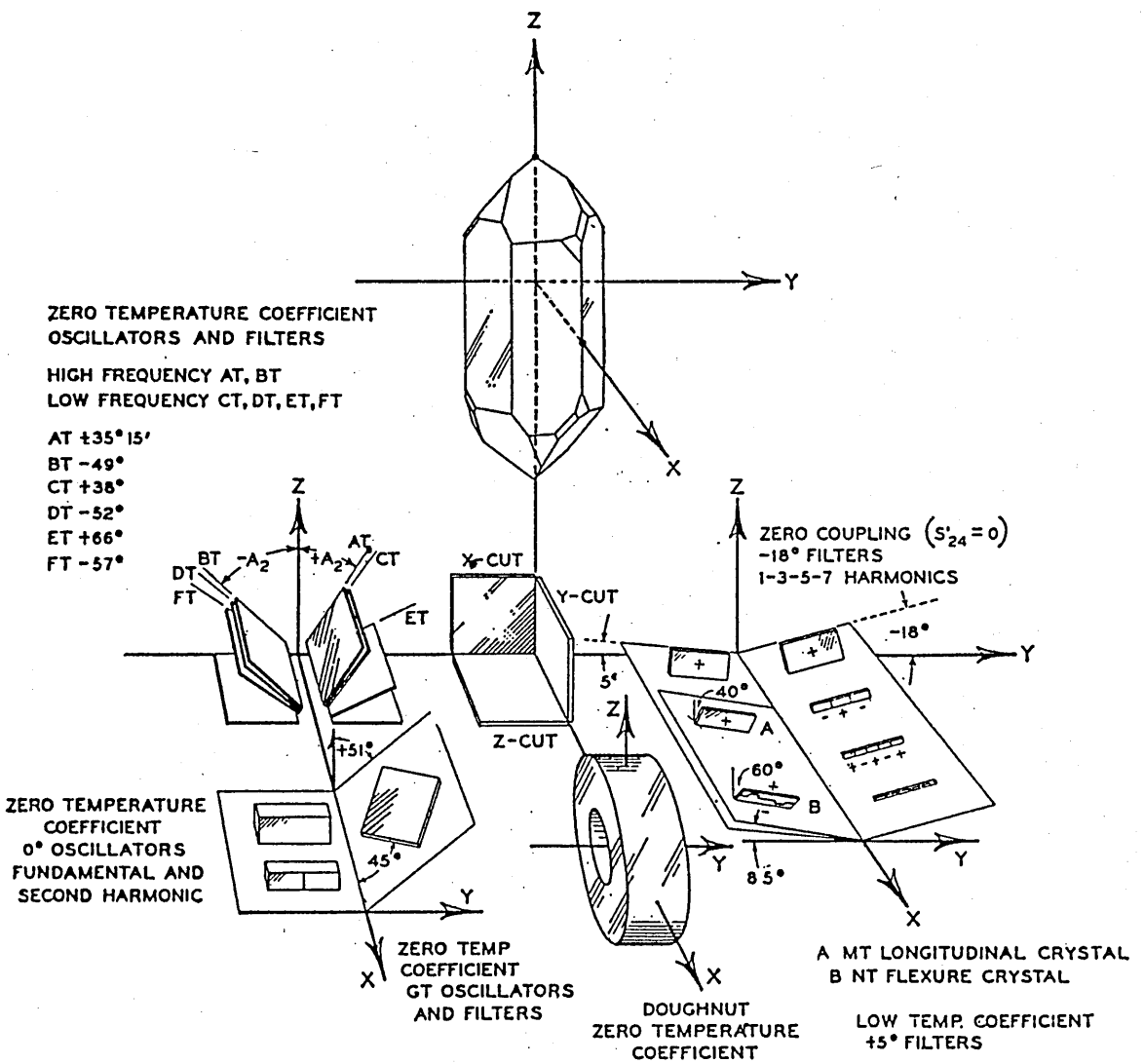

Figure 3.9. Oriented quartz crystal cuts in relation to the natural crystal.
(Heising)

3.10. Description of resonator construction.

In this section the construction of the resonator used in this investigation is described [12][13]. Reference is made to alternative methods or techniques and the advantages and disadvantages are commented on.

In the early days of the crystal industry, natural quartz, mined in Brazil, was used in the production of crystal resonators because this was the only source of resonator grade material. Resonator grade quartz must effectively be a solid single crystal, single handed and free from air pockets and impurities. Today all the quartz used within the quartz industry is manufactured. It is grown at high pressure and elevated temperatures. However the temperature must never exceed 573°C because the finished crystals must be one handed. (Section 3.2 [14][15]).

Blocks of quartz are first cut into bars and then into slices which are called blanks. The blanks are a little thicker than is required for finished resonators. In figure 3.10 the use of a multibladed saw is shown, indicating how a number of bars are cut simultaneously and how the saw is presented at an angle [16].

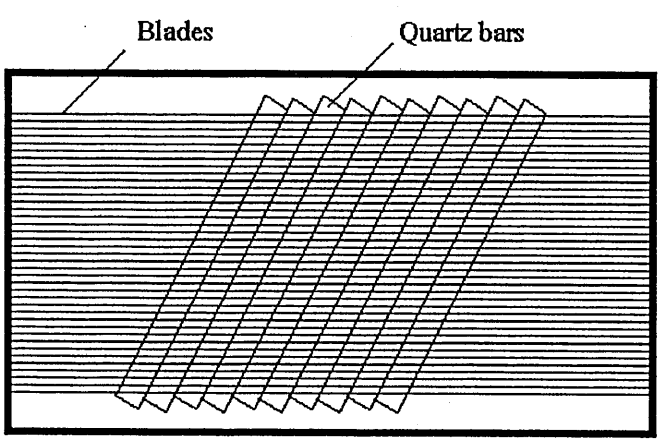

Figure 3.10. Multibladed saw used to cut bars of quartz into resonator blanks.

At this stage the blanks are selected by their lattice orientation which is checked by a goniometer using Bragg diffraction of X rays. The blanks at this stage are rectangular and are made round by grinding. Then they are tuned to a little above the required frequency by lapping. When this phase is complete the crystals are etch-cleaned in hydrofloric acid, the only solvent of quartz, in preparation for the formation of electrodes. The electrical connection to the quartz is made using electrodes, usually of silver or gold, evaporated onto the surface of the quartz. Formation of electrodes has two stages:

Basecoating lays down the bulk of the electrode material and is performed on many resonators simultaneously.

Tuning adds small amounts of the electrode material in order to tune the resonator to the required frequency. Tuning is performed on each resonator individually and its resonant frequency is monitored as the material is deposited.

Other techniques for forming the electrical connection with the blank have been investigated and used but these are outside the scope of this research.

Mechanical support of and electrical connection to the electroded crystal resonator are made by means of a two pronged clip. Each prong is connected to a lead which will connect the crystal to the electronic circuit. The crystal resonator is held in place by conductive epoxy which ensures good mechanical strength and good electrical contact between crystal and holder.

It is important for the performance of the resonator that there is protection from the atmosphere. This protection prevents deposits forming on the surface of the resonator which would degrade performance. To this end each crystal resonator is sealed in some form of holder in an inert gas or vacuum, as in figure 3.11. Shown

in figure 3.12 is an edge view of a resonator which shows the arrangement of the electrodes.

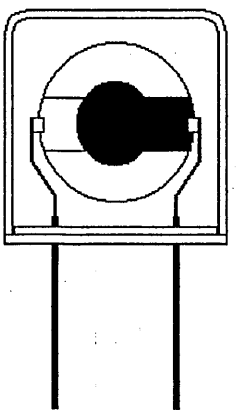

Figure 3.11. Crystal resonator mounted in a holder

Figure 3.12. Edge view of a crystal resonator showing the arrangement of the electrodes

Holders are of nickel plated copper, or glass. The body of the holder comes in two parts which have to be joined; the metal holders are welded and the glass holders are sealed. For the metal holders two forms of welding are commonly used; cold weld where the joint is made under great pressure and resistance weld where the joint is made by the heating effect of a large electrical current. During the research resonators mounted in two types of holder were used. Initially resistance weld crystals were used but problems were encountered with these for which the solution was found in the use of glass holder crystals.

3.10.1. Electrical crystal models

The electrical model of the crystal resonator uses the properties of standard electrical devices, capacitors, inductors and resistors, to describe how a crystal behaves when the crystal is considered as an electrical component. This is a very common practice in the study of electrical and electronic components.

The first successful model to describe accurately the behaviour of a crystal resonator was derived independently by Butterworth and Van Dyke [11], and is used widely today. The model is only representative in the region of resonance. Models which represent the behaviour on the crystal over the whole frequency range are beyond the scope of this thesis. The Butterworth-Van Dyke model represents the crystal as in figure 3.13.

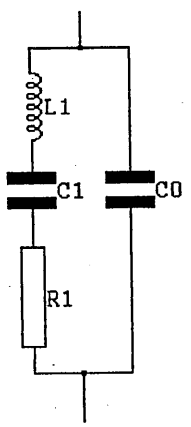

Figure 3.13. Commonly used crystal model

C_0 is the capacitance formed by the electrodes of the crystal and C_1, L_1 and R1 are the motional parameters of the quartz blank. The order of magnitude for the components in the model are C_0 = 10pF, C_1= 10fF, L_1 = 10mH and R =10Ω.

Parzen [17] extends this model to incorporate the effects of the holder. However, over the frequency range of the research described in this thesis the effects of the holder are typically ignored.

3.11. Effect of temperature on AT cut crystals

3.11.1. Static temperature characteristic

The AT cut crystal resonator has a linear temperature coefficient of frequency deviation against temperature of zero. However, higher-order temperature coefficients are non-zero. In the vicinity of the AT angle small changes in the lattice orientation with respect to the physical boundaries of the resonator give rise to different frequency deviations against temperature characteristics. Figure 3.14 shows the family of curves normalised and in angular changes of 2 minutes of arc. The zero angle reference is that angle which has zero temperature coefficient.

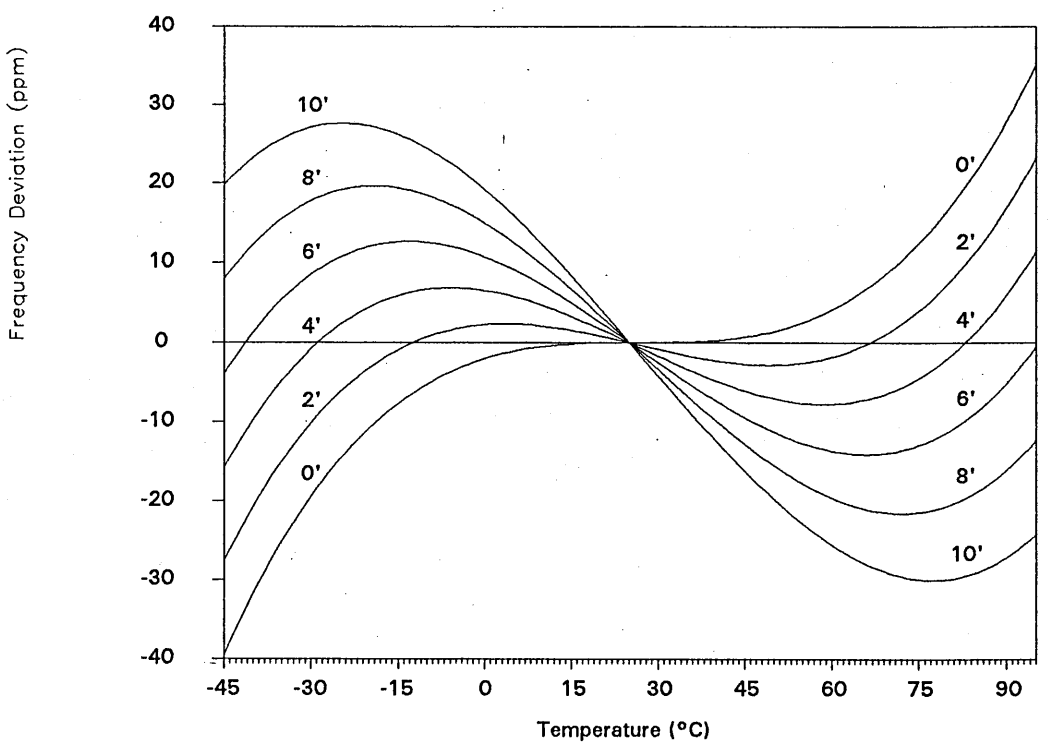

Figure 3.14. Frequency deviation against temperature characteristics for AT cut crystal resonators for a variety of lattice angles.

Bechmann [18][19] showed that the frequency deviation against temperature characteristic for the AT cut crystal resonator could be described very well over the temperature range -200°C to +250°C by a cubic polynomial

$$\frac{\Delta F}{F_0} = a(T-T_0) + b(T-T_0)^2 + c(T-T_0)^3 \qquad (3.30)$$

where T is ambient temperature, T_0 is the reference temperature, usually taken as 25°C (298°Kelvin), ΔF is the frequency deviation from the nominal frequency F_0, $a=a_1\theta$, $b=b_0 + b_1\theta$ and $c=c_0 + c_1\theta$. θ is the angular offset of the crystal lattice from the AT angle. For practical AT cut crystal resonators only a, b_0 and c_0 need be considered because θ is small. Experimentally determined values of these parameters [20][21] are given in table 3.2.

Table 3.2.
AT cut crystal temperature characteristic constants.

a_1	$-5.08\times10^{-6}/K/°\theta$
b_0	$-0.45\times10^{-9}/K^2$
b_1	$-4.7\times10^{-9}/K^2/°\theta$
c_0	$108.6\times10^{-12}/K^3$
c_1	$-20.0\times10^{-12}/K^3/°\theta$

If the reference temperature is the inflection temperature then the coefficient of the square term becomes zero. However, in practice it is more practical to take a nominal temperature close to the inflection temperature hence the use of 25°C as mentioned above.

3.11.2. Dynamic temperature effects

When AT cut resonators were used in oven controlled crystal oscillators it was found that the level of frequency stability was lower than anticipated. The cause for this was identified as stress developed in the resonator due to unequal

temperature distribution throughout its volume. This effect was called *Dynamic Frequency response* and is characterised by modifying the linear coefficient of (3.30) [22]. Hence the dynamic frequency deviation against temperature expression is

$$\frac{\Delta F}{F} = \left[\tilde{a}\frac{dT}{dt} + a\right](T-T_0) + b(T-T_0)^2 + c(T-T_0)^3 \qquad (3.31)$$

where $\tilde{a}$ is the thermal rate coefficient which has been determined experimentally as $-2.27\times10^{-7}s/K^2$. For temperature compensated crystal oscillators this behaviour is of little concern.

Warner [23] and Oura, Kuramochi, Nakamura and Ogawa [24] showed that ring shaped electrodes, which excited the thickness shear vibrations by a lateral field, were not sensitive to the dynamic frequency deviations. However, this form of electrical connection has not been widely adopted. Another approach to the problem was that which led to the discovery of the AC and BC cuts. This was to look for the cause of the problem from a crystallographic viewpoint, and then to determine coefficients that caused the problem and identify ways to reduce them to zero. The result was the doubly rotated SC cut resonator, SC standing for stress compensated. The analysis and application of this crystal cut is widely reported in the literature. It has application in digital temperature compensation and its use is described in chapter 7.

3.11.3. Ageing

The change of resonant frequency of the resonator with time is called *ageing.* There are four major causes for ageing; stress release in the quartz and holder, holder leakage giving rise to a change of pressure, chemical changes at the boundary between quartz and electrode, and variations in mass loading [25]. In

general the rate of frequency deviation caused by ageing decreases with time and the ageing process is accelerated by increasing the resonator temperature. The effects of ageing in an oscillator are reduced by using a resonator which has been pre-aged. Pre-aging involves storing the resonator at a temperature above its anticipated operating temperature range. The time of storage depends on the application. It is standard practice to recalibrate crystal oscillators periodically and compensate any drift by varying the load capacitance in the resonator circuit. However, this can degrade the performance of temperature compensated crystal oscillators because the tuning sensitivity of the varactor diode is changed at the same time. Galla and McVey [26] show that the position of a calibration capacitor within the crystal circuit is important and conclude that the most favourable results are obtained with the capacitor connected in series with the crystal. Clark [27] showed that improved results were obtained if the bias voltage for the varactor diode was changed instead of directly changing the capacitance in the circuit.

The resistance weld holder crystals used in the early stages of the research were not pre-aged. The glass holder crystals were stored at 80°C for two weeks [28] and a further two weeks at 95°C [23]. This pre-ageing was performed to ensure that ageing would not interfere with measurements of hysteresis.

3.11.4. Hysteresis

When a crystal is subjected to a temperature cycle which involves measuring its resonant frequency with increasing and decreasing temperature it is anticipated that the frequency will be equal, independent of the direction of temperature change. However in practice hysteresis is observed. There are several conditions that can cause hysteresis; three of these are surface contamination, moisture in the holder condensing on the surface and stress within the crystal resonator. A review paper on this subject with 54 references has been presented by Kusters and Vig [29].

During the research presented in this thesis hysteresis was encountered which was attributed to three sources; the environmental chamber, see section 5.5, the oscillator drive circuit, see section 4.6, and the resonator. Hysteresis within the resonator was found to be related to the type of holder used; the resistance weld holder crystals used initially had hysteresis of the order of 0.5ppm. Inspection of the resistance weld crystals and some available glass holder crystals under a microscope showed surface contamination of small particles on the surface of the crystals and in the electrodes. This contamination could only be deposited during their manufacture. New crystals were ordered which were cleaned at important stages of their manufacture to ensure the removal of all contamination. The differences from the usual processes were that the crystal blanks were brush washed with isopropyl alcohol before and after base plating and the plating masks were cleaned in a similar way. When these crystals were viewed under a microscope there was no visible surface contamination. The level of hysteresis obtained with these crystals is shown in section 4.6. Problems of this nature differ between different manufacturers of crystal resonators [30].

3.11.5. Bandbreaks

Bandbreaks, also called activity dips, appear on the frequency deviation against temperature characteristic of a crystal resonator as spurious frequencies which do not lie on the smooth characteristic. Bandbreaks occur when the crystal vibrates in a mode other than the desired mode. The tendency to couple to the undesired mode is related to the power dissipated in the crystal resonator which, is referred to as the *drive level.* Bandbreaks are a serious problem for temperature compensated crystal oscillators because they cannot be compensated for. Hence the level of stability is degraded if the resonator used in a TXCO has a bandbreak. Glass holder crystals used in the research exhibited a significant bandbreak problem and the steps taken to find a solution are described in section 4.6.

3.11.6. Apparent angular offset

When the frequency deviation against temperature characteristic is plotted for an AT cut crystal resonator which has a capacitor connected in series, often refered to as the series load capacitor, there is an apparent change in the lattice angle of the crystal when compared with the characteristic obtained without the series capacitor. This effect is sometimes refered to as skewing. A similar effect is caused by mass loading brought about by the deposited electrode material. Ballato [31] explains how mass loading and series capacitance modify the cubic expression which describes the frequency deviation characterisitc. In this thesis the same result is derived by from a different starting point.

The difference between the loaded resonant frequency and the unloaded, or series, resonant frequency of the crystal alone is given as a fraction of the series resonant frequency by:

$$\frac{f_L - f_s}{f_s} = \frac{\Delta f}{f_s} = \frac{C_0}{2r(C_0 + C_L)} \tag{3.32}$$

where f_S is the series resonant frequency of the crystal, f_L is the resonant frequency with the series capacitor C_L, C_0 is the capacitance formed by the two electrodes of the resonator and r is the ratio $\frac{C_0}{C_1}$.

When the effect of temperature is taken into consideration using the linear coefficient for each term the result is

$$\frac{f_L(1+T_{fL}T) - f_s(1+T_{fs}T)}{f_s(1+T_{fs}T)} = \frac{C_0(1+T_{C_0}T)}{2r(1+T_rT)(C_0(1+T_{C_0}T)+C_L(1+T_{C_L}T))} \tag{3.33}$$

where T_X is the linear temperature coefficient of x. T_{fS} is the linear coefficient, a, in (3.30). Differentiating this result with respect to temperature gives the linear temperature coefficient for frequency deviation

$$\frac{f_L}{f_s}(T_{fL}-T_{fs}) = \frac{C_0}{2r(C_0+C_L)}\left[-T_r + \frac{C_L}{(C_0+C_L)}(T_{C0} - T_{CL})\right] \qquad (3.34)$$

Now

$$\frac{f_L}{f_s} \approx 1$$

So

$$(T_{fs}-T_{fL}) \approx \frac{C_0}{2r(C_0+C_L)}\left[T_r + \frac{C_L}{(C_0+C_L)}(T_{CL} - T_{C0})\right] \qquad (3.35)$$

This result is in agreement with Ballato's simplification after he neglects mass loading. It shows how the linear coefficient of the cubic expression is modified by the load capacitance.

When specifying a crystal resonator an allowance has to be made for the apparent angular offset to ensure that the crystal will operate within the required frequency tolerance over the temperature range.

3.11.7. Higher order tuning effects

The cubic nature of the frequency deviation against temperature for an AT cut crystal resonator is well understood. When the required cubic compesnation voltage is determined, by some means of curve fitting, and applied to a varactor diode it is found experimentally that a fourth order error characteristic is obtained as shown is section 8.5. Salt [32] gives the following expression for obtaining the required compensation capacitance.

$$\frac{C_0 + C_L}{C_{00}+C_{L0}} = \frac{C_1}{C_{10}}(1 + \Delta f_T)\left[1 + \frac{\Delta f_T}{\Delta f_L}\right] \qquad (3.36)$$

Where C_{00} and C_{10} are the values of the crystal capacitances C_0 and C_1 at the reference temperature T_0 and C_{L0} is the value of the series load capacitance C_L at T_0, Δf_T is the cubic polynomial for frequency deviation and $\Delta f_L = \frac{f_L - f_{s0}}{f_{s0}}$ where f_L is the frequency that the oscillator is set to by the compensation process and f_{s0} is the series resonant frequency, at T_0, of the crystal without a series load capacitor.

Assuming that the temperature dependance of C_1 is represented by

$$C_1 = C_{10}(1 + T_{C1}(T - T_0)) \tag{3.37}$$

then (3.36) becomes

$$\frac{C_0 + C_L}{C_{00}+C_{L0}} = (1 + T_{C1}(T - T_0))(1 + \Delta f_T)\left[1 + \frac{\Delta f_T}{\Delta f_L}\right] \tag{3.38}$$

In practice $\Delta f_T \ll 1$ and a fourth order term is obtained with a coefficient of $\frac{cT_{C1}}{\Delta f_L}$ where c is the third order coefficient of Δf_T.

There is a possible discrepancy between the way the linear coefficient is modified here and in Ballato's expression (3.32). Swanson and McVey [33] give a similar expression to that of Salt for the required compensation capacitance but the two forms are not identicle. Their expression is

$$\Delta C = \left[\frac{C_0 + C_x}{P}\right]\Delta f_T \tag{3.39}$$

where $C_x + \Delta C \approx C_L$ and $P \approx \Delta F_L$. Here ΔC is the temperature dependant capacitance needed to compensate the crystal. Expressing P in terms of the circuit capacitances gives

$$\Delta C = \left[\frac{2(C_0 + C_x)^2}{C_1}\right]\Delta f_T \tag{3.40}$$

When coefficients of temperature are taken a different result to that of Salt is obtained which has a linear term closer to Ballato's because all the capacitance values are considered. Part of the difficulty here is the approximations used and neglected terms which form the approximations. Future work will aim to determine whether the discrepancies are real and if so how they are resolved.

3.12. References

[1] Glazer, A. M. (1987). The Structure of Crystals, *Adam Hilger, Bristol*, pp. 14-21.

[2] Glazer, A. M. (1987). The Structure of Crystals, *Adam Hilger, Bristol*, pp. 1-11.

[3] Nye, J. F.(1985, 2nd ed.). Physical Properties of Quartz, *Oxford University Press, Oxford*, pp. 276-288.

[4] IEEE Standard on Piezoelectricity. ANSI/IEEE Std.176-1987.

[5] Voigt, W. (1910, 1st ed.). Lehrbuch der Kristallphysik, *B. G. Teubner, Leipzig.*

[6] Nye, J. F.(1985, 2nd ed.). Physical Properties of Quartz, *Oxford University Press, Oxford*, pp.150-169.

[7] Heising, R. A.. Sykes, R. A. (1946). Quartz Crystals for Electrical Circuits, *Van Nostrand Company Inc., New York*, pp. 205-248.

[8] Heising, R. A.. McSkimin, H. J. (1946). Quartz Crystals for Electrical Circuits, *Van Nostrand Company Inc., New York*, pp. 249-275.

[9] Bottom, V. E. (1982). Introduction to Quartz Crystal Design, *Van Nostrand Reinhold Company Inc., New York*, pp. 63-81.

[10] Lack, F. R., Willard, G. W. and Fair, I. E. (1934). Some improvements in quartz crystal circuit elements. *Bell System Technical Journal, vol.13*, pp. 453-463.

[11] Cady, W. G. (1946, 1st ed.). Piezoelectricity, *McGraw-Hill, New York*, pp. 333-334.

[12] Heising, R. A.. Bond, W. L. (1946). Quartz Crystals for Electrical Circuits, *Van Nostrand Company Inc., New York*, pp. 290-316.

[13] Salt, D. (1987). Handbook of Quartz Crystal Devices, *Van Nostrand Reinhold (UK) Co. Ltd.*, pp. 63-87.

[14] Doxey, W. L. (1986). Quartz crystals paved the way. *Proc 40th Annu. Freq. Control Symp.*, pp. 9-14.

[15] Gerber, E. A. and Ballato, A. (editors), Halliburton, L. E., Martin, J. J. and Koehler, D. R. (1985). Precision Frequency Control, vol. 1, *Academic Press Inc. (London) Ltd.*, pp. 23-29.

[16] Dowsett, J., Spencer, R. B. and Wood, A. F. B. (1987). Use of annular saw for cutting Quartz resonator blanks and comparison with other methods. *Proc 41st Annu. Freq. Control Symp.*, pp. 548-522.

[17] Parzen, B. (1982). Theoretical and practical effects of the resonator specifications and characteristics upon precision crystal oscillator design and performance. *Proc 36th Annu. Freq. Control Symp.*, pp. 480-485.

[18] Bechmann, R. (1956). Frequency-temperature-angle characteristics of AT-type resonators made of natural and synthetic quartz. *Proceedings of the IRE, vol. 44*, pp. 1600-1607.

[19] Bechmann, R. (1960). Frequency-temperature-angle characteristics of AT and BT type quartz oscillators in an extended temperature range. *Proceedings of the IRE, vol. 48*, p. 1494.

[20] Miljković, M. R., Brajović, V. J. and Trifunović, G. Lj. (1987) Frequency-temperature characteristics of AT crystal units. *IERE Internstional Conference on Frequency Control and Synthesis, publ. no. 75,* pp. 3-10.

[21] Ballato, A. (1978). Frequency-temperature-load capacitance behaviour of resonators for TCXO application. *IEEE Transactions on Sonics and Ultrasonics, vol. su-25, no. 4.* pp. 185-191.

[22] Ballato, A. and Vig, J. R. (1978). Static and dynamic frequeny-temperature behaviour of singly and doubly rotated, oven-controlled quartz resonators. *Proc 32nd Annu. Freq. Control Symp.*, pp. 180-188.

[23] Warner, A. W. (1963). Use of parallel-field excitation in the design of quartz crystal units. *Proc 17th Annu. Freq. Control Symp.*, pp. 248-266.

[24] Oura, N., Kuramochi, N., Nakamura, J. and Ogawa, T. (1982). Thermal frequency behaviour in contoured quartz crystal plates induced by direct irradiation of laser beam. *Proc 36th Annu. Freq. Control Symp.*, pp. 133-139.

[25] Gerber, E. A. and Ballato, A. (editors), Gerber, E. A. (1985). Precision Frequency Control, vol. 1, *Academic Press Inc. (London) Ltd.*, pp. 271-279

[26] Galla, W. D. and McVey, E. S. (1980). TCXO error due to aging adjustment. *Proc 34th Annu. Freq. Control Symp.*, pp. 504-508.

[27] Clark, R. L. (1985). Reducing TCXO error after aging adjustment. *Proc 39th Annu. Freq. Control Symp.*, pp. 166-170.

[28] Hardcourt, R. Cathodeon Crystals Ltd.. Private communication.

[29] Kusters, A. and Vig, J. R. (1990). Thermal hysteresis in quartz resonators - a review. *Proc 44th Annu. Freq. Control Symp.*, pp. 165-175.

[30] Förster, H. J. (1982). Thermal hysteresis of AT and SC-cut quartz crystal resonators. *Proc 36th Annu. Freq. Control Symp.*, pp. 140-158.

[31] Ballato, A. (1977). Temperature compensated crystal oscillator (TCXO) design aids: frequency-temperature resonator characteristics as shifted by series capacitors. *Technical report ECOM-4498, US Army Electronics Command, Fort Monmouth, NJ*

[32] Salt, D.. Private communication.

[33] Swanson, C. T. and McVey, E. S. (1979). A non-iterative solution for a two-thermistor TCXO. *Proc 33rd Annu. Freq. Control Symp.*, pp. 425-430.

4. OSCILLATORS

4.1. Introduction

At the start of the research presented in this thesis it was intended that an available oscillator drive circuit would be used. However, problems with the crystal drive level were encountered which showed that the oscillator design could not be ignored. Initially, attempts were made to modify the existing design. These attempts improved the results but the drive level was still too high. Finally, a new oscillator drive circuit was designed which solved the problem. In this chapter, first the principle of harmonic oscillators is presented then a description of the oscillator designs used during this research is given.

4.2. The Barkhausen Criterion

The Barkhausen Criterion gives the two conditions that have to be satisfied by a feedback loop, as in figure 4.1, in order for the loop to maintain harmonic oscillation. These are:

1: the gain around the loop must be unity

2: the total phase shift around the loop must be 0° or n×360° where n is a positive integer.

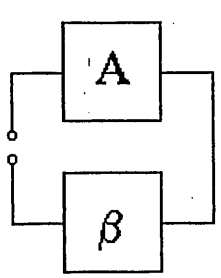

Figure 4.1. Feedback loop

A system which has a forward gain A and feedback gain β is shown in figure 4.1. The gain criterion for sustained oscillation is met when $A\beta=1$. The feedback signal is shown disconnected from the input. This break in the loop could be made at any point and the following would still hold. If the system shown in figure 4.1 represents an oscillator with a signal $v_{in}=V_I\sin 2\pi ft$, where f is the resonant frequency of the loop, applied to the input. The output of the loop, v_{out}, will be a signal of the same magnitude and phase as the applied signal. If the frequency of the input signal is changed the output signal will change so that one or both of the conditions will not be met.

In a practical circuit $v_{out}=kV_I\sin 2\pi ft$ where $k>1$ to ensure that the oscillator will start to oscillate spontaneously. The signal amplitude will then increase until nonlinearities, such as clipping, reduce the loop gain to 1 as required by the Barkhausen Criterion. Alternatively, the gain could be controlled by an addition to the circuit which maintains the amplitude of the output signal. This is called automatic gain control (agc).

4.3. Linearity

When the input signal to the system element is a sine wave the element is said to have a linear gain if the output comprises only a sine wave of the same frequency as the input. If the output signal includes harmonics of the input signal which have been generated within the element, the element has a nonlinear gain function. Nonlinearities can be of many forms but the two that are of interest for oscillators are clipping and device characteristics.

Clipping occurs when the input signal is too large, for example the output voltage cannot be larger than the power supply voltage, so if the magnitude of the input signal is too great part of the output signal will be clipped off, figure 4.2.

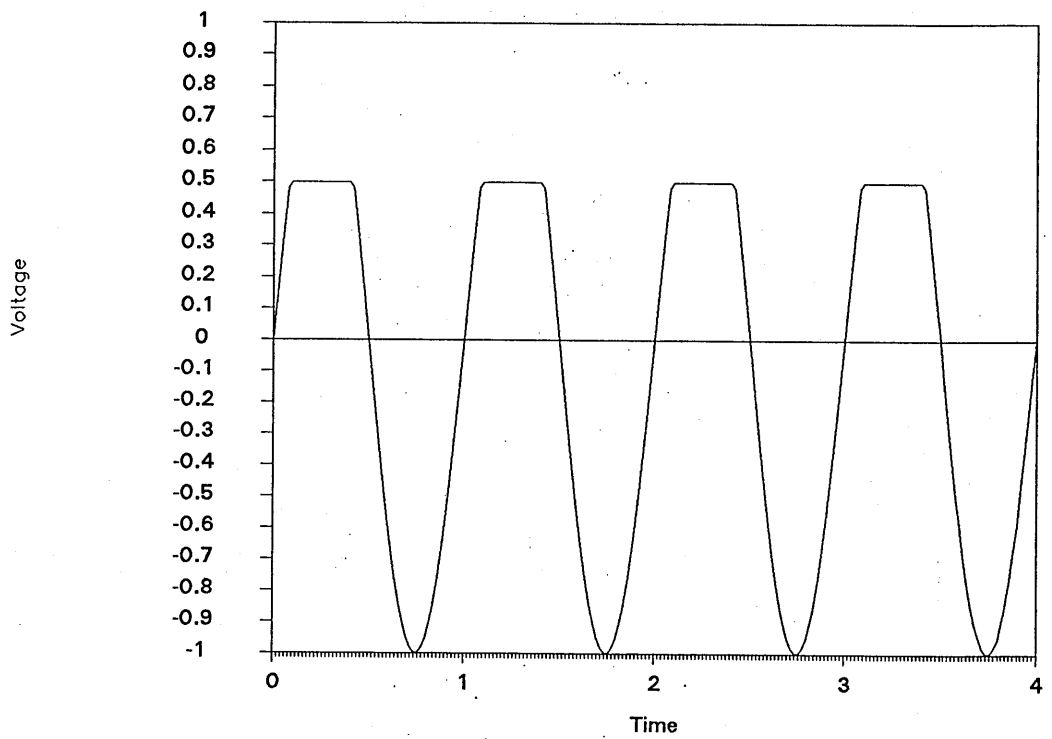

Figure 4.2. Sine wave clipped at +0.5 volts

There are two effects clipping has on the circuit:

i. the average of a sine wave is zero but when clipping of the form shown in figure 4.2 occurs the average is offset which in a circuit takes the form of a DC bias;

ii. the gain of the amplifier is reduced and is dependant on the level of the input signal.

The device characteristics of transistors and thermionic valves are not linear because of their nature of operation. However, when small signals are to be amplified the gain can be considered as being linear, so there is a distinction in the mode of operation of these devices, linear called small signal operation and nonlinear called large signal operation. The effects of the nonlinear device characteristics are similar to those of clipping; change in DC bias and reduced gain. The gain of the device might also be affected by the change in the bias conditions.

4.4. Varactor diode

A varactor diode, also known as a varicap diode, is a semiconductor diode which behaves as a voltage controlled capacitor. Diodes are electronic components which will only allow current to flow in one direction. Semiconductor diodes achieve the two states by having part of their structure able to switch between being an insulator and a conductor, depending on the polarity of the applied voltage. When the diode conducts the applied voltage is said to forward bias the diode, as in figure 4.3.

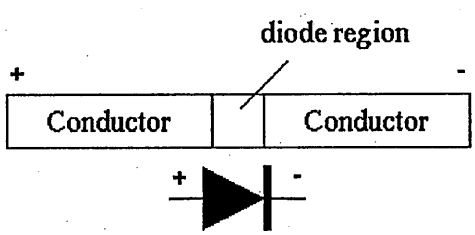

Figure 4.3. Forward biased diode model shown with diode circuit symbol.

When the diode is reverse biased part of the diode becomes an insulator, shown shaded in figure 4.4.

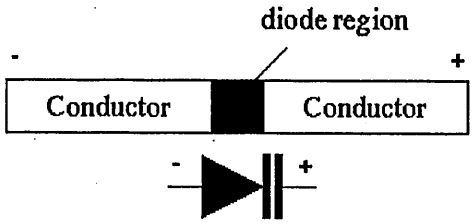

Figure 4.4. Reverse biased diode model shown with varactor diode circuit symbol.

The width of the insulating region depends on the magnitude of the reverse voltage. In this condition the device is an insulator between two conductors and hence is a capacitor. Because the width of the insulator is voltage dependant the capacitance is also voltage dependent. Hence a voltage dependant capacitor is formed. The relationship between the capacitance and the bias voltage is given by

$$C = \frac{k}{(\psi - V)^n} \tag{4.1}$$

where k, n and ψ are constants and V is the potential across the varactor diode. The value of n can be controlled by the manufacturing process to be between $\frac{1}{3}$ and $\frac{1}{2}$ so a variety of characteristics is possible. For silicon diodes ψ is 0.78volts.

4.5. Practical oscillator circuits

In the following examples some practical oscillator circuits are presented. The first two are included as examples of how the conditions for oscillation are applied but have no application in crystal oscillator circuits. For each circuit the factors that determine its frequency of oscillation and the required forward gain A that is required to sustain oscillation are presented. When the circuits that are used for crystal oscillators are described they are presented in a simplified form where the crystal is replaced by an inductor. Further discussion of these circuits may be found in refs [1] to [5]

4.5.1. Wien oscillator

The general arrangement of the Wien oscillator is shown in figure 4.5. It comprises a voltage amplifier which has 0° phase shift between input and output and a feedback circuit of two resistors and two capacitors which will exhibit 0° phase shift at the frequency of oscillation.

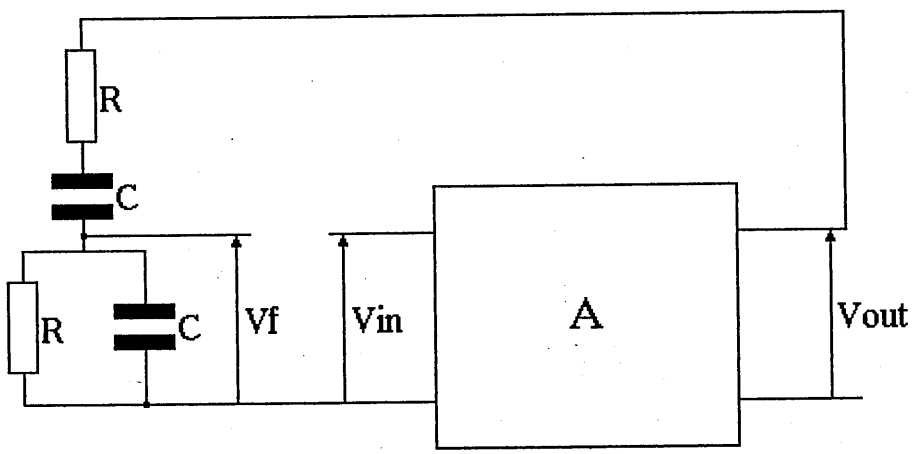

Figure 4.5. Wien oscillator circuit.

The gain of the feedback circuit is given by

$$\beta = \frac{1}{3 + j\left[\omega CR - \frac{1}{\omega CR}\right]} \tag{4.2}$$

When the imaginary part=0 the phase condition for oscillation is met and the frequency of oscillation can be determined:

$$f = \frac{1}{2\pi CR} \tag{4.3}$$

The gain of the feedback will be 1/3 hence for the gain condition to be met the forward gain A of the amplifier must be 3.

There is an alternative starting point for the mathematics which describes the behaviour of the feedback circuit of the Wien oscillator.

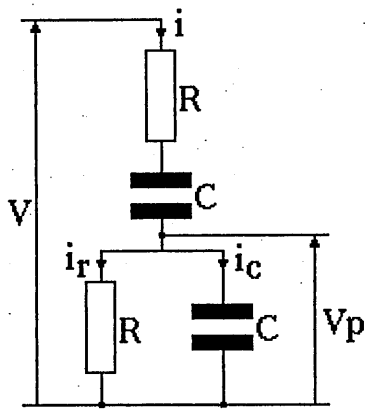

Figure 4.6. Wien oscillator feedback circuit showing currents and voltages

The feedback circuit is redrawn in figure 4.6 to show three currents, i, i_C, and i_r with two voltages labelled V and V_p. Using the relationship between voltage and current for a capacitor given in section 3.8, the voltage V is given in terms of the current i and the voltage V_p by

$$V = iR + \frac{1}{C}\int i\,dt + V_p \tag{4.4}$$

and the current i is given in terms of V_p by

$$i = \frac{V_p}{R} + C\frac{dV_p}{dt} \tag{4.5}$$

Substituting (4.5) into (4.4) gives V in terms of V_p:

$$V = 3V_p + CR\frac{dV_p}{dt} + \frac{1}{CR}\int V_p\,dt \tag{4.6}$$

The two voltages V and V_p are related by the gain A of the amplifier so that when $V=3V_p$ (4.6) is in the form of the lossless sinusoidal case which gave a constant amplitude sine function. Hence, here is a system which produces an undamped sine function.

4.5.2. Phase shift oscillator

The phase shift oscillator, figure 4.7, comprises an inverting voltage amplifier which has a phase shift of 180°, represented by the gain -A. Hence the feedback circuit has to introduce a further 180° phase shift to meet the phase condition of the Barkhausen Criterion.

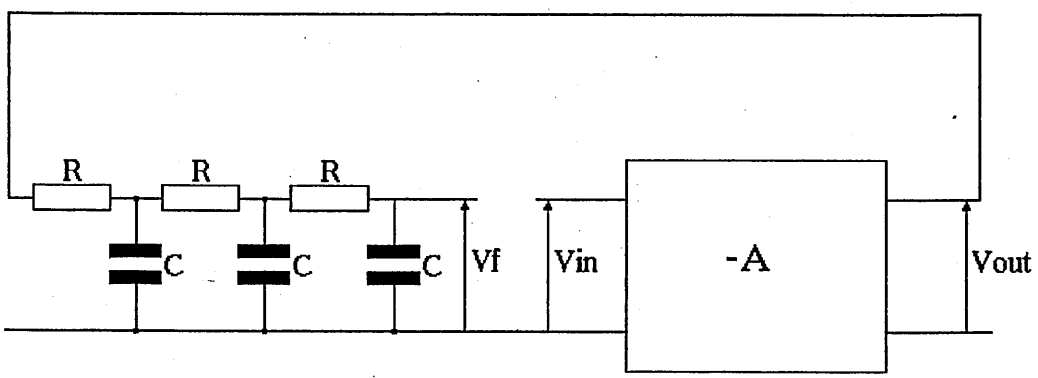

Figure 4.7. General circuit arrangement of the phase shift amplifier

The gain of the feedback circuit, provided by the three capacitors and three resistors, is given by the expression

$$\beta = \frac{1}{1 - \frac{5}{\omega^2C^2R^2} - j\left[\frac{6}{\omega CR} - \frac{1}{\omega^3C^3R^3}\right]} \qquad (4.7)$$

For the phase condition to be statisfied the imaginary term in (4.7) has to be zero which occurs in practical terms to give the frequency of oscillation

$$f = \frac{1}{2\pi CR\sqrt{6}} \qquad (4.8)$$

Putting (4.8) into the real part of (4.7) gives the gain β at the required frequency

$$\beta = \frac{-1}{29} \qquad (4.9)$$

4.5.3. Colpitts family of oscillators

The theory of the oscillators described in this section covers more than one common circuit [6][7]. The circuit in figure 4.8 shows a simplified hybrid π transistor equivalent circuit and a feedback circuit comprising Z_1, Z_2 and Z_3. Here the other components of the equivalent circuit are considered to be negligible.

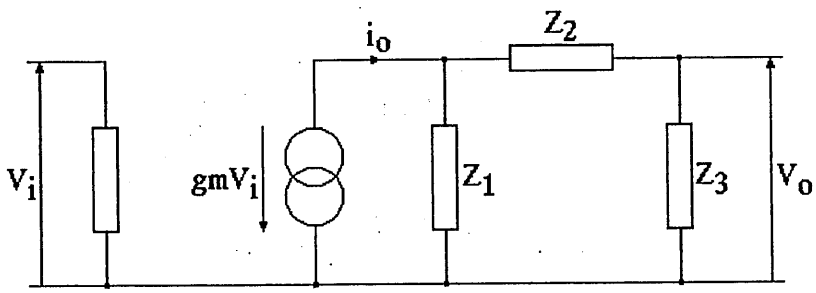

Figure 4.8. General arrangement of the Colpitts family of oscillators

The two port network represents the device that provides the forward gain. In a contemporary circuit this would be a transistor but historically this would have been a thermionic valve. The transfer function of the feedback network is

$$\frac{V_f}{i_o} = \frac{-Z_1 Z_3}{Z_1+Z_2+Z_3} \tag{4.10}$$

However

$$i_o = g_m V_i \tag{4.11}$$

Where g_m is the transconductance of the amplifier. Putting (4.11) into (4.10) gives the voltage gain:

$$\frac{V_f}{V_i} = \frac{-Z_1 Z_3 g_m}{Z_1+Z_2+Z_3} \tag{4.12}$$

The gain condition for oscillation is $V_f = V_i$. For the phase condition of oscillation to be met the reactances Z_1 and Z_3 have to be the same type, either both

are capacitors or both are inductors then Z_2 is taken as the other type of reactive component. For crystal oscillators, Z_1 and Z_3 are capacitors and the crystal is used in place of the inductor for Z_2. For the description here the circuit is presented with an inductor in the place of Z_2 in order to simplify the mathematics.

Putting $Z_1 = \frac{1}{j\omega C_1}$, $Z_2 = j\omega L + r$, and $Z_3 = \frac{1}{j\omega C_3}$ into the circuit gives

$$\frac{V_f}{V_i} = \frac{-g_m}{-r\omega^2 C_1 C_3 + j\omega(C_1 + C_3 - L\omega^2 C_1 C_3)} \tag{4.13}$$

For oscillation the imaginary part of the denominator has to be zero. The non-trivial case gives a resonant frequency:

$$f = \frac{1}{2\pi\sqrt{\frac{LC_1C_3}{C_1 + C_3}}} \tag{4.14}$$

Hence the frequency of oscillation is determined by the inductor and the capacitors in series combination.

Putting (4.14) into (4.13) gives an expression for the transconductance required to sustain oscillation

$$g_m = \frac{r(C_1 + C_3)}{L} \tag{4.15}$$

Hence the transconductance required to sustain oscillation is independent of frequency.

When the electrical requirements are compared with an npn bipolar junction transistor a practical circuit arrangement can be determined. For the BJT current

flows into the collector and out of the emitter under the control of the base to emitter voltage. An npn transistor symbol is shown in figure 4.9.

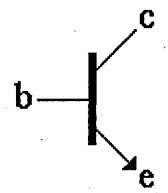

Figure 4.9. Circuit symbol of an npn transistor

Comparing figure 4.9 with figure 4.8, Z_1 will connect between the collector and the emitter, Z_2 will connect between the collector and the base and Z_3 will connect between the base and emitter. The general arrangement for the whole family of oscillators is shown in figure 4.10 and the specific arrangement for the Colpitts, Pierce and Clapp oscillators in figure 4.11.

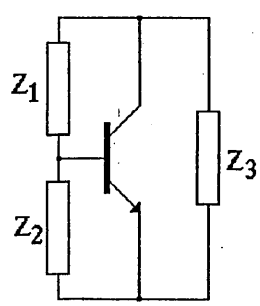

Figure 4.10. Transistor with general impedances for Colpitts family of oscillators.

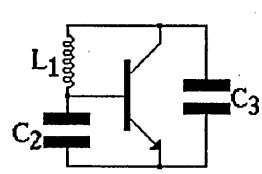

Figure 4.11. Transistor with components for Colpitts, Pierce and Clapp oscillators.

In a crystal oscillator the crystal is connected in the place of the inductor. Hence in operation the crystal will appear electrically as an inductor of the same value as the replaced component. The usual form of the Colpitts crystal oscillator with biasing resistors is shown in figure 4.12.

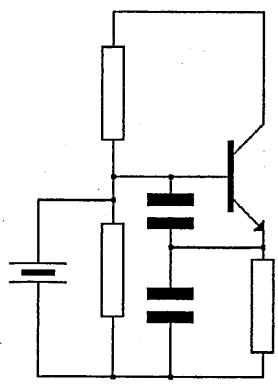

Figure 4.12. Usual Colpitts crystal oscillator circuit.

An important consideration for this circuit when a crystal is used in place of the inductor is the magnitude of the current that flows through the crystal. This is related to the drive level which is important when bandbreaks have to be considered. The current through the inductor i_L is equal to the current through C_3 which is given by

$$i_L = j\omega C_3 V_f \tag{4.16}$$

Putting (4.11) and (4.16) into (4.13) and rearranging at resonance gives

$$i_L = \frac{-i_o}{j\omega C_1 r} \tag{4.17}$$

This relates the current through the inductor to the Q of the resonant circuit which is given by

$$Q = \frac{1}{\omega(C_1+C_2)r} \tag{4.18}$$

4.5.4. Buttler oscillator

The final circuit presented here is the Buttler oscillator. This oscillator, in its simplest form, has a crystal as the only reactive component in the circuit. Hence the frequency of the oscillator is only dependent on the series resonance of the crystal with any associated tuning components. The forward gain A is a voltage gain which has zero phase shift and is a little greater than unity. The feedback gain β is a resistive ratio formed by the series resonant crystal and the input resistance of the amplifier [8], as in figure 4.13.

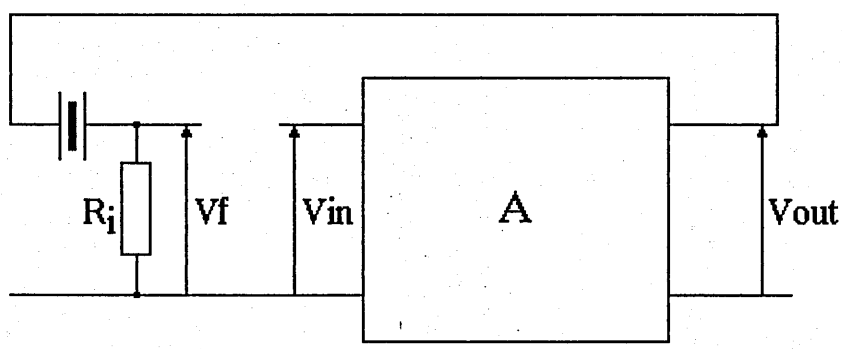

Figure 4.13. Buttler oscillator circuit.

The break in the loop shown in figure 4.13 is not possible in the practical circuit shown in figure 4.14 because R_i is the input resistance of the common base transistor.

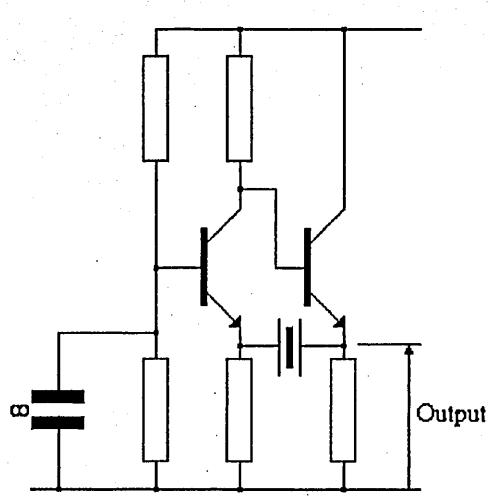

Figure 4.14. Practical implementation of Buttler oscillator

The frequency of oscillation is the series resonant frequency of the crystal and the forward gain needed to sustain oscillation is given by

$$A = \frac{r_{in}}{R_1 + r_{in}} \tag{4.19}$$

where R_1 is the motional resistance of the crystal and r_{in} is the input resistance of the common base amplifier stage. Typically $r_{in} \approx 10 \times R_1$. Hence the gain $A \approx 1$.

In this circuit arrangement there is no magnification of the current through the crystal due to resonance so the drive current through the crystal is much lower than for the Colpitts oscillator. Hence the circuit is less prone to coupling with bandbreaks.

4.6. Oscillator circuits used during the research

In the remainder of this chapter the oscillator circuits used to drive the crystal resonators are presented. The principal objective for the research described in this thesis was to investigate temperature compensation of crystal oscillators. The oscillator circuit was considered to be transparent, being the means by which oscillation was sustained. Hence only at the latter stages was a new design undertaken when it was considered that an alternative approach was required. The first circuit used for the research was a modified commercial design. Two modifications were made, one initially because the oscillator was designed to operate from 6 volts, whereas for the research described in this thesis the oscillator was required to operate from 4 volts. Further modifications were found to be necessary when hysteresis and bandbreaks appeared in the frequency deviation against temperature characteristics of the crystals being used. It was found that the

modifications made to the circuit had not fully addressed the problem of bandbreaks and an alternative circuit was adopted.

4.6.1. First oscillator circuit

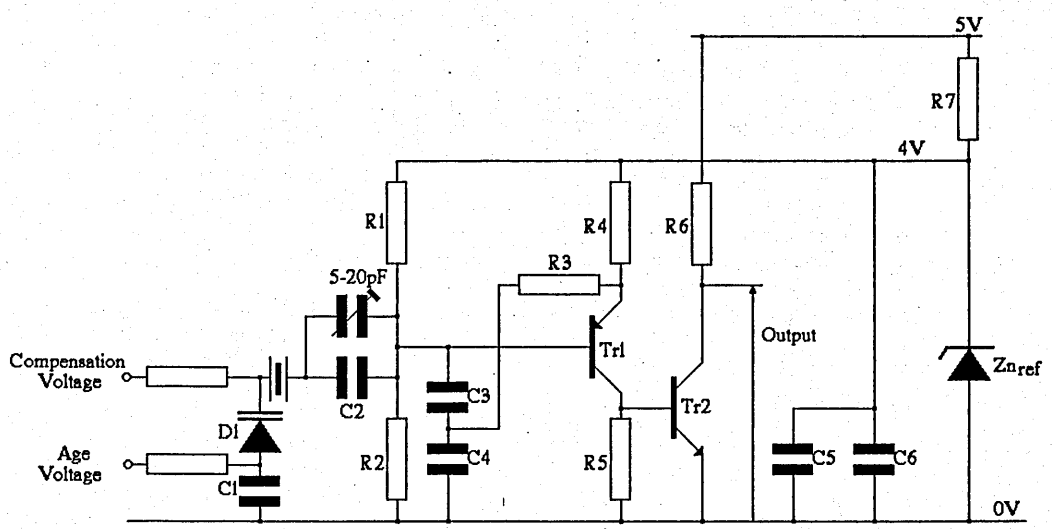

R1	33kΩ	C1	1nF
R2	33kΩ	C2	82pF
R3	100Ω	C3	150pF
R4	see text	C4	150pF
R5	1.5kΩ	C5	10nF
R6	1.5kΩ	C6	10nF
R7	470Ω		
D1	BBY 40		
Tr1	BF 569		
Tr2	BSV 52		

Figure 4.15. Circuit of the modified Colpitts oscillator

The Colpitts oscillator circuit used for much of the experimental work is shown in figure 4.15. Originally the oscillator had been designed to operate from a supply voltage in the range 6 volts to 15 volts. In order to operate from a supply of 4 volts resistor R4 was changed from 3.3kΩ to 2.2kΩ because the output transistor was not initially biased correctly to operate from the lower voltage. This oscillator circuit was used in the temperature compensated oscillator experiments described

in section 6.2 and initially in testing the new glass holder crystals described in section 6.8. Throughout, the age voltage was set at 0.18 volts using a potential divider formed by a 105kΩ resistor between the reference voltage and the age voltage input and a 5kΩ resistor between the age voltage input and 0 volts. In normal operation the age voltage is adjusted to correct for resonator ageing.

4.6.2. Second oscillator circuit

Glass holder crystals are evacuated whereas the resonators used previously were resistance weld crystals which have an atmosphere of nitrogen which acts as damping on the motion of the crystal. One effect of the damping is to reduce coupling to bandbreaks. Hence the new crystals were more prone to bandbreaks which were observed when the crystals were temperature cycled. Dr da Silva [9] suggested that the emitter resistor should be increased in value in order to increase the time constant of C_4 and R_4. This would reduce the DC bias voltage across the base and emitter of Tr_1, so reducing its gain as the level of oscillation increased. The circuit had to be modified to that shown in figure 4.16.

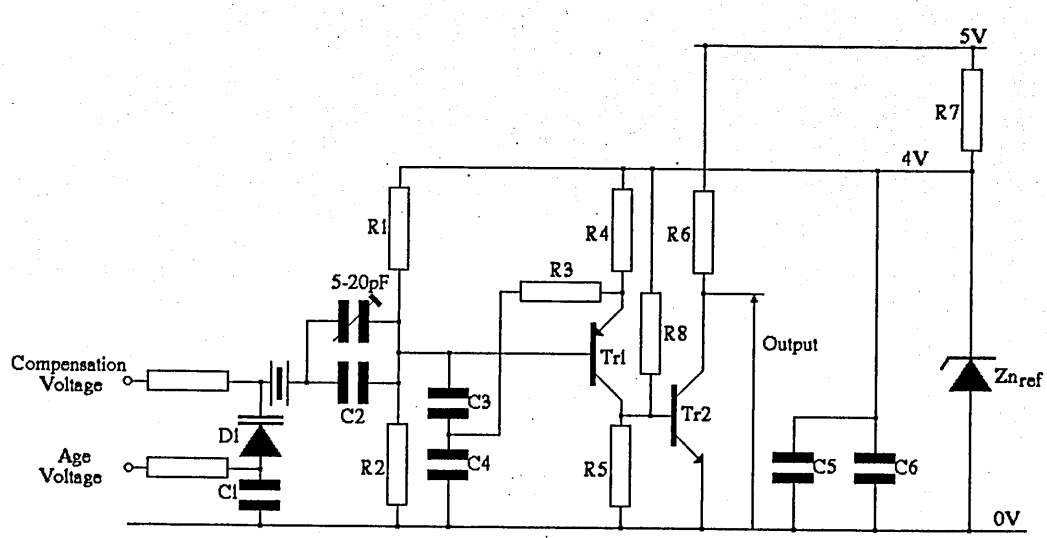

Figure 4.16. Oscillator modified to reduce the drive on the crystal.

The resistor R_8 had to be included in the circuit to provide the DC bias for Tr_2 because the voltage across R_5 was not sufficient due to the reduced collector current in Tr_1. The value used for R_8 was 12.1kΩ. Using 9 crystals with large bandbreaks and one with no apparent bandbreaks as a control, the resistance of R_4 was increased in stages and the ten oscillators temperature cycled. The results for one of these oscillators are shown in figure 4.17.

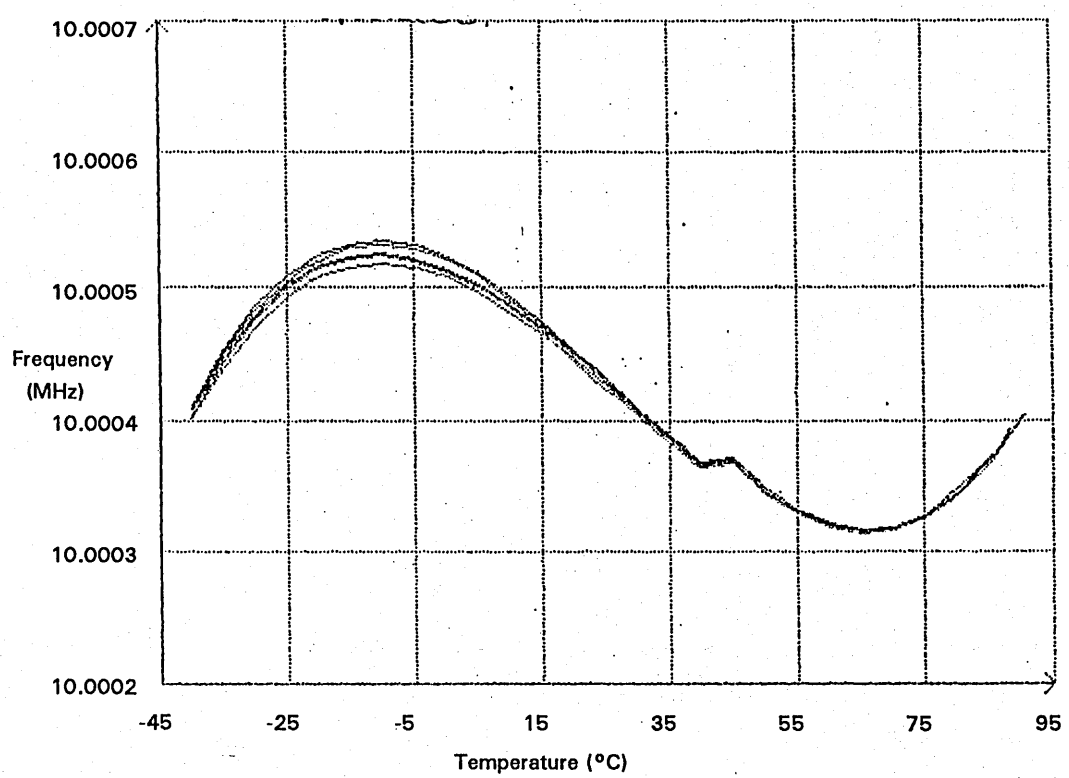

(a)

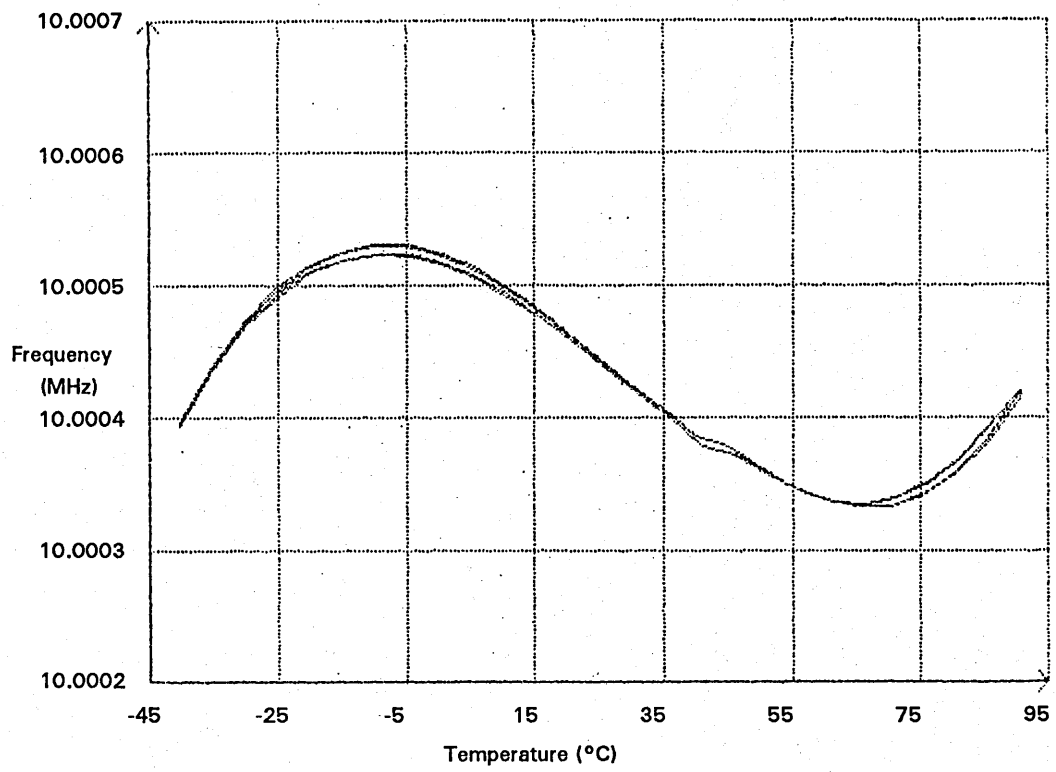

(b)

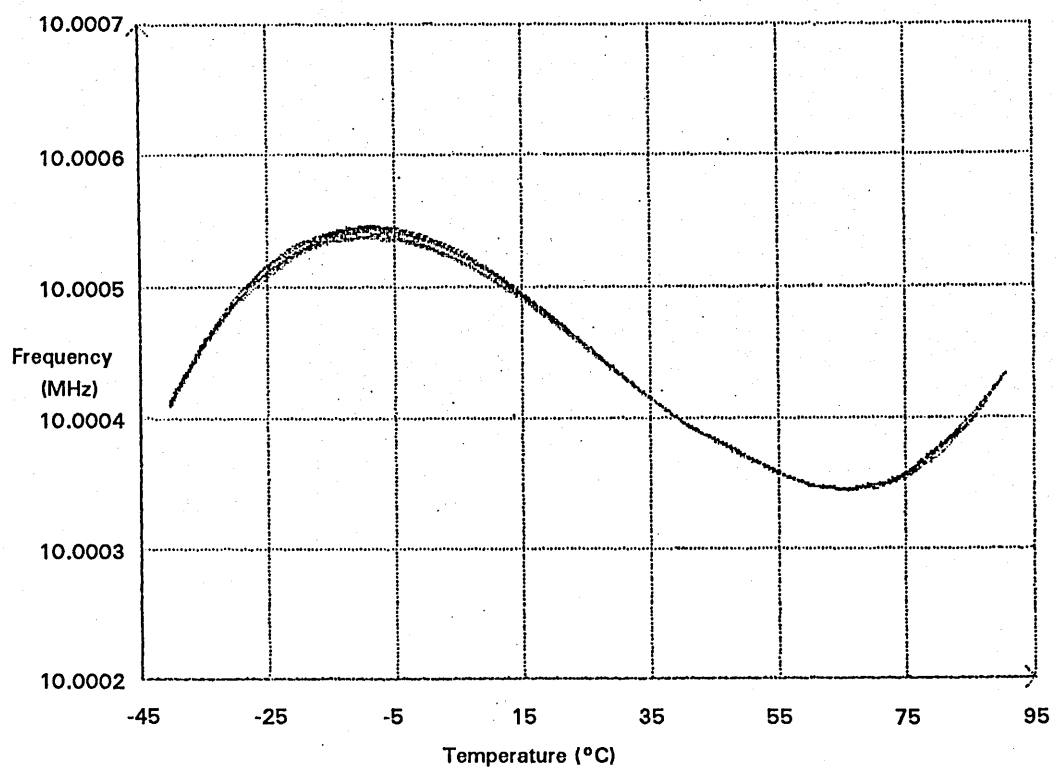

(c)

Figure 4.17. Three stages of oscillator gain set by R_4
(a) 2.2kΩ, (b) 4.7kΩ, (c) 8.2kΩ

The bandbreak is no longer apparent with $R_4 = 8.2k\Omega$. For these measurements the varactor diode was connected to the reference voltage, which makes the frequency higher than normal.

The hysteresis in figure 4.17 was typical of that observed for all the crystals. It was considered that the higher than usual varactor diode bias voltage might be a contributing factor. The bias to the varactor diode was reduced to 2 volts using a potential divider formed from two 30kΩ resistors. This appeared to increase the level of hysteresis. Figure 4.18 shows this.

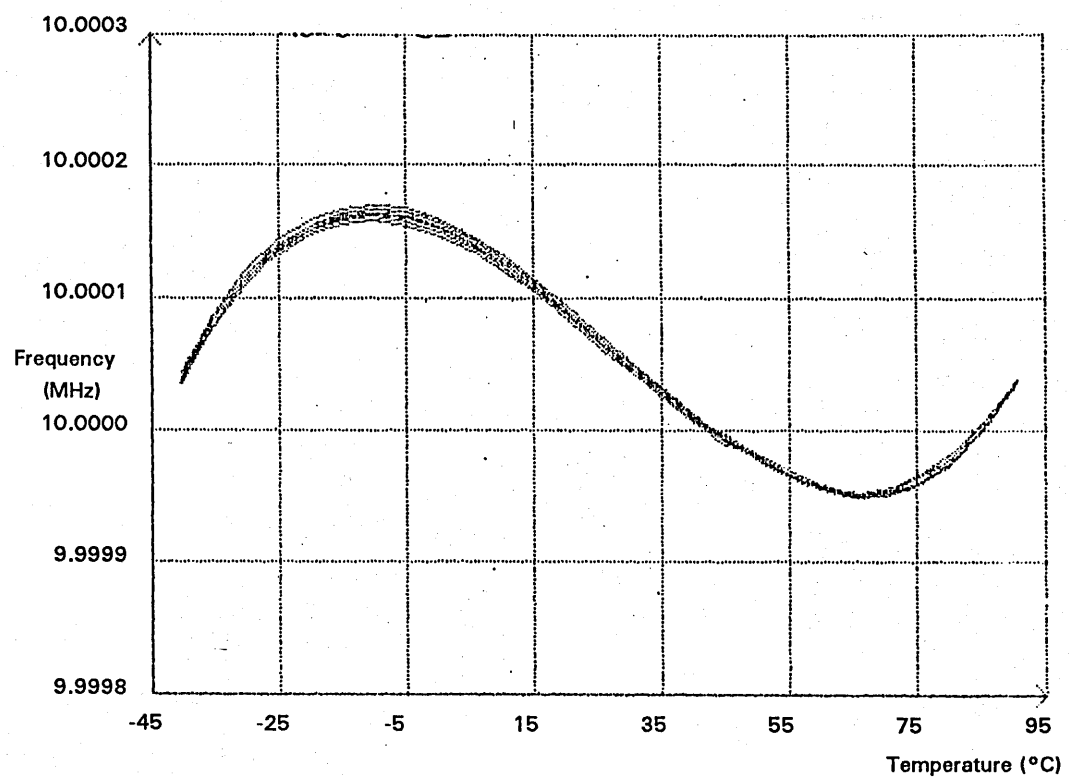

Figure 4.18. Compensation voltage fixed at 2 volts

The cause of the hysteresis seen here was confirmed as being associated with the oscillator circuit by swapping crystals between the oscillators and observing that the hysteresis went with the oscillators and not the crystal. The trimmer capacitor was identified as the cause of the hysteresis. This was confirmed by temperature

cycling 5 oscillators which had their varactor diode replaced by a short circuit, and 5 oscillators which had their trimmer replaced in a similar manner. To avoid this problem, the trimmer capacitor was replaced by a fixed capacitor whose value was calculated to ensure that the required nominal frequency of the oscillator was obtained when the varactor bias voltage was 2 volts. The capacitance against bias voltage characteristic of the varactor diode showed that a nominal 2 volts bias voltage gave a capacitance of 34pF. The capacitance required to tune the crystal was 15pF so the required fixed series capacitance was calculated as

$$\left[\frac{34\times15}{34-15}\right]\text{pF} = 26.8\text{pF} \qquad (4.20)$$

The parallel combination of a 22pF and a 5.6 pF capacitor gave a nominal capacitance of 27.6pF.

$$\left[\frac{27.6\times15}{27.6-15}\right]\text{pF} = 32.8\text{pF} \qquad (4.21)$$

Hence a slightly higher voltage would be needed across the varactor diode to produce the required capacitance. This voltage corresponds to approximately 2.5V.

A typical characteristic obtained with these modifications is shown in figure 4.19. The hysteresis at the turning points it is now less than 0.04ppm. At this level crystal ageing and dynamic thermal effects in the crystal cannot be ignored. Hence the changes to the resonator and drive circuit have significantly reduced the level of hysteresis within the oscillator.

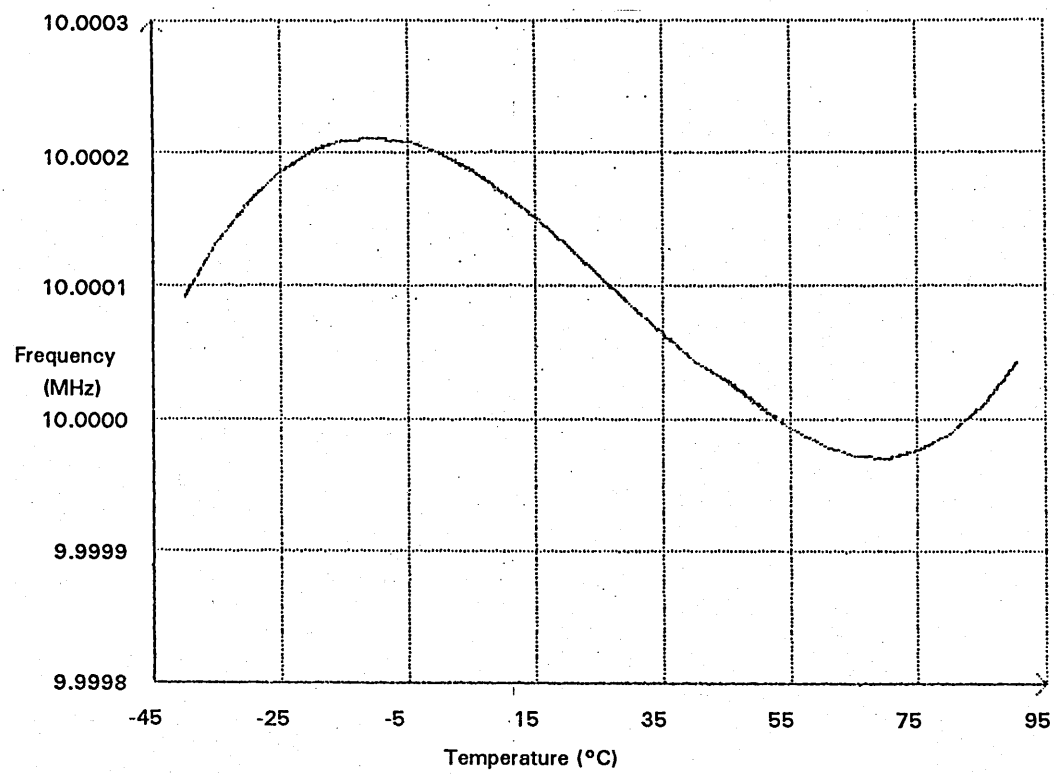

Figure 4.19. Typical frequency deviation against temperature characteristic using the modified oscillator circuit.

Apparatus for holding the oscillators during these experiments was only available on loan and had to be returned before the original metal holder crystals could be tested in this manner. A comparison was made by putting two oscillators through the company's sample process for TCXO's. The oscillator circuit used was that of figure 4.16; one oscillator had a glass holder crystal, the other had a resistance weld crystal. The results of the verification of these two oscillators are shown in figure 4.20. The resistance weld holder crystal has hysteresis of approximately 0.5ppm and the glass holder crystal has no detectable hysteresis. However there is a bandbreak in the glass holder crystal characteristic.

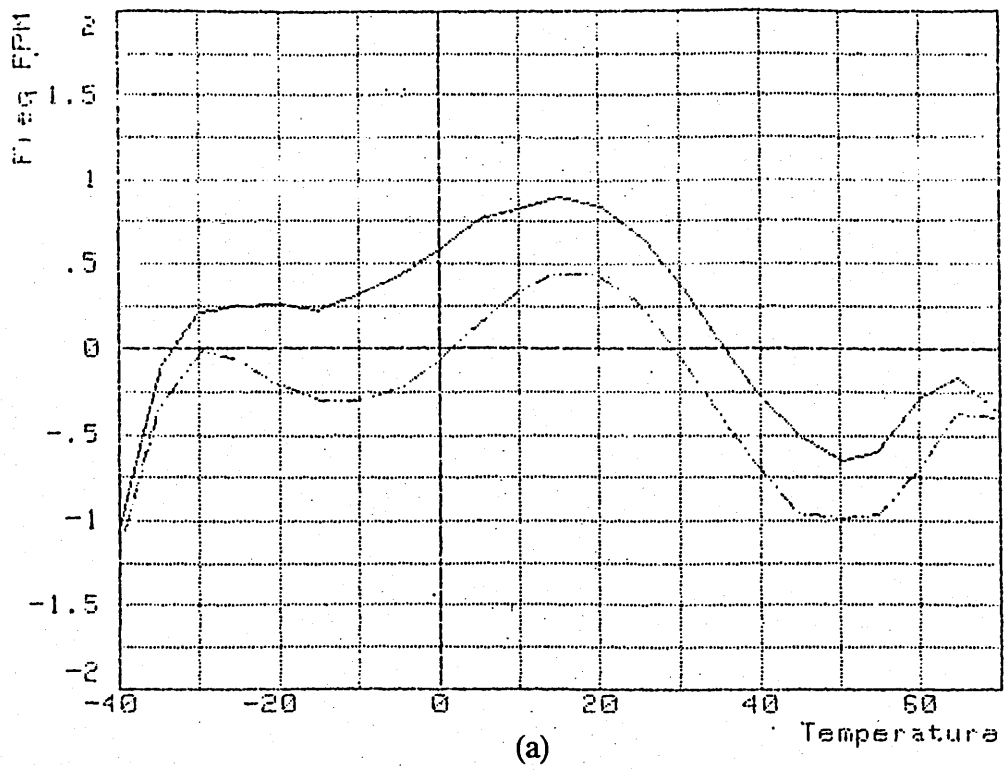

(a)

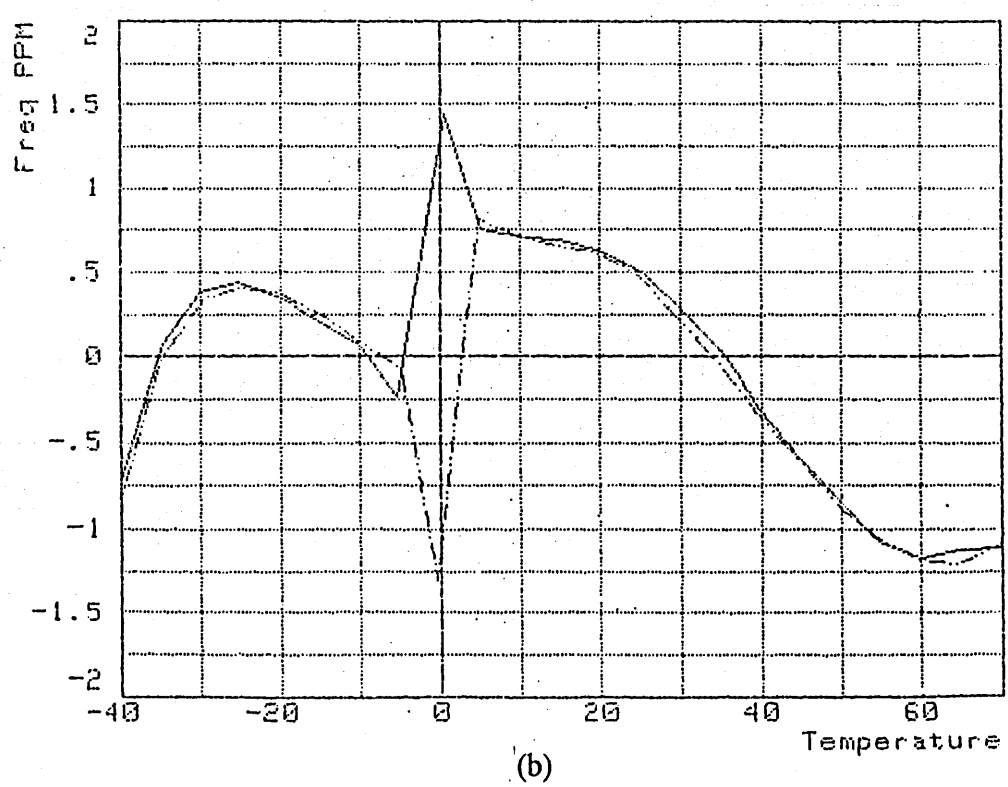

(b)

Figure 4.20. Comparison of hysteresis for (a) resistance weld crystal and (b) glass holder crystal in TCXO's.

4.6.3. Third oscillator circuit

It was discovered that bandbreaks were still occurring when a third order curve fit of the data was performed on tuning data, shown in figure 4.21.

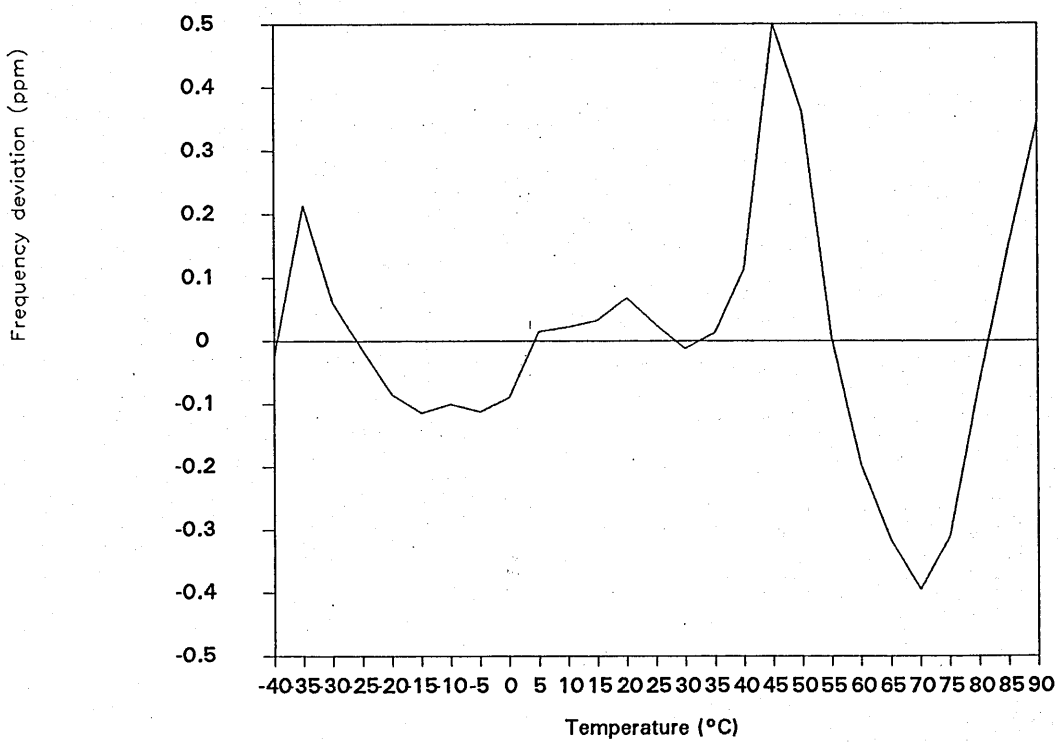

Figure 4.21. Third order curve fit on tuning data.
(The bandbreak is still evident.)

Bandbreaks of this level are difficult to detect by visual inspection of the frequency deviation against temperature characteristics shown in figure 4.19. However, these results show that at this level the problem of bandbreaks had not been adequately resolved. When figure 4.21 is compared to the results of the second attempt at experimental verification of the compensation network in section 6.8.4 there is much similarity over the top half of the temperature range. Hence the bandbreak is the reason why the optimisation failed.

It was considered that the parallel resonant circuit formed by the crystal and the two capacitors C_3 and C_4 in the Colpitts oscillator was magnifying the current through the crystal. An alternative approach would be to use an oscillator circuit which drove the crystal without the need for extra reactive components. Such a circuit is the Buttler oscillator circuit, introduced in section 4.5. The new circuit designed to reduce the drive level problem is shown in figure 4.22.

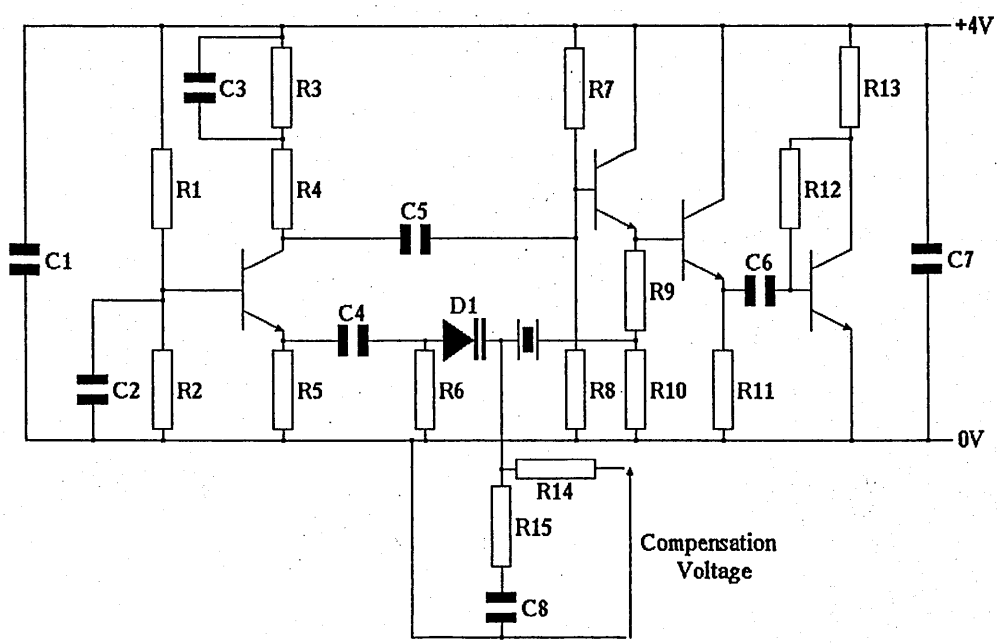

R1	12kΩ	C1	10nF
R2	5.6kΩ	C2	10nF
R3	3.9kΩ	C3	10nF
R4	180Ω	C4	25.6pF
R5	1kΩ	C5	10nF
R6	100kΩ	C6	10nF
R7	100kΩ	C7	10nF
R8	100kΩ	C8	10nF
R9	56Ω		
R10	560Ω	C4	was (2×10+5.6)pF
R11	560Ω		
R12	120kΩ	D1	BBY 40
R13	3.9Ω	Transistors	BFS 20
R14	100kΩ		
R15	100kΩ		

Figure 4.22. Buttler oscillator circuit used to reduce the crystal drive level.

Under the same conditions as those used to obtain figure 4.21 it was found that the Buttler oscillator gave no detectable bandbreaks.

4.7. Discussion

Originally the intention of the investigation had been to use an existing oscillator circuit with a minor modification to accommodate a reduced operating voltage. However, problems with hysteresis in the characteristics of the resistance weld hold crystals resulted in the use of glass holder crystal crystals. This second type of crystal suffered from bandbreaks and showed signs of hysteresis. With these crystals the cause of the hysteresis was found to be the trimmer capacitor used to initially adjust the frequency of oscillation. After this had been corrected the level of hysteresis was of the same order as crystal ageing and dynamic thermal effects within the crystal. Attempts to solve the bandbreak problem by reducing the drive to the crystal were only partially successful. A new design of oscillator based on the Buttler oscillator circuit was found to overcome the problem of bandbreaks. The difference between the two circuits lies in way the crystal is used in each circuit.

4.8. References

[1] Millman, J. (1979, 1st ed.). Microelectronics: Digital and Analog Circuits and Systems, *McGraw-Hill, New York*, pp. 646-657.

[2] Gerber, E. A. and Ballato, A. (editors) Smith, W. L. and Parker, T. E. (1985). Precision Frequency Control, vol. 2, *Academic Press Inc. (London) Ltd.*, pp. 45-98.

[3] Henny, K. (editor-in-chief), Sarbacher, R. I. and Fielder, D. C. (1950). Radio Engineering Handbook, *McGraw-Hill, New York*, pp. 416-460.

[4] Kraus, H. L., Costain, C. W. and Raab, F. H. (1980). Solid State Radio Engineering, *John Wiley and Sons Inc., New York*, pp. 128-162.

[5] Salt, D. (1987). Handbook of Quartz Crystal Devices, *Van Nostrand Reinhold (UK) Co. Ltd.*, pp. 127-140.

[6] Sherman, J. H. (1959). Designing transistor oscillators for crystals. *Proc 13th Annu. Freq. Control Symp.*, pp. 182-190.

[7] Ohata, Y. (1974). A new approach to the design of crystal oscillators. *Proc 28th Annu. Freq. Control Symp.*, pp. 221-

[8] Hillstrom, T. L. (1988). Design method yields low-noise, wide-range crystal oscillators. *EDN March*, pp. 141-146.

[9] da Silva, E., Open University. Private communication.

5. APPARATUS and METHOD

5.1. Introduction

The apparatus and an overview of the method used for the experimental work involving practical oscillator and temperature compensation circuits presented in this thesis are described in this chapter. Under the heading of apparatus are included the instruments used for making measurements and performing the experiments and some software which is closely tied to the use of the instruments. This software forms an integral part of the experimental apparatus and was used many times with little or no modification. First, the aim of temperature compensation and the apparatus required to meet the aim are presented, then some of the apparatus is described in greater detail.

5.2. Description of the temperature compensation process

The purpose of the temperature compensation process is to customise a general compensation circuit to meet the requirements of the specific crystal resonator used for that particular temperature compensated crystal oscillator.

5.2.1. Method

The method used in this thesis is divided into three stages: characterisation, optimisation and verification.

Characterisation involves subjecting the TCXO to a number of discrete temperatures over the whole specified operating temperature range. At each temperature measurements are made on each of the subsystems. The measurements are: the output voltage of the voltage regulator, the correcting voltage needed to be applied to the varactor diode and the temperature as indicated by the temperature sensitive elements of the compensation circuit. In the software written to control the characterisation and verification stages the temperature increments are referred to as temperature steps. One of the conclusions described more fully in section 6.8 was that the optimisation program used to customise the compensation network needed the temperatures used for characterisation to be equally spaced to prevent undesirable weighting being introduced.

Optimisation uses the data gathered during characterisation to customise the compensation circuit to the requirements of the crystal oscillator. For a TCXO which has a compensation circuit comprising a network of resistors and thermistors the values of the resistors are determined. The term *optimisation* used here is specific to the method adopted during this research to determine the required resistor values in the resistive compensation networks. The more general term *customisation* gives a better description of what is being achieved at this stage. In the case of a TCXO comprising a digital compensation circuit the correction data is generated using techniques other than optimisation.

Verification ensures that the optimisation and the customising of the compensation circuit have been performed correctly by again subjecting the oscillator to temperatures over a specified temperature range. The temperature conditions used for the verification can be the same as those used for the characterisation or the conditions may be different. For the purpose of this research it was decided that the verification conditions should be different from those used for characterisation because it was considered that this would give a more general verification. This

form of verification is harder to achieve because it requires a greater level of thermal stability in the environmental chamber to ensure that all the components are at the same temperature.

In the early days of TCXO's the selection of the compensation components was an iterative one where the compensation circuit was assembled, temperature cycled and adjustments made to the circuit to improve the performance of the compensation until the frequency deviation was within the required levels. With the advent of the digital computer, alternative techniques have been employed. These have included solution of explicit mathematical expressions [1] or the use of an optimisation program. Both have resulted in the need for fewer temperature cycles.

5.2.2. Apparatus

The requirements of the apparatus and the pieces of apparatus used are specified in this section. The pieces of apparatus are:-

1. An environmental chamber which can provide a temperature range of -45°C to +90°C and which is continuously controllable over that range. During the course of the research the laboratory was relocated. Before the move the environmental chamber used carbon dioxide (CO_2) refrigeration. After the move the new laboratory did not have a supply of CO_2. An environmental chamber cooled by vapour compression refrigeration was purchased as a replacement.

2. A power supply that is able to meet the voltage, current and stability requirements of the oscillator(s) being compensated.

3. A frequency meter with accuracy and resolution of better than 0.01ppm. In the arrangement used for the research the accuracy was achieved by using a Rubidium frequency standard which was checked against a national frequency reference.

4. A digital multimeter (DMM) capable of measuring voltage and resistance with accuracy and resolution of about 0.1% of the reading. The DMM is used to measure the output of the voltage regulator and the thermistor resistance.

5. A precision voltage source (PVS) with a resolution of 1mV and a minimum range of 0 to 5 volts. The PVS is used to apply the required tuning voltage to the oscillator during characterisation.

6. A switch box which is used to select each device in turn for measurement by the DMM. When the new environmental chamber computer interface was designed the control electronics were incorporated and relays were mounted on the circuit board used to hold the oscillator in the chamber. The design of this new switch arrangement allowed up to 16 oscillators to be characterised or verified concurrently.

7. A computer to control the experiments and to process the gathered data in order to produce the custom compensation circuit. All the pieces of apparatus are under the control of the computer so that the experimental procedures are repeatable and, as they take a long time, can be performed without human supervision.

5.2.3. Apparatus configuration

In the previous section, the use of two types of environmental chamber and two switch box arrangements are mentioned. Despite these changes, the function of the apparatus remained consistent. In this section the arrangement of the apparatus as it was used for much of the experimental investigation is presented. The measurements that have to be made over the temperature range during the characterisation of a temperature compensated crystal oscillator (TCXO) which uses a resistive network to produce the compensation voltage are

(i) resistance of each thermistor

(ii) oscillator frequency

(iii) output of the voltage regulator (V_{ref})

(iv) required tuning voltage (see section (4.6.1))

All these measurements have to be made remotely because the environmental chamber must remain sealed throughout in order to maintain the thermal environment. A buffer amplifier is necessary because the frequency meter has a 50Ω input resistance which might otherwise affect the operation of the oscillator. The circuit used for the characterisation of the analogue TCXO's is shown in figure 5.1. The switches shown in figure 5.1 are the contacts of relays in the switch box.

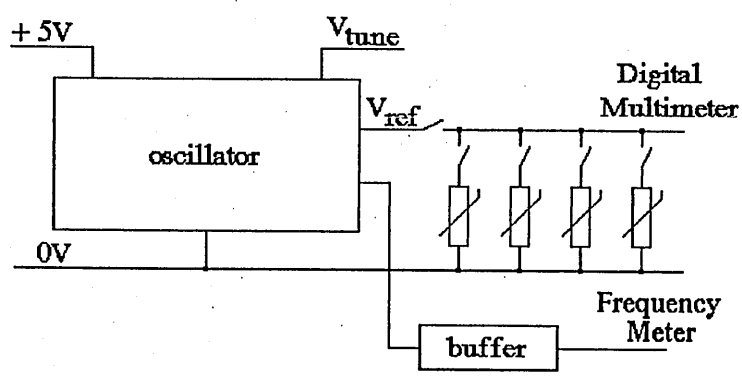

Figure 5.1. Oscillator characterisation circuit

In the first arrangement of the apparatus, shown in figure 5.2, the environmental chamber uses liquid carbon dioxide CO_2 refrigeration. Problems that were experienced using this environmental chamber are discussed in section 5.4. The switches used to select each device for measurement by the digital multimeter were in the commercial switch box external to the environmental chamber. Use of a switch box external to the environmental chamber means that many wires have to be brought out of the chamber. This is not a significant problem when only one oscillator is being characterised but with multiple oscillators it is a substantial problem. A better approach is to have the relays inside the chamber and steer the signals which close the contacts.

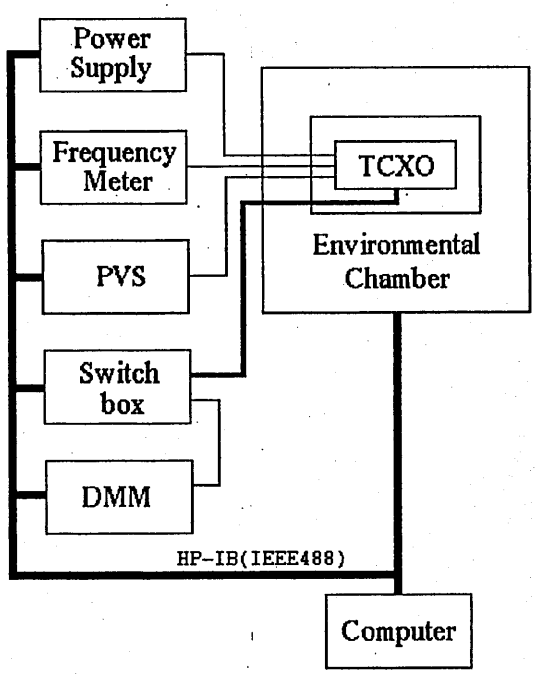

Figure 5.2. First arrangement of the apparatus.

In the second arrangement, of figure 5.3, the relays were mounted on a printed circuit board which also held the oscillators during characterisation and verification. These printed circuit boards, called daughter cards, were designed to hold multiple oscillators and the operation of these cards was controlled by the computer by means of the new environmental chamber interface.

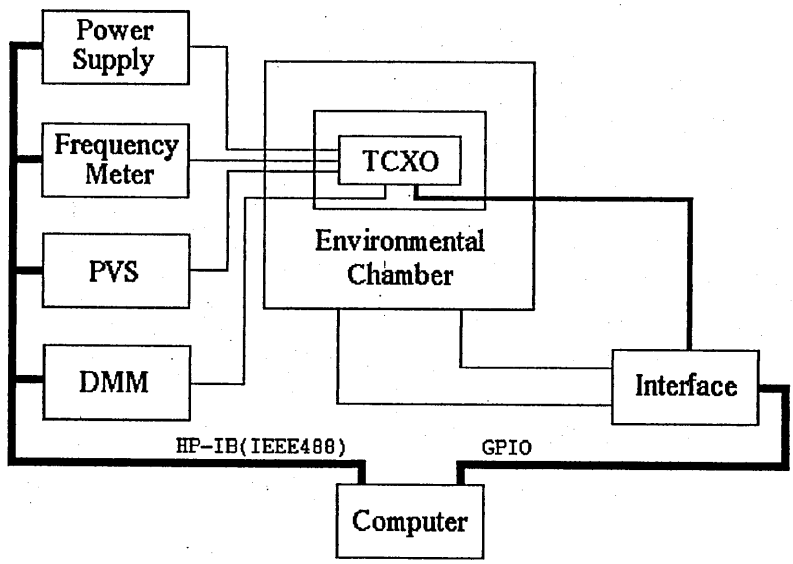

Figure 5.3. Second arrangement of the apparatus

A third configuration of the apparatus was adopted to perform the digital temperature compensation experiments, as in figure 5.4. The chamber control interface was not used for this work because it was considered that a higher level of resolution would be required in the control of the chamber. The PVS and the DMM were not needed in connection with the oscillator. The PVS was used to provide the reference voltage of required temperature and the DMM was used to measure the voltage provided by the chamber which represented the temperature within the chamber. The interface was designed for the digital compensation circuit.

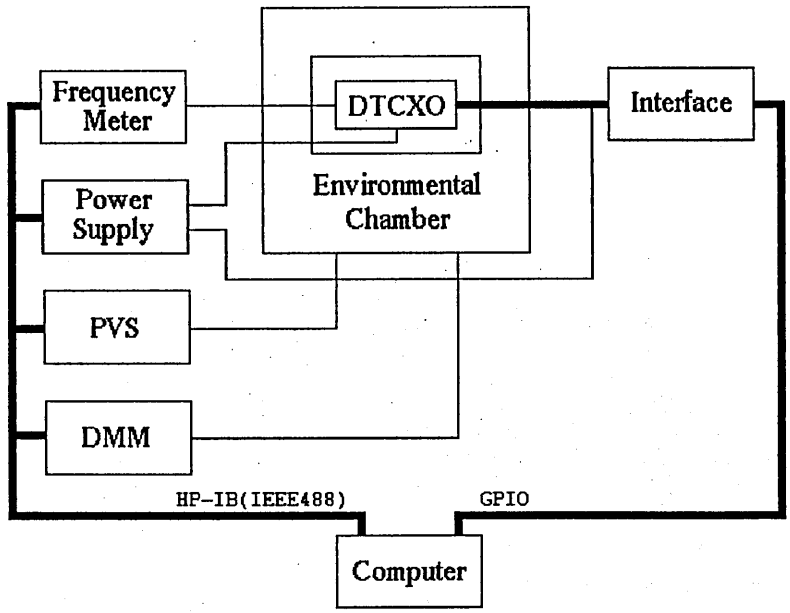

Figure 5.4. Third arrangement of the apparatus.

5.3. Operation of environmental chambers

During the course of the investigation two different types of environmental chambers have been used. The environmental chamber are used to provide and control the thermal environment that the oscillators have to be subjected to for characterisation and verification stages of making a temperature compensated crystal oscillator (TCXO). Temperature control within the environmental chamber is performed by two different mechanisms; one for heating and one for cooling. Air within the chamber is circulated by a fan which draws air over the control elements and reduces thermal gradients within the chamber. During the investigation two environmental chambers were used. Both used a resistive heating element to heat the chamber but one used liquid carbon dioxide (CO_2) vented to the atmosphere as the cooling agent, and the other used a vapour compression refrigerating system similar to that used in the domestic food freezer.

5.3.1. Carbon dioxide refrigeration

Carbon dioxide (CO_2) stored as a liquid under great pressure at room temperature is released into the environmental chamber. The liquid CO_2 rapidly vaporises, taking up latent heat of vaporisation due to the reduction in pressure. Hence the environmental chamber is cooled. The CO_2 gas is vented to the atmosphere and lost. When the store of CO_2 is exhausted it has to be replaced with a fresh supply of liquid CO_2.

5.3.2. Closed cycle cooling

In this system the liquid is vaporised in a vessel called a vaporiser instead of the vapour venting to the atmosphere as in the case of CO_2 cooling. The gas is collected from the vaporiser, then compressed and cooled to form a liquid again ready to pass back through the vaporiser. This means that the refrigerant is constantly being replenished instead of being exhausted so it does not have to be replaced.

5.4. Temperature regulation

Regulation of the temperature within the chamber is achieved using limit cycle control. The heater and the cooler can only be in one of two states, either on or off. If the heater, for example, is switched on the chamber temperature will rise until the rate of energy being supplied by the heater is equal to the rate at which energy being lost through the chamber walls. The rate that energy is being lost (the power loss) through the walls is proportional to the temperature difference across the wall, so the greater the difference between ambient temperature and the chamber temperature, the greater the power loss through the wall. If the heater is

repeatedly on for a short time and off for a short time then the average power being supplied is lower so the equilibrium temperature will be lower. Limit cycle control allows the temperature to wander about the required temperature within defined limits, say $\pm 0.5°C$. When the temperature drifts outside the range the appropriate correction, either heater or cooler, is applied.

5.5. Environmental chamber problems

When a steady temperature is being maintained within the environmental chamber CO_2 is released in short pulses. The longer the pulses, the greater the cooling effect. When a short pulse is released the latent heat of vaporisation for the CO_2 is supplied by the air in the chamber. As the air is circulated it comes into contact with the walls of the chamber and the item under test and heat energy is transferred to the cooler air hence a new equilibrium temperature is achieved. If the pulse of CO_2 is of the order of a second the temperature of the air within the chamber may fall by as much as 2°C and as the thermal time constants of the crystal and the thermistors are different the measurements may be made at effectively different temperatures so introducing errors into the system. This was the problem encountered with the CO_2 refrigerated environmental chamber initially used for the investigation. The temperature control system of the chamber would have had to be redesigned in order to reduce the pulse length. The method adopted to overcome the problems with this chamber was to make the measurements at each temperature five times and record the average, in order to reduce the effects of the CO_2. Events overtook the use of this chamber when the use of carbon dioxide for refrigeration was made impractical when the laboratory was relocated.

5.5.1. Thermal hysteresis in the second environmental chamber.

The experiments that will be described in section 6.8 indicated the presence of hysteresis within the environmental chamber. It was necessary to establish the cause and find possible remedies of the hysteresis in order to verify experimentally the theoretical temperature compensation research.

5.5.2. Method

A temperature cycle was devised comprising 6 equally spaced temperatures, stepped through in order from the highest temperature to the lowest and back to the highest as follows; 85, 60, 35, 10 -15, -40, -40, -15, 10, 35, 60, 85 °C. The environmental chamber remained at each temperature for one hour. A thermistor with nominal resistance 4.7kΩ at 25°C and 17 seconds thermal time constant, was mounted in free air in the middle of the environmental chamber. Resistance of the thermistor was measured at intervals of 10 seconds.

5.5.3. Results and discussion

The full set of data gathered is shown in figure 5.5 and two details are shown in figure 5.6. The fuzziness observed in these figures is due to the cycling of the temperature within the environmental chamber, explained in section 5.4, which means that the control mechanism of the environmental chamber has the impression that the chamber is at the correct temperature. The change of temperature in the form of a gradual drift with an exponential form observed suggests that there is a long thermal time constant somewhere in the control system of the environmental chamber. The cause of these effects was found to be the manner in which the temperature transducer, used by the control system to monitor

the temperature within the chamber, was mounted. The temperature transducer was a thermistor which was mounted on an aluminium plate so that the thermistor was in the air flow. However, when there was a change of temperature within the chamber the aluminium plate was slow to achieve the new temperature and the mounting of the transducer formed a good thermal path between the plate and the transducer, causing an error in the measured temperature within the chamber. It was decided that allowing 20 minutes between the controller going into limit cycle control and starting to take measurements was sufficient time for the system to stabilise to within 0.5°C for increasing and decreasing temperature.

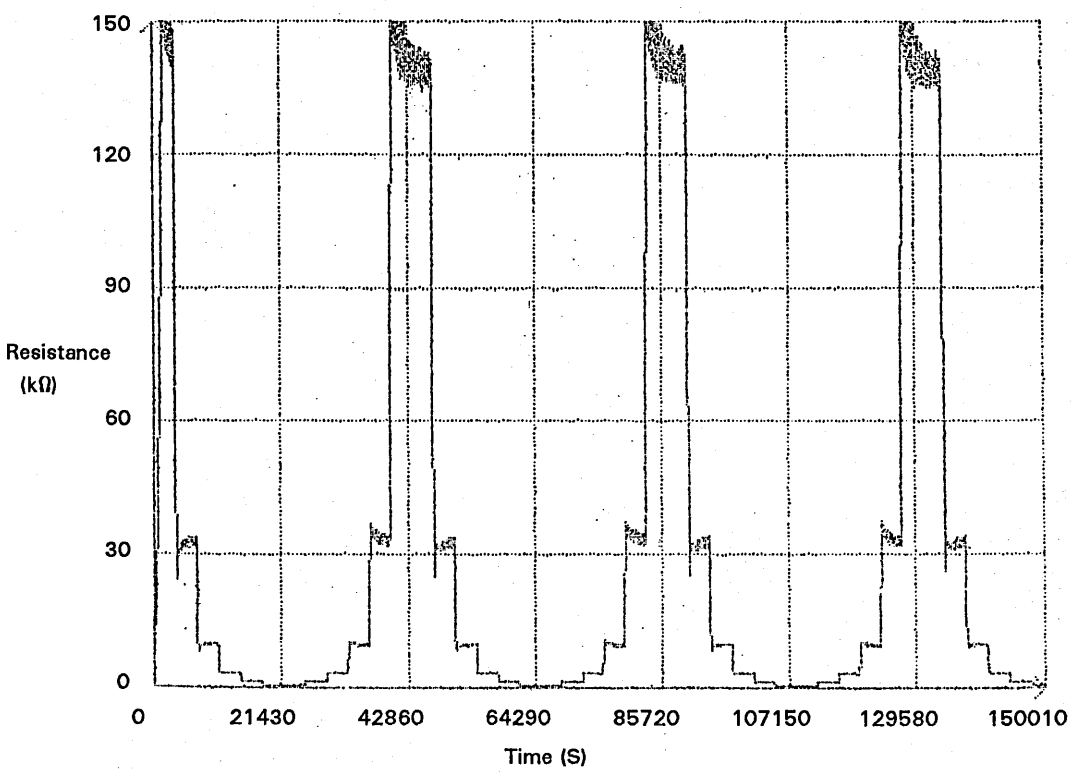

Figure 5.5. Thermistor resistance against time over 3½ temperature cycles.

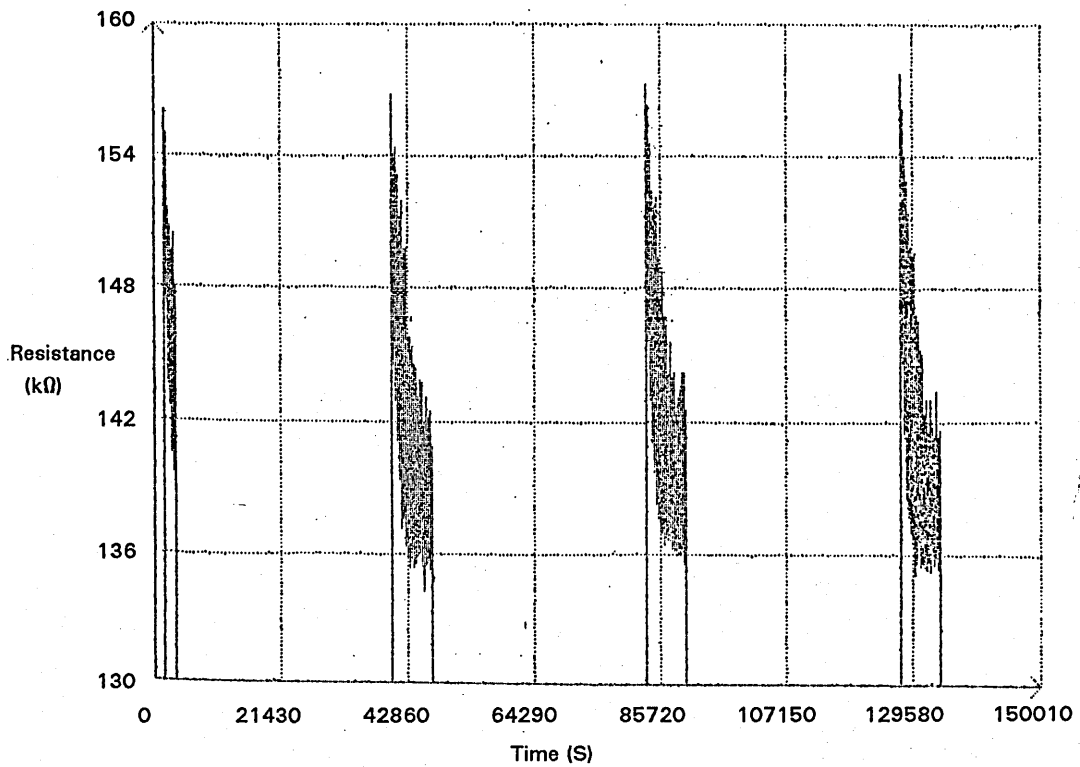

(a)

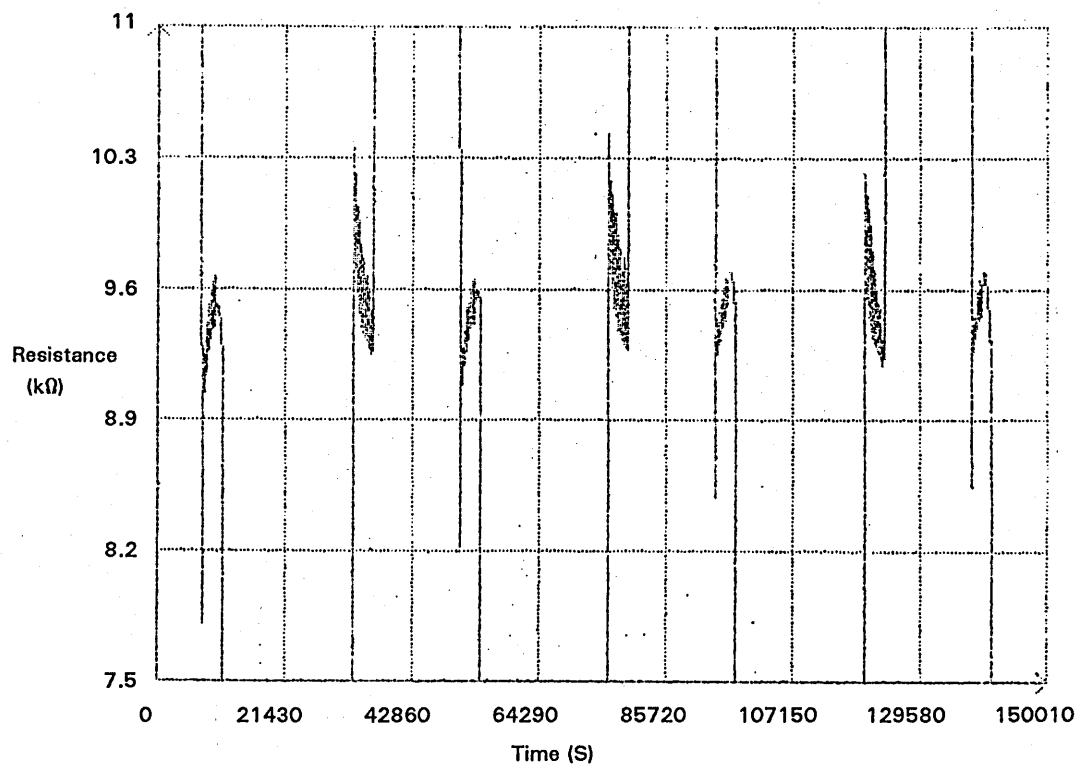

(b)

Figure 5.6. Details of thermistor resistance against temperature (a) -40°C, (b) 10°C.

5.5.4. Limit cycle effects

The limit cycle control of the environmental chamber was approximately $\pm 0.5°C$ of the required temperature. The thermal time constants of the thermistors and the crystal are different. However, the thermal time constants of both components are short enough for their values to be affected by the thermal cycling within the environmental chamber. Hence the temperature of each device could be different because the measurements of all the components of a temperature compensated crystal oscillator could not be made instantaneously with the apparatus available.

5.5.5. Method

A thermistor and a crystal oscillator were set up in the environmental chamber which had been at 85°C for many hours. The oscillator frequency and the thermistor resistance were measured at 10 second intervals. The thermistor used had a nominal resistance of 10kΩ and a thermal time constant of 1 second.

5.5.6. Results and discussion

The results shown in figure 5.7 show (a) oscillator frequency and (b) thermistor resistance and figure 5.8 shows the same data averaged over 10 measurements. Here, in comparison, the noise is significantly reduced. It was considered that the data gathered during characterisation would be improved if it were averaged in this way. The full range of the thermistor resistance in these figures corresponds to approximately 0.5°C.

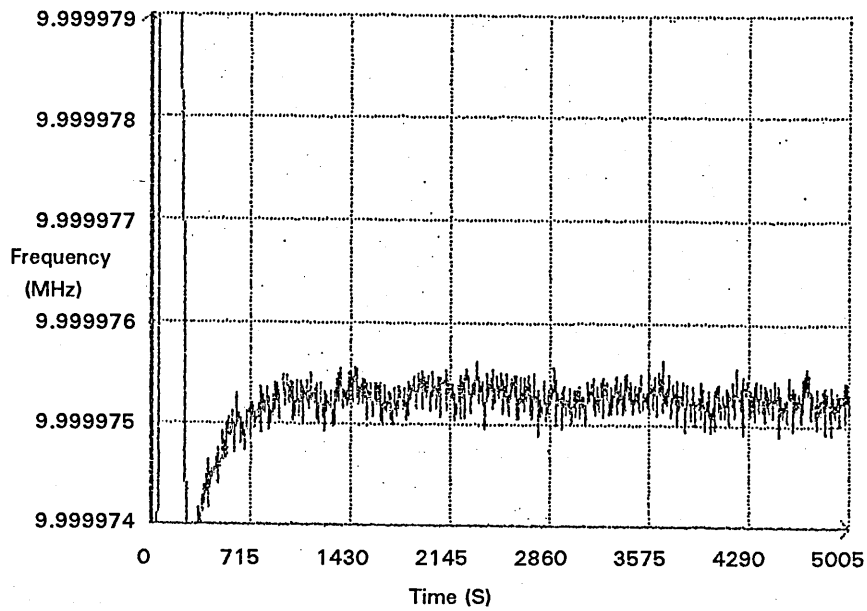

(a)

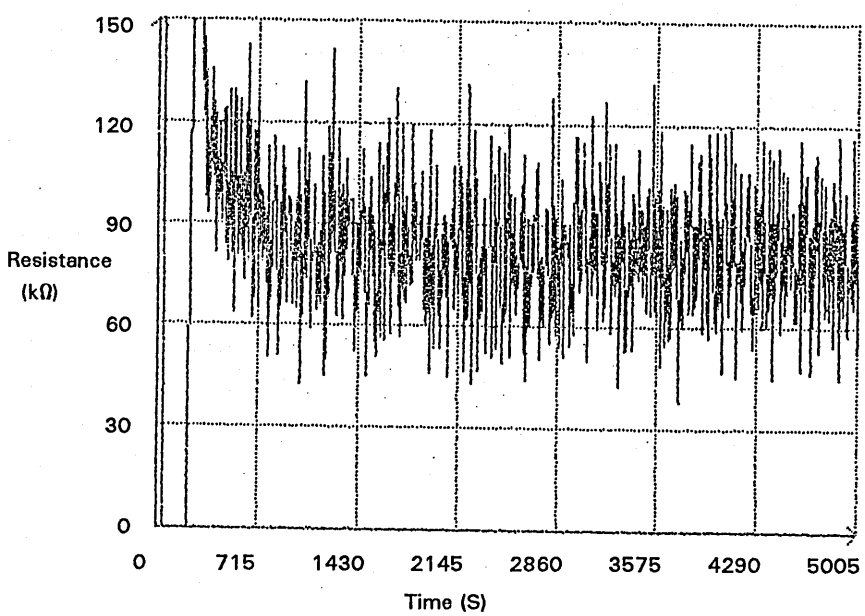

(b)

Figure 5.7. Raw data, (a) oscillator frequency and (b) thermistor resistance.

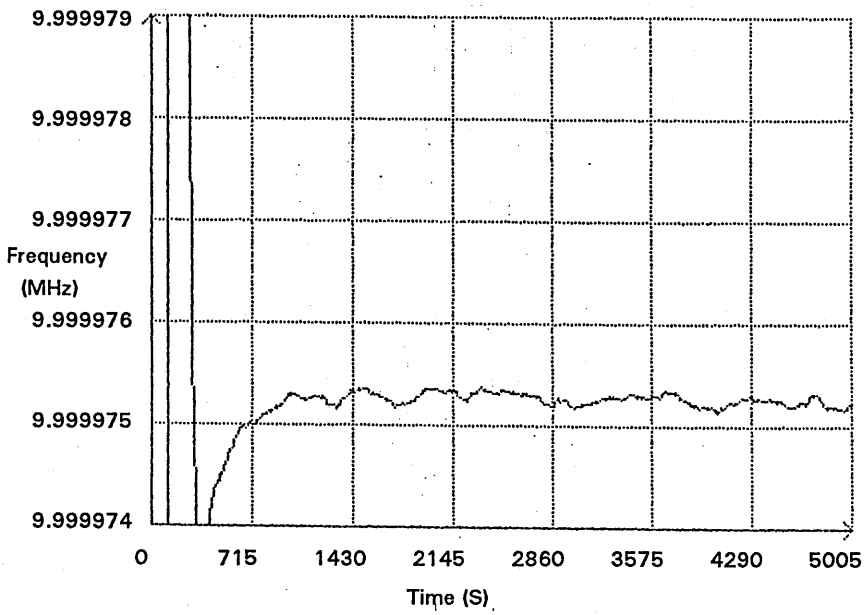

(a)

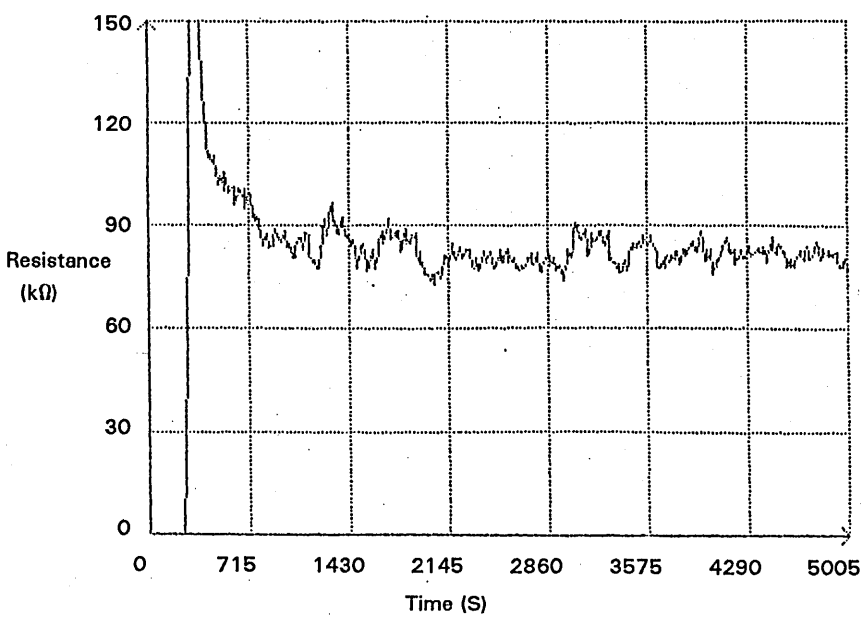

(b)

Figure 5.8. Data averaged over 10 measurements, (a) oscillator frequency and (b) thermistor resistance.

5.6. Characterisation and verification software

Experiments on oscillators which required making measurements over a range of temperatures were controlled by computer. Computer control enabled the experiments to be performed without human intervention. Hence experiments could run continuously and it ensured that the measurement cycles were repeatable. The software which controlled the characterisation was developed by an evolutionary process. Initally the measurements were printed out on paper as they were made and only a single oscillator could be temperature cycled at a time. In the final versions many oscillators could be temperature cycled and measurements, processed to reduce equipment difficulties, were stored on a floppy disc.

In principle, the processes of characterisation and verification are the same; the environmental chamber is set to an initial temperature and allowed to stablise, the appropriate measurements are made and the chamber is set to the next temperature in the cycle. This is repeated until measurements at all the required temperatures have been made, then the environmental chamber is set to room temperature, ready for retrieval of the oscillators. The difference between the two programs lies in the measurements; during characterisation the components of the compensation circuit are measured and the required compensating voltage is determined; during verification only the output frequency of the oscillator is measured.

5.6.1. Algorithm for tuning voltage

As part of the characterisation of an oscillator for temperature compensation, the required compensation voltage has to be determined. This cannot be measured directly but has to be found by an iterative method which is based on the knowledge of the tuning sensitivity of the oscillator and the frequency error for a

known tuning voltage. From this information the required tuning voltage is determined.

The sensitivity of the oscillator frequency to changes of the tuning voltage is determined by taking two frequency measurements at two different tuning voltages. Then the sensitivity is determined by:

$$P = \frac{(f_1 - f_2) \times 10^6}{(V_1 - V_2) \times f_r} \tag{5.1}$$

where P is the tuning sensitivity in ppm/V, f_1 and f_2 are the oscillator frequencies for tuning voltages V_1 and V_2 and f_r is the required oscillator frequency. The voltage needed to tune the oscillator to the required frequency is determined by measuring the frequency at a nominal voltage V_n and then calculating the required tuning voltage V_t:

$$V_t = \frac{(f_{V_n} - f_r) \times 10^6}{F_r \times P} + V_n \tag{5.2}$$

The new voltage V_t is used in the place of V_n and the process is repeated until the frequency error is below the required level. Ideally there should only need to be one iteration to find the required tuning voltage but in practice changing the tuning voltage changes the required tuning voltage and more iterations may be needed. Also temperature variations within the chamber will mean that two successive readings with the same tuning voltage may give a different frequency because the temperature has changed.

5.6.2. Device drivers

Each of the pieces of apparatus had an associated piece of software called a device driver. The device drivers communicated between the characterisation or verification software and each piece of apparatus, either to set up the apparatus or to make a measurement. The advantage of this approach was that the drivers were reusable so that the time taken to write a new program was reduced because the software required to communicate with the apparatus, which formed a major part of these programs, was already written and tested.

5.7. Optimisation

Optimisation is the process by which a system depending on a number of factors has the factors adjusted so that the system gives the best result. Usually in optimisation a function is maximised or minimised. Negotiation is a form of optimisation where each party has an initial point of view and then, through discussion and compromise, each changes their point of view until agreement is reached.

In figure 5.9 there are two functions; r(x) which is the required function and a(x) which is an attempt at matching r(x). If the number of independent variables is greater than unity, x is replaced by a n dimension vector where n is the number of independent variables.

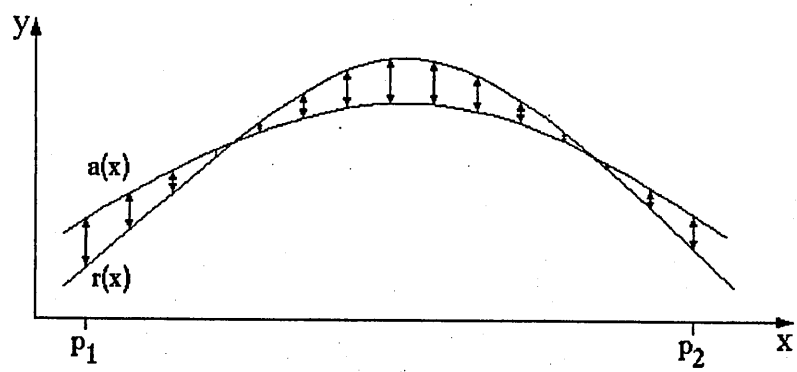

Figure 5.9. Two functions r(x) and a(x)

At a point p on the x axis the corresponding difference between the two functions r(p) - a(p) gives the error in a(x) at x=p.

Over a range $x=p_1$ to $x=p_2$ a number of error measurements are made. When their magnitudes are summed, a figure of error or merit for the fit can be obtained. This is expressed mathematically by:

$$\text{error} = \sum_{x_n=p_1}^{p_2} |r(x_n) - a(x_n)| \qquad (5.3)$$

The modulus of the difference is used in the summation to prevent the positive and negative differences cancelling each other.

An alternative to taking the magnitude is to use the square of the difference between the two functions at each point. The result is similar to taking the magnitude because the positive and negative errors do not cancel each other. The usefulness of raising the difference to a power greater than 1 is that the emphasis of the error function is changed so that as the power that each difference is raised to is increased so the error is more sensitive to the larger differences. The limit is

with very large powers which are equivalent to only considering the largest difference.

Weighting of the error function may be used to emphasize specific parts of the required function, where, for instance, a small error is required or conversely, where a close match may be less important. Inclusion of a weighting factor is represented mathematically by:

$$\text{error} = \sum_{x_n=p_1}^{p_2} |r(x_n) - a(x_n)| \times Wx_n \qquad (5.4)$$

where Wx_n is a weighting value required for the difference at $x = x_n$.

If the function a(x) is modified a new value for error will result. Using the same set of weights and the same power for the differences, the version of a(x) which gives the lowest value of error is the one that best matches the function r(x), the limit being when the error=0. Then the two functions are equal at the points of testing although they may not be equal for all x over the range p_1 to p_2 as shown in figure 5.10.

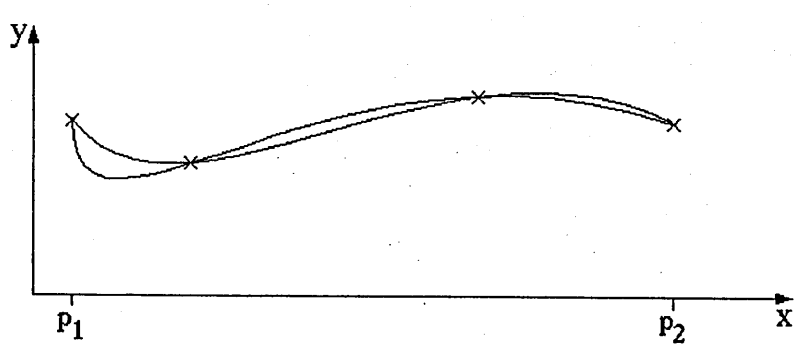

Figure 5.10. Two functions equal at the sampling points.

5.7.1. Hooke and Jeeves Optimisation

As many networks were to be tried it was important that it should be a simple matter to introduce a new network into the optimisation routine. The Hooke and Jeeves univariant search algorithm was chosen for this reason and because it forms a good introduction to optimisation techniques. A disadvantage with the Hooke and Jeeves algorithm is that convergence to a result can be slow compared with some alternative approaches. However, these other approaches require some preparation of the function to be optimised so were less convenient for the research being undertaken.

In general terms optimisation procedures fall into two categories; those that use the function to be optimised and those that use both the function and its derivatives. The Hooke and Jeeves optimisation process [2][3] uses only the function being optimised.

The function being optimised using Hooke and Jeeves optimisation is a mathematical function comprising one or more independent variables. It is based on knowing the value of the function at some starting vector in the space being searched. The function is then recalculated with one of the variables changed by a small amount and the two values of the function compared. The process has two operations; the exploratory move and the pattern move.

The exploratory move involves changing one of the independent variables by a small amount δi, by either increasing or decreasing its value. A new value for the function being optimised is calculated and compared with the current best value. If the new result is more favourable, the variable takes on the new value otherwise the variable is changed in the other direction and the comparison is made again. If the second result is not more favourable the variable is left with its original value.

When exploratory moves have been performed on all the independent variables which are included in the optimisation process the exploratory move operation is complete. If the position has changed as a result of the exploratory moves a pattern move will follow otherwise the previous pattern move has overshot and the search will return to the position which represents the current best result. If the search is at the position which gives the current best known result and the exploratory moves fail to find a more favourable result the optimisation process has converged to a result and so it terminates.

The pattern move works on the basis that the exploratory move has found a good direction so it takes a further step in that direction then another exploratory move is attempted. The position before the pattern move is made is the currently known best result and this is the position that the search will return to when a pattern move fails. If the exploratory moves after the first pattern move result in a further reduction in the value of the function then the direction of the second exploratory move is added to the first hence the pattern move grows in length and direction as the search progresses. If the exploratory move after a pattern move fails to reduce the value of the function the pattern move has failed so the search returns to the currently known best result and a new pattern move is started.

After each successful set of exploratory moves the direction and magnitude of the δi of a variable is added to a running total for that variable and the pattern move results from adding the running total onto the last successful vector.

An example based on Fidler [3] is given here to illustrate Hooke and Jeeves optimisation.

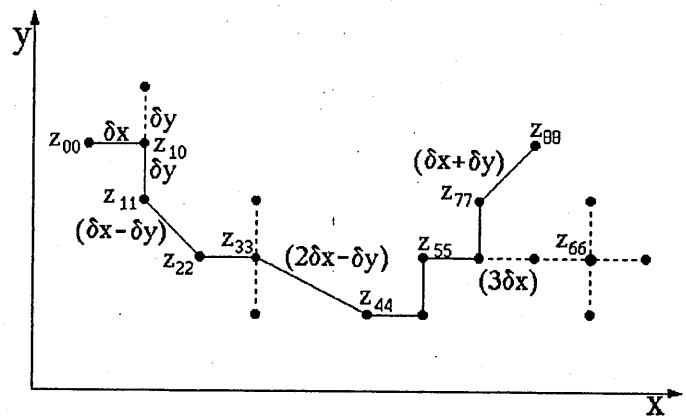

Figure 5.11. Exploratory and pattern moves of Hooke and Jeeves optimisation

Consider a function in a three dimensional space

$$z=f(x,y) \tag{5.5}$$

The intention is to find the values of x and y when z is at its minimum value. The actions in the xy plane which are described in this section are shown in figure 5.11.

At an arbitrary starting vector

$$x=x_0 \text{ and } y=y_0,\ z_{00}=f(x_0,y_0).$$

A small value δx is added to x_0 to give a new result

$$z_{00}+x = f(x_0+\delta x,y_0)$$

$z_{00}+x < z_{00}$ so x_1 is given the value $x_0+\delta x$.

A small value δy is added to y_0 to give a new result

$$z_{10}{}^{+}y = f(x_1, y_0+\delta y)$$

$z_{10}{}^{+}y > z_{10}$ so try $y_0-\delta y$.

$$z_{10}{}^{-}y = f(x_1, y_0-\delta y)$$

$z_{10}{}^{-}y < z_{10}$ so y_1 is given the value $y_0-\delta y$.

Now that the exploratory moves are complete and a lower value for z has been found a pattern move is performed which takes x to x_2 and y to y_2 so

$$z_{22} = f(x_2, y_2).$$

At this position a better value for z is found for x at $x_2+\delta x$ which becomes x_3, but the exploratory moves for y both fail to improve on the value for z so y is left unchanged and $y_2=y_3$.

At position z_{66} both variables fail to improve the value of z so the pattern move has failed. The optimisation now makes a fresh start at position z_{55} and the running total of the pattern move is reset back to zero for all of the variables. If at this position the exploratory moves fail to improve on the value of z the optimisation has found a minimum position otherwise the process continues as before.

5.7.2. Modifications to the optimisation program

During the search for a new network it was found either necessary or beneficial to make modifications to the program. The two main reasons for introducing the

changes were the time taken to converge to a solution and limiting the results to realistic component values for the thermistors.

Squared variables were adopted [4] when it was found that the optimisation process gave negative values for some of the resistances when the program was initially being tested. This transformation was used throughout the research in order to prevent negative values of resistance being returned.

Fixed variables were intended to increase the speed of convergence of the optimisation program by reducing the number of variables that were included in the process. Fixed variables were also used at one time to find a good starting vector, see section 6.7.

Sine limiting function was introduced to the error function to limit the range of the B value for each thermistor model in the network after a network was found that gave the required level of frequency deviation when the B value of one of the thermistors was outside the practical limits of available thermistors. The limit was achieved by (5.6).

$$B = \text{mean} + \text{peak} \times \sin(x) \tag{5.6}$$

Where mean was the middle of the range of the allowable values of B, peak was half of the range of the allowable values of B and x was the variable that was varied as part of the optimisation process, see section 6.7.

Changing the δi value was an attempt to increase the speed of convergence of the optimisation process without loosing resolution. The first program used a single δi value that applied to all the variables that were included in the optimisation process. However it was quickly found that the range of magnitudes of the

variables meant either some variables were smaller than δi or δi was so small compared to other variables that the time taken to find a minimum was many times longer. First each variable was given its own δi for the exploratory moves. Later the magnitude of each δi was made to reflect the success of the pattern moves. This was achieved by multiplying each δi by a preset factor greater than 1.0 after a number of consecutive pattern move successes and multiplying by a factor less than 1.0 after each pattern move failure. The δi values were decreased until a limit was reached then the optimisation was deemed to have finished. This was mainly used during stage 2 in section 6.7.7 and section 6.7.10.

5.8. Discussion

The Hooke and Jeeves software was used extensively during the research to find a new temperature compensation network as described in the following chapter. The software was found to be slow at the time, and sometimes a run could take many hours. It is likely that the same software will take less time on the faster computers that are now available. However, now that new networks have been identified it might be appropriate to consider alternative optimisation algorithms.

5.9. References

[1] Sarkar, S. K. (1974). Explicit expressions for TCXO design. *Proc 28th Annu. Freq. Control Symp.*, pp. 232-236.

[2] Hooke, R. and Jeeves, T. A. (1960). "Direct search" solution of numberical and statistical problems. pp. 212-229.

[3] Fidler, J. K.. Introduction to optimisation in electronics and communications. Mathematical Topics in Telecommunications, vol 1: Optimisation Methods in Electronics and Communications, chapter 6.

[4] Fidler, J. K. Private communication.

6. RESISTIVE NETWORK TEMPERATURE COMPENSATION

6.1. Introduction

Temperature compensation for crystal oscillators is usually achieved by applying an appropriate voltage to a varactor diode to offset the small, temperature induced, frequency deviations of a crystal resonator. Resistive networks, comprising resistors and thermistors, were the first means used to produce the required tuning characteristic for compensation. This type of compensation still finds widespread application. However, alternative analogue circuits and digital techniques used to generate the compensation voltage have surpassed the level of stability that resistive networks have achieved. The objective of the research was to identify new resistive networks capable of providing higher frequency stability using a relatively low supply voltage. In this chapter, first an investigation to determine compensation levels achievable by a distinct commercial compensation network is described then a description of the research which resulted in the identification of the new resistive compensation circuit is presented.

6.2. Initial experimental work

The initial experimental work formed an introduction to the practical aspects of temperature compensating crystal oscillators. The intention was to determine whether the compensation network used by Cathodeon Crystals in their manufacture of commercial temperature compensated crystal oscillators (TCXO's) was capable of achieving the stability level given in table 6.1. Over this temperature range the compensation network was used to compensate oscillators to

a frequency stability of ±3ppm. Table 6.1 also shows the power supply requirements that were loosely applied to the investigation.

Table 6.1
Oscillator stability goal

Temperature range	-40°C to +85°C
Frequency stability	< ±0.5ppm
Supply voltage	5volts ±10%
Supply current	1.5mA

This temperature range and frequency stability level were chosen because they were representative of the level of stability being claimed for other analogue compensation techniques [1][2]. The supply voltage was chosen to reflect the widespread use of transistor logic (TTL) devices which means that it is increasingly rare to find a new electronic system which does not have this voltage supply available. The supply current reflects the battery operated applications that this type of oscillator is often used in.

The temperature compensation network being investigated here was distinct compared with published literature. This network used a positive temperature coefficient (PTC) thermistor as the temperature sensitive element to compensate over the high temperature part of the characteristic, whereas it is usual to find only negative temperature coefficient (NTC) thermistors used. The high temperature part of the characteristic refers to the region between the high temperature turning point and the highest temperature of the characteristic. The compensation network circuit diagram is shown in figure 6.1.

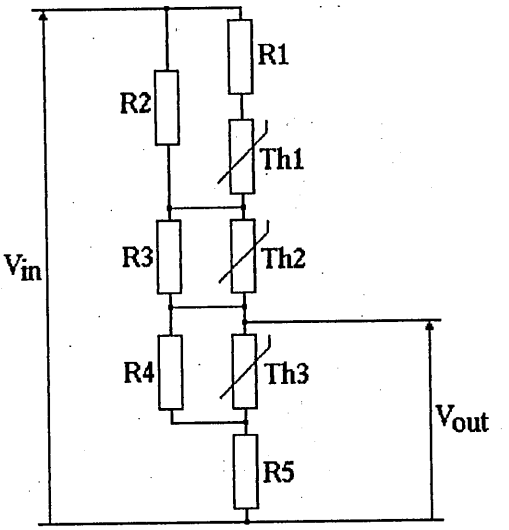

Figure 6.1. The compensation network with PTC thermistor (Th2)

The type of PTC thermistor used in this compensation network is effectively a temperature sensitive switch with a temperature threshold. Below the threshold temperature the PTC thermistor has a resistance of the order of 100Ω and is relatively insensitive to temperature change. However, above that temperature its resistance rapidly increases as its temperature increases. See figure 6.2 to compare the characteristics of the PTC thermistor with the more usual negative temperature coefficient (NTC) thermistor.

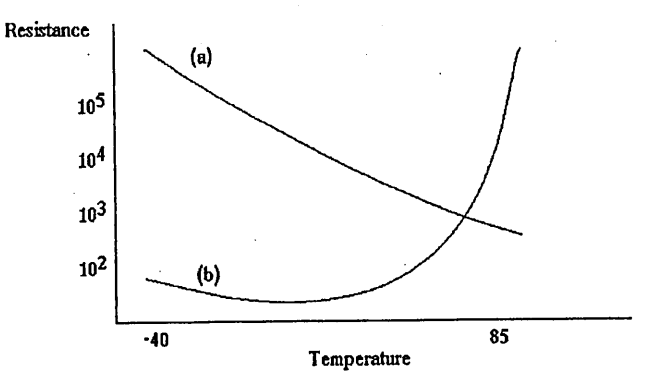

Figure 6.2. Comparison of thermistor characteristics (a) NTC (b) PTC

The lattice orientation angle of the crystal resonator used in the oscillator was chosen so that the switching temperature of the PTC thermistor corresponds with the high temperature turning point in the crystal frequency deviation against temperature characteristic.

6.3. Experiment

The apparatus used for this experimental work was described in section 5.2 and the oscillator circuit was described in section 4.6. In order to simplify the connections within the equipment, thermistors were placed in sockets external to the oscillator for characterisation, then soldered onto the circuit board after this stage was complete. This was the method used by the company for commercial oscillators. The measurements made on the components during characterisation are shown in table 6.2.

Table 6.2
Data gathered during characterisation.

Temperature (°C)	V_{ref} (V)	Therm1 (kΩ)	Therm2 (kΩ)	Therm3 (kΩ)	V_{tune} (V)
84.8	4.034	5.322	36.08	.558	2.187
74.6	4.037	7.676	8.325	.802	2.319
65.0	4.039	9.900	2.878	1.034	2.338
54.8	4.041	15.13	.579	1.550	2.256
44.7	4.043	22.16	.223	2.248	2.115
34.8	4.045	32.17	.154	3.248	1.937
25.0	4.046	47.03	.128	4.700	1.748
14.9	4.047	70.45	.117	7.029	1.573
4.9	4.048	108.3	.113	10.81	1.435
-15.0	4.048	275.2	.115	27.36	1.346
-25.0	4.050	461.5	.126	45.42	1.437
-35.0	4.049	755.6	.141	76.91	1.627
-40.0	4.048	1009.	.150	102.7	1.780

The optimising program was allowed to run to its limit to achieve better results than were usually achieved. The practice within the production procedure was to have a maximum error level so that when the optimisation gave a predicted error below that level the optimisation terminated. This procedure reduces the time taken to optimise a batch of oscillators.

Improvements over the production oscillators were:-

1. improved voltage reference
2. improved quality of characterisation measurements achieved by averaging
3. limits removed from optimisation program.

The resistor values selected by the optimisation program are shown in table 6.3 and the predicted error and verification error are plotted in figure 6.3.

Table 6.3
Resistors selected by the optimisation of characterisation data.

	Required value (kΩ)
R1	11.8
R2	187
R3	13.3
R4	1020
R5	29.4

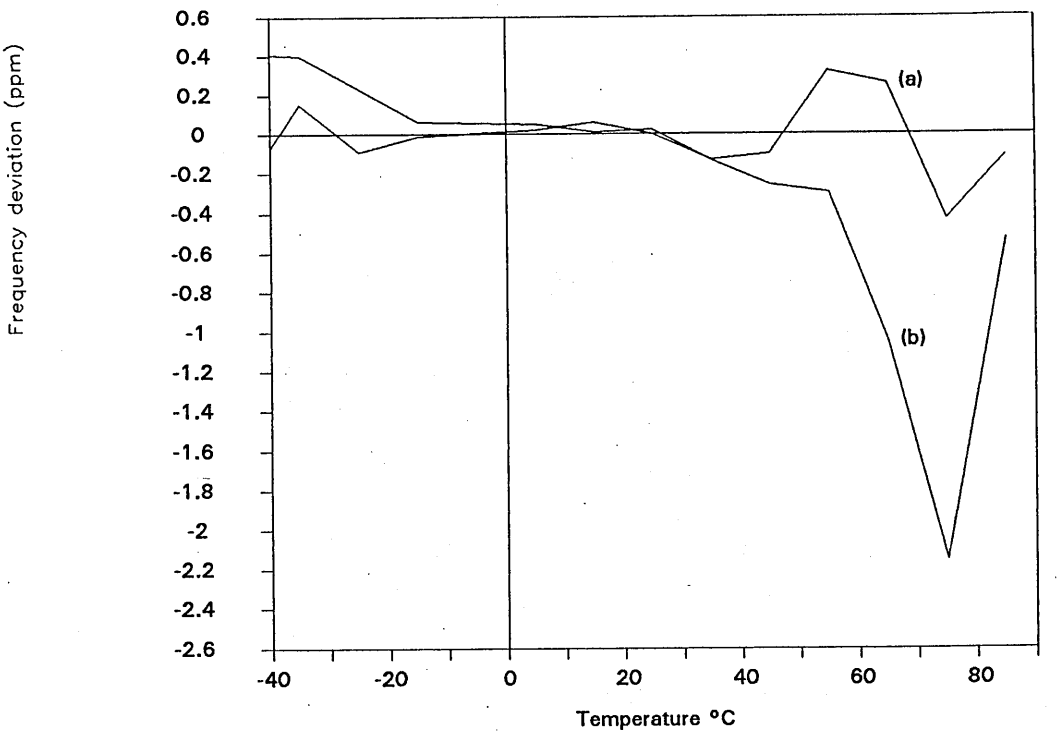

Figure 6.3. Comparison of predicted and measured verification data. (a) optimisation, (b) verification

The results show that there is a problem in the higher temperature range which is the part of the temperature range compensated by the PTC thermistor. The region covered by the NTC thermistors matched very well the predicted results. The discrepancy at the lower temperatures was caused by the rapid changes in the chamber temperature as described in section 5.4. The conclusion drawn about the discrepancy at the higher temperatures was that the characteristic of the PTC thermistor had changed between characterisation and verification.

6.4. Experiment to test stability of the PTC thermistor

Following the results obtained in the first experiment, it was necessary to determine whether soldering the PTC thermistor changed its characteristic. To this end, an experiment which simulated soldering the PTC devices into the circuit was carried out on four thermistors.

6.4.1. Method

The experiment was performed at room temperature which was monitored throughout using a digital thermometer. The resistance of the thermistors being tested was measured and recorded. A soldering iron was applied to one lead for 2 seconds and then removed for 1 second. Then the soldering iron was applied to the other lead for 2 seconds. On each contact of the soldering iron with a thermistor lead, the tip of the soldering iron was placed approximately 5mm from the body of the thermistor. When the thermistor had stabilised to room temperature, after the simulated soldering operation, its resistance was again measured. This procedure was repeated several times on each thermistor.

6.4.2. Conclusion on soldering the PTC thermistor

The results obtained in this experiment showed that a change occurred within the PTC thermistors when they were soldered, as shown in figure 6.4.

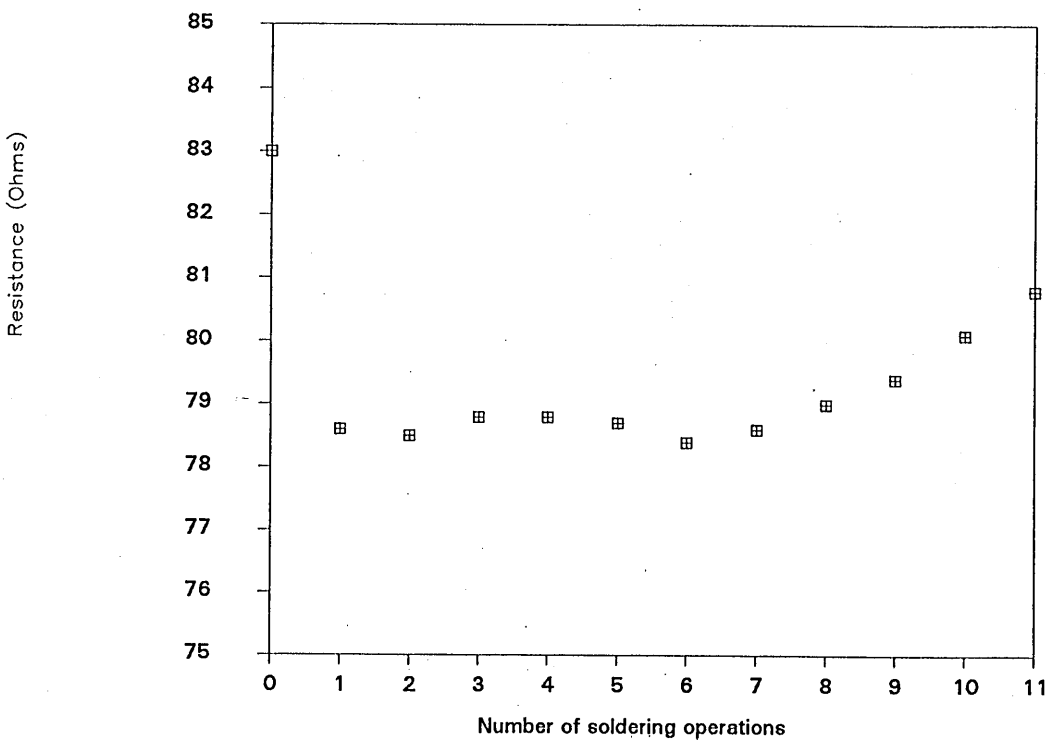

Figure 6.4. Typical changes in room temperature resistance of the PTC thermistors.

The cause of the change within the component was brought about by the ingression of atmospheric gases. However, this was not a problem for the thermistor's intended application which was over-temperature protection of electrical equipment [3].

6.5. Conclusion on the mixed thermistor network

The distinctive network for temperature compensated crystal oscillators is shown to be capable of compensating crystal oscillators to below ± 0.5 ppm over the temperature range -40°C to +85°C. However, the component which makes the network distinctive, the positive temperature coefficient thermistor, is unstable and has to be considered unsuitable for high stability analogue temperature compensation.

Negative temperature coefficient thermistors are manufactured using an alternative technology [4] and have greater stable with both time and temperature so a new network is needed based on these devices. However, it is networks that use only NTC thermistors which have fallen behind the alternative methods of compensation so a new network was needed. The investigation undertaken to identify a new network is described in the remainder of this chapter.

As a result of my investigations the manufacturing process of temperature compensated crystal oscillators within Cathodeon Crystals was changed to soldering the thermistors into the circuit-boards before characterisation, with a corresponding improvement in yield.

6.6. New temperature compensation circuit

In the remainder of this chapter the research to find a new temperature compensation network using only negative temperature coefficient (NTC) thermistors as the temperature sensitive elements is presented.

6.6.1. Aim

The aim of the investigation was to find a new network comprising resistors and negative temperature coefficient (NTC) thermistors that would compensate a crystal oscillator to $< \pm 0.5$ppm over the temperature range -40°C to +85°C. The approach was to build a model of a network using $Ae^{\frac{B}{T}}$ to represent the thermistors and to use optimisation to determine the component values. Once a network was identified, the nearest commercial thermistors were to be selected and the optimiser run to determine whether a network built from the practical thermistors was still capable of achieving the compensation levels. Once this was confirmed, a real oscillator would be tested.

6.6.2. Method

The frequency deviation against temperature for an AT cut crystal resonator is described by a cubic polynomial:

$$\frac{\Delta f}{f} = a(T - T_0) + b(T - T_0)^2 + c(T - T_0)^3 \qquad (6.1)$$

The requirement of the compensation network is to produce the inverse characteristic to offset these deviations. Using a varactor diode to tune the crystal frequency, the required compensation voltage is also taken to be cubic in

appearance, although in section 6.7 it is shown that this does not allow exact compensation. However, at this stage of the investigation the general form of the required compensation voltage against temperature was regarded as a cubic function.

The negative temperature coefficient (NTC) thermistors that were used for this investigation were taken to have a resistance against temperature characteristic which is an exponential function given by

$$R=Ae^{\frac{B}{T}} \qquad (6.2)$$

A compensation circuit has to transform a constant voltage to the required temperature dependent compensation voltage. Alternatively, a compensation circuit comprising resistors and thermistors is a resistive circuit which has a temperature sensitive transfer function.

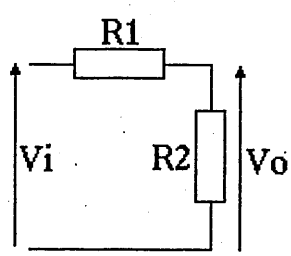

Figure 6.5. Potential divider

The voltage transfer function of the potential divider circuit is

$$\frac{V_o}{V_i}=\frac{R_2}{R_1+R_2} \qquad (6.3)$$

A NTC thermistor in the position of R_1 gives a voltage which increases with temperature and a NTC thermistor in the position of R_2 gives a voltage which decreases with temperature. The required compensation characteristic has a cubic characteristic which can be regarded as having three sections each identified by the sign of the gradient. With rising temperature the first section has a negative gradient, the second section has a positive gradient and the third section has a negative gradient, as shown in figure 6.6.

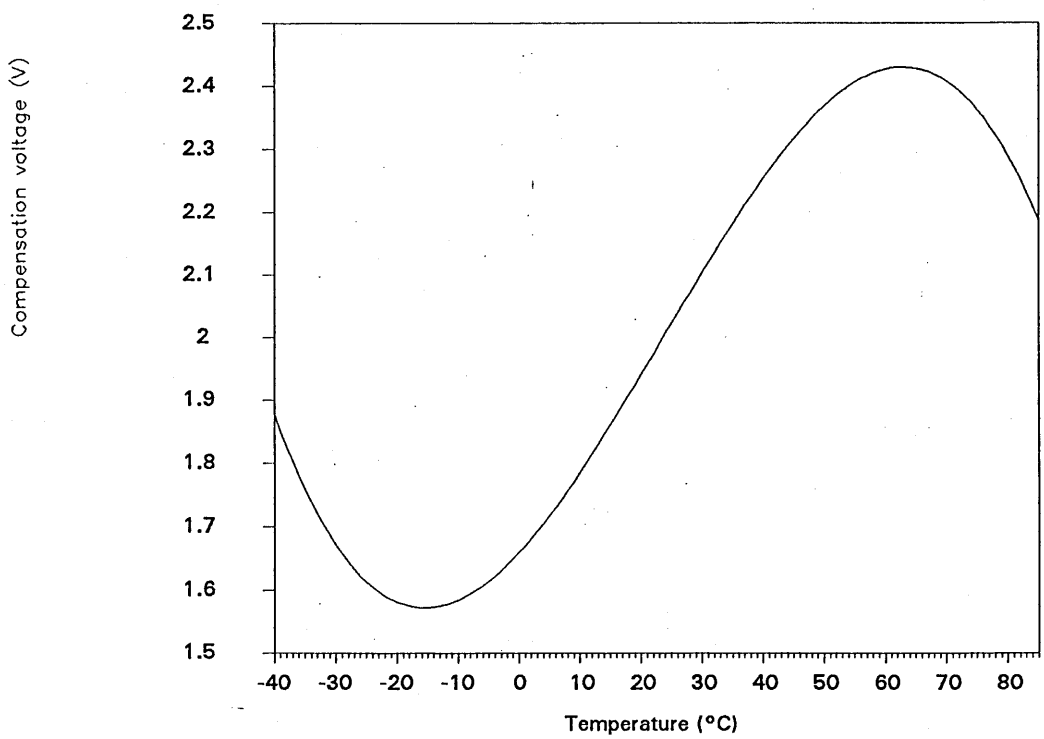

Figure 6.6. General form of the compensation voltage.

A single thermistor in a potential divider circuit can only have a single gradient, either positive or negative, whereas the required characteristic effectively has three gradients. Hence a network comprising three potential dividers, each with a single thermistor would appear to be required [5]. This was the basis of the first network investigated using the Hooke and Jeeves optimisation program.

The method was to build the network into the optimisation program by determining the transfer function of the network, to choose a starting vector and to let the optimiser search for an optimum position from that vector. The transfer function was used as the optimised parameter because when the optimiser is working on real data it is given the output of the voltage regulator and the required compensation voltage, the network has to have a transfer function that is equal to the compensation voltage divided by the regulator voltage.

6.7.3. Network number 1

The first circuit to be investigated, comprises three cascaded potential dividers as illustrated in figure 6.7.

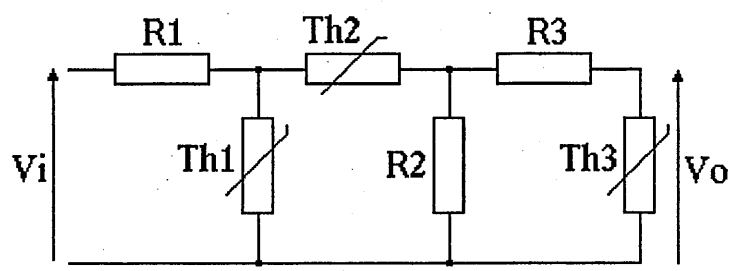

Figure 6.7. The first network.

The transfer function of this circuit is

$$\frac{R2Th1Th3}{\left[\begin{array}{c} R2Th1Th3+R1R2Th3+Th1Th2Th3+R1Th2Th3+R1Th1Th3+Th1R2R3 \\ +R1R2R3+Th1Th2R3+R1Th2R3+R1Th1R3 \\ +Th1Th2R2+R1Th2R2+R1Th1R2 \end{array}\right]} \qquad (6.4)$$

Where $Th1 = A_1 e^{\frac{B_1}{T}}$, $Th2 = A_2 e^{\frac{B_2}{T}}$, and $Th3 = A_3 e^{\frac{B_3}{T}}$.

A simple gain against temperature characteristic for the network to match was devised as in table 6.4. This characteristic reflected the required form of the general compensation characteristic.

Table 6.4
Simple characteristic used at the start of the investigation

Temperature (K)	Transfer function
300	0.50
320	0.45
340	0.50
360	0.55
380	0.50

There was no restriction placed on the way the network behaved between the coordinates of the devised characteristic. It was intended to do this by introducing further points to the devised characteristic once the optimisation process had established that the circuit was able to produce a characteristic that passed through these initial data points.

6.7.4. Results and discussion for network number 1

A typical set of results obtained for this circuit during the optimisation process is shown in table 6.5.

Table 6.5.
Typical results obtained for the first network.
(a) transfer function, (b) component values

(a)

Temperature (K)	Transfer function
300	0.474
320	0.504
340	0.517
360	0.517
380	0.506

(b)

Component	Initial vector	Final vector
R1	100Ω	110000Ω
A1	100Ω	1000Ω
B1	2000K	2200K
A2	10000Ω	2500Ω
B2	2000K	1400K
R2	100Ω	380000Ω
R3	1000Ω	$3.44\times10^{17}\Omega$
A3	10000Ω	111Ω
B3	10000K	15550KΩ

This circuit appears to be unable to achieve the required gain characteristic. The network has formed a maximum turning point. However, from a wide range of starting vectors the network did not achieve two turning points.

Possible reasons for this are considered to be

(i) the optimisation was starting from unfavourable initial vectors which were resulting in the process falling into local minima

(ii) the network is unable to provide the required characteristic.

Considering the operation of the network, the initial assumption about its behaviour depends on each thermistor controlling the transfer function of the circuit over part of the temperature range. Instead, in this circuit the thermistors have the potential of being active over the whole temperature range. Hence reason (ii) would appear to offer the better explanation for this circuit not being able to

produce the required cubic form. The conclusion was drawn that the circuit was based on an over simplification of how a potential divider circuit would meet the requirements of the compensation characteristic. Subsequent theoretical work presented in chapter 7 confirms this conclusion. The transfer function of this network does not have sufficient terms in the numerator to be able to produce the cubic form. In chapter 7 it is shown that a third order function is required in both the numerator and denominator whereas in the transfer function of the circuit here (6.4) there is only a single term in the numerator.

6.7.5. Network number 2

The starting requirements of the basic network were extended to include restrictions on the temperature range over which each thermistor governed the gain of the circuit. The thermistor which governs the gain over the low part of the temperature range must not operate above the minimum turning point. The thermistor which governs the gain over the mid temperature range must not operate outside of the temperature range bounded by the two turning points. The thermistor which governs the gain over the high part of the temperature range must not operate for temperatures below the maximum turning point. A detailed discussion on modifying the thermistor characteristics is presented in section 7.4 and only an outline is given here. The resistance of a thermistor decreases with temperature quite rapidly. Hence, an upper temperature limit is achieved by connecting a fixed resistor in series with a thermistor and a lower temperature limit is achieved by connecting a fixed resistor in parallel with a thermistor.

Developing these new assumptions the circuit modelled in the optimisation program was modified to that shown in figure 6.8.

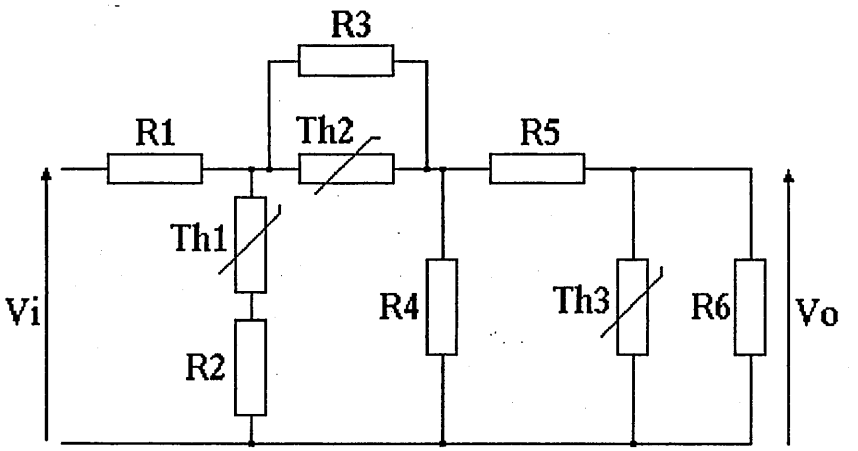

Figure 6.8. Modified circuit of the compensation circuit.

In the modified circuit, R2 sets the upper temperature limit for Th1, R3 sets the lower limit for Th2, the combination of R1 and R5 set the upper limit for Th2 and R6 sets the lower limit For Th3.

In an attempt to address problem (i) mentioned in the discussion of network 1, an attempt was made to find a good starting vector. The basic circuit of figure 6.9 comprising six fixed resistors was used in the optimisation program.

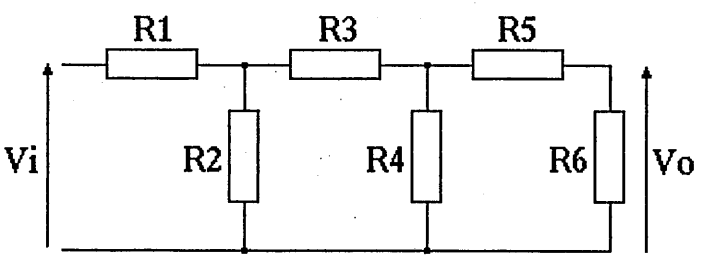

Figure 6.9. Circuit used to find a good starting vector.

First the required transfer function was set to 0.5 and a variety of optimisations was performed. From these a suitable result was chosen. This result gave all the resistances in the network values which contributed to the gain, shown in table 6.6.

Table 6.6
Resistance values used to give a transfer function of 0.5.

Resistor	Initial vector (Ω)	Final vector (Ω)
R1	100	992
R2	10000	6320
R3	100	900
R4	10000	6400
R5	100	900
R6	10000	6400

Next the facility within the program of removing variables from the optimisation process was used, see section 5.7. Only one of the thermistors was left free and the gain appropriate for where it finished governing the activity of the network was set as the required gain. In the first instance R2 was left free and the required gain was set to 0.45 which gave R2 a new value of 3190. When the procedure was performed for R3 and R6, a value of 0 was returned for R3 when the network had to give a value of 0.55, and a value of 4500 was returned for R6 when the network had to give the final gain of 0.5. The actual value the network gave with R3=0 was 0.54, however it was considered that this was close enough to start the optimisation program. Having obtained these values which described the required range of the components, values for the B component of each thermistor model were chosen based on practical values and appropriate values for each A component and R2, R3 and R6 were calculated and these are given in the initial vector of table 6.8(b).

The actual characteristic that these starting values gave is shown in table 6.7

Table 6.7.
Gain characteristic given by the initial vector

Temperature (K)	Gain
300	0.506
320	0.492
340	0.483
360	0.479
380	0.478

6.7.6. Results and discussion for network number 2

A sample of the results is given in table 6.8.

Table 6.8.
Typical results obtained for the second network
(a) gain characteristic, (b) component values

(a)

Temperature (K)	Gain
300	0.500
320	0.498
340	0.500
360	0.502
380	0.500

(b)

Component	Initial vector	Final vector
R1	992Ω	992Ω
R2	3025Ω	3025Ω
A1	0.152Ω	0.152Ω
B1	3000K	2580K
R3	1000Ω	1000Ω
A2	0.16Ω	0.16Ω
B2	3500K	1400K
R4	6400Ω	8100Ω
R5	900Ω	900Ω
R6	7000Ω	7000Ω
A3	1.25Ω	1.25Ω
B3	4000K	3790K

The first sets of results were encouraging. The first result from the optimisation process using this network gave a transfer function that had two turning points. Hence the transfer function had the correct form. However, the peak to peak range of the turning points was small. Some of the subsequent results were slight improvements on this, but, the range of the results did not get close to the requirements.

Considering the different magnitudes of the components, the single δi magnitude governing the amount that variables are changed by during an exploratory move in the Hooke and Jeeves algorithm was changed so that each element had its own δi. The results obtained after making this change are shown in table 6.9.

Table 6.9.
Typical results obtained when each variable has its own δi value.
(a) gain characteristic, (b) component values

(a)

Temperature (K)	Gain
300	0.468
320	0.482
340	0.501
360	0.518
380	0.531

(b)

Component	Initial vector	Final vector	δ size
R1	930Ω	930Ω	1.0
R2	3025Ω	3136Ω	1.0
A1	0.152Ω	0.01Ω	0.1
B1	3004K	3224K	10
R3	2172Ω	2172Ω	1.0
A2	0.16Ω	0.16Ω	0.1
B2	3332K	3242K	10
R4	7056Ω	7056Ω	1.0
R5	841Ω	900Ω	1.0
R6	10340Ω	10340Ω	1.0
A3	1.25Ω	2.16Ω	0.1
B3	3641K	3801K	10

The optimisation has terminated at a vector where the points have lost the cubic form. With this approach the problem has been further extended to finding good δi magnitudes alongside finding an initial vector which converges to the required result.

A new starting point was considered to be needed. It was considered at this stage that the network was not necessarily at fault, just that something which still needed to be identified was failing to fall into place.

6.7.7. Network number 3

The mixed thermistor compensation network, described in section 6.3, was known to match the required characteristic over approximately 3/4 of the temperature range using negative temperature coefficient (NTC) thermistors. It was decided that this network in a modified form would provide the new starting point considered to be needed at this point in the investigation. The circuit in its new form is shown in figure 6.10. It was whilst working with this network that the idea of the two Res combinations, Res_s and Res_p described in chapter 7, was developed.

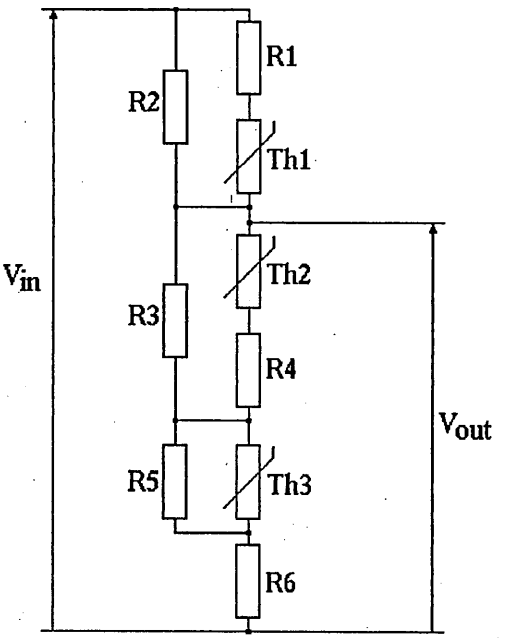

Figure 6.10. Network based on the mixed thermistor network

The positive temperature coefficient thermistor of the original network was replaced by a Res_s combination comprising Th2, R3 and R4 and the position that the output voltage is taken from was moved.

This network is in the form of a single potential divider with R1 of figure 6.5 being replaced by Th1, R1 and R2 in a Res_s combination and R2 of figure 6.5 by the remaining components, Th3, R5 and R6 being in a Res_p combination. The two resistors associated with each thermistor are intended to limit the temperature range that the thermistor governs the gain of the network. The intended operation of the circuit was for Th3 to govern the low temperature range, Th1 to govern the mid temperature range and Th2 to govern the high temperature range. Where appropriate, this intention was reflected in the choice of values used in the initial vectors.

The investigation performed with this network to determine the network's suitability for temperature compensating crystal oscillators is described in three stages.

Stage 1

Professor Fidler [5] suggested that the optimisation program might work better if more temperatures were simulated. The increased number of simulated temperatures would improve the detail of the thermistors and the required gain. Hence, the number of simulated temperatures was increased to 17. This number was arrived at by dividing the required gain characteristic into 9 levels instead of the 3 levels used previously. The new characteristic and the best results obtained under these conditions are shown in table 6.10.

Table 6.10
Best results obtained with the new network and the extended gain characteristic
(a) gain characteristic, (b) component values

	(a)	
Temperature (K)	Required gain	Network gain
300	0.500	0.500
305	0.485	0.476
310	0.460	0.459
315	0.467	0.453
320	0.450	0.452
325	0.467	0.454
330	0.460	0.461
335	0.485	0.476
340	0.500	0.500
345	0.525	0.523
350	0.540	0.540
355	0.547	0.549
360	0.550	0.551
365	0.547	0.547
370	0.540	0.537
375	0.525	0.522
380	0.500	0.505

(b)

Component	Initial vector	Final vector	δ size
R1	185000Ω	187900Ω	1.0
R2	12000Ω	107000Ω	1.0
A1	0.02Ω	0.0188Ω	0.01
B1	4400K	5980K	10
R3	20000Ω	32400Ω	1.0
R4	3000Ω	3025Ω	1.0
A2	0.083Ω	0.0010Ω	0.01
B2	4650K	8800K	10
R5	841Ω	55230Ω	1.0
R6	1025000Ω	23720Ω	1.0
A3	0.00237Ω	0.0001Ω	0.01
B3	4350K	4140K	10

Two conclusions were drawn from these results

(i) The Hooke and Jeeves program is working as required and is able to determine suitable component values to achieve the required gain characteristic of a suitable network. This was never seriously in doubt but until a set of good results had been obtained there was the possibility that there was a problem with the software or the way in which it was being used.

(ii) This proposed compensation network is able to produce a cubic gain against temperature characteristic with a good level of matching to the devised data.

It was later noted that the characteristic was shifted on the temperature scale relative to the crystal characteristic. This was a relatively small shift and did not interfere with the aims of the investigation.

Stage 2

Having shown that the network is able to produce a cubic gain against temperature characteristic, the next aim was to use real data for the required gain characteristic with a view to identifying real thermistors that could be used to make a practical

compensation circuit. Data gathered during the experiment described in section 6.3 was used to form this new characteristic. The required gain at each temperature was calculated by

$$\text{gain} = \frac{V_{tune}}{V_{ref}} \tag{6.5}$$

The new required gain characteristic is shown in table 6.11

Table 6.11.
New gain characteristic formed using real data.

Temp. °C	V ref	V tune	gain
84.8	4.034	2.187	0.543
74.6	4.037	2.319	0.574
65.0	4.039	2.338	0.579
54.8	4.041	2.256	0.559
44.7	4.043	2.115	0.525
34.8	4.045	1.937	0.480
25.0	4.046	1.748	0.432
14.9	4.047	1.573	0.388
4.9	4.048	1.435	0.353
-15.0	4.048	1.346	0.333
-25.0	4.050	1.437	0.356
-35.0	4.049	1.627	0.402
-40.0	4.048	1.780	0.440

The best set of results that was obtained is shown in table 6.12. The frequency deviation expected is calculated by

$$\text{error} = V_{ref} \times (\text{gain difference}) \times \text{pulling} \tag{6.6}$$

where gain difference is the difference between the required gain and the network gain. The measured tuning sensitivity of the oscillator was 22.5ppm/volt. This figure was taken as 25ppm/volt so that $V_{ref} \times \text{pulling} = 100$.

Table 6.12.
Best results achieved with the new gain characteristic
(a) gain characteristic, (b) component values

(a)

Temperature (°C)	Frequency deviation (ppm)
84.8	0.17
74.6	-0.16
65.0	-0.18
54.8	0.13
44.7	0.06
34.8	0.03
25.0	0.00
14.9	-0.08
4.9	0.05
-15.0	0.05
-25.0	-0.14
-35.0	0.16
-40.0	0.07

(b)

Component	Final vector
R1	9056Ω
R2	133433Ω
A1	0.106Ω
B1	4116K
R3	304507Ω
R4	0
A2	0.00114Ω
B2	6875K
R5	46851Ω
R6	0
A3	0.0001Ω
B3	4170K

The results show that the network is able to match the required compensation data points to $< \pm 0.2$ppm. An error allowance of ± 0.05 ppm has to be made for the resolution of the required gain data used in the optimisation program being only to 3 decimal places. However, the results show that the network is able to achieve compensation well below ± 0.5ppm. When the component values are considered a problem emerges. The value B_2, which is the B value of the thermistor which

governs the gain of the network over the high temperature part of the characteristic, is much larger than values that are obtainable for practical thermistors. A series of commercial thermistors was selected to determine practical values of thermistor variables used in the optimisations. The range was the Philips Components 2322 642 6 series. This range was selected because it had a wide spread of thermistor resistances at 25°C and a wide range of B values. An extract of the available thermistors in this range is shown in table 6.13. Clearly the value of $B_2 = 6875$ lies considerably outside the range covered in the table.

Table 6.13.
An extract of the 2322 642 6 series of thermistors.

Resistance at 25°C (kΩ)	$B_{25/85}$ (K)
.1	3300
.15	3375
.22	3475
.33	3575
.47	3650
.68	3725
1.0	3825
1.5	3975
2.2	4125
3.3	5250
4.7	4350
6.8	4400
10	4275
15	4200
22	4275
33	4350
47	4400
68	4450
100	4500
150	4550
220	4600
330	4625
470	4650

(Table extract reproduced courtesy of Philips Components Ltd.)

Stage 3

Up to this stage the variables which represent the components of the network in the optimisation program have been unbounded. Under this condition the results that have been obtained have established that a good match to the required data is obtainable. For this next stage the values for B were bounded using the sine function described in section (4.7). The boundary was initially set at 3665 ± 990 which actually covered all the thermistors in the selected range of available thermistors. Later the boundary was set to 4150 ± 500 which covered the thermistors in the series which had practical resistances for use in the compensation circuits. Now that the optimisation process was restricted to only using realistic values of B in the thermistor models the level that the network compensated to was about ± 0.8ppm. This result was obtained many times using different starting vectors and arrangements of the program such as weighting factors and δ values for the variables. A set of typical results is shown in table 6.14.

Table 6.14.
Typical results obtained using bounded B values for the thermistors.
(a) gain characteristic, (b) component values

(a)

Temperature (°C)	Frequency deviation (ppm)
84.8	0.83
74.6	-0.48
65.0	-0.75
54.8	-0.18
44.7	0.16
34.8	0.36
25.0	0.27
14.9	-0.03
4.9	-0.14
-15.0	-0.12
-25.0	-0.09
-35.0	0.3
-40.0	-0.16

(b)

Component	Final vector
R1	153181Ω
R2	2096087Ω
A1	0.229Ω
B1	4650K
R3	742048Ω
R4	0
A2	1.00Ω
B2	4650K
R5	2800788Ω
R6	0
A3	0.00614Ω
B3	4458K

Two factors were common with all these results

(i) The B_2 value was always at the maximum of 4650.

(ii) The maximum error always occurred at the high temperatures.

6.7.8. Results and discussion for network number 3

Network 3 has been shown capable of achieving a gain against temperature characteristic which corresponds to the required level of compensation of $< \pm 0.5$ppm over the temperature range -40°C to +85°C using theoretical thermistors. When the range of available thermistors is restricted to practical limits the level that the compensation circuit can achieve is degraded by a factor of 4. This gives a reason why the mixed thermistor network was able to achieve good results and why thermistor based compensation networks might be considered to have reached their limit. The PTC thermistor has a resistance against temperature characteristic which is equivalent to a B value of approximately 7000 [6].

6.7.9. Network number 4

Having established that the network in its basic form could not achieve the required level of compensation when the thermistors were limited to practical components it was decided to attempt to modify the network. The first modification took two forms; in the first form a Res combination was added in the R1 position of the potential divider, figure 6.11 (a); in the second form a Res combination was added in the R2 position, figure 6.11 (b). Neither of these forms improved the level of compensation that the network provided.

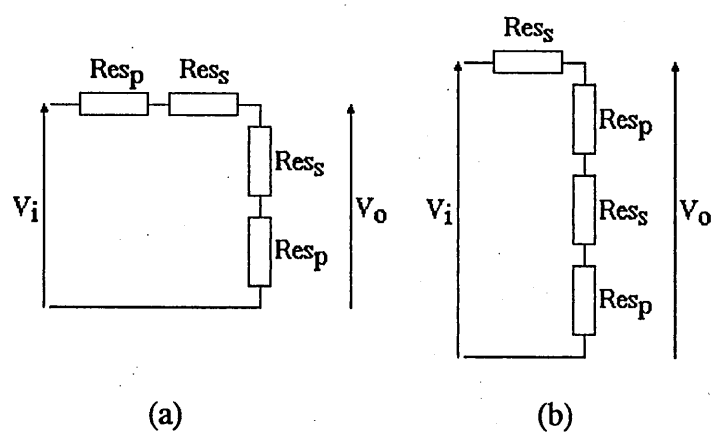

Figure 6.11. Two forms of potential divider using a fourth Res combination. (a) in R1, (b) in R2

6.7.10. Network number 5

It has been established that using theoretical negative temperature coefficient (NTC) thermistors it is possible to provide a compensation voltage to the level of $< \pm 0.5$ppm but when the thermistors characteristics are restricted to realistic values the level of compensation is limited to about ± 0.8ppm. It was considered that the way to proceed was to identify a means of making practical thermistors behave in a similar way as the theoretical thermistors.

The thermistor characteristic of resistance against temperature is represented by an exponential function, section 7.2. The term that had to be modified was B which forms part of the exponential power and which can be altered by forming a product of two thermistors so that the values of B for the two thermistors form a sum:

$$A_1 e^{\frac{B_1}{T}} \times A_2 e^{\frac{B_2}{T}} = A_1 A_2 e^{\frac{B_1+B_2}{T}} \qquad (6.7)$$

In electronic circuits product expressions are obtained by gain. Hence the required result could be obtained by using an amplifier with its gain set by a temperature sensitive component. The amplifier would then be included in the circuit so that the output of the network was multiplied by the gain of the amplifier, figure 6.12.

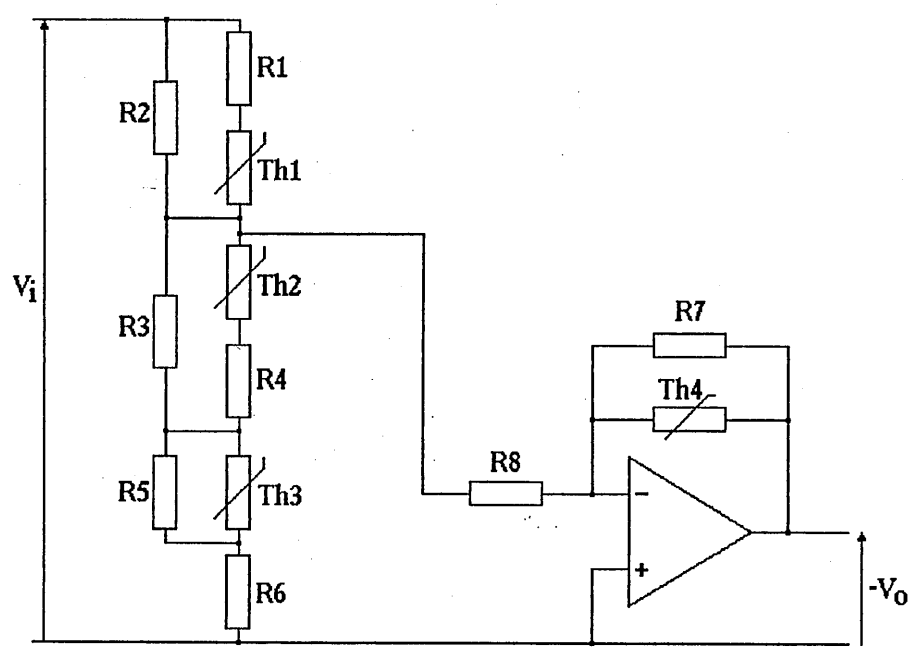

Figure 6.12. Compensation circuit with temperature sensitive amplifier

The amplifier in figure 6.12 is shown in a simplified form. It can be followed by an invertor to give a positive overall transfer function. A nominal characteristic for the amplifier showing gain against temperature is shown in figure 6.13.

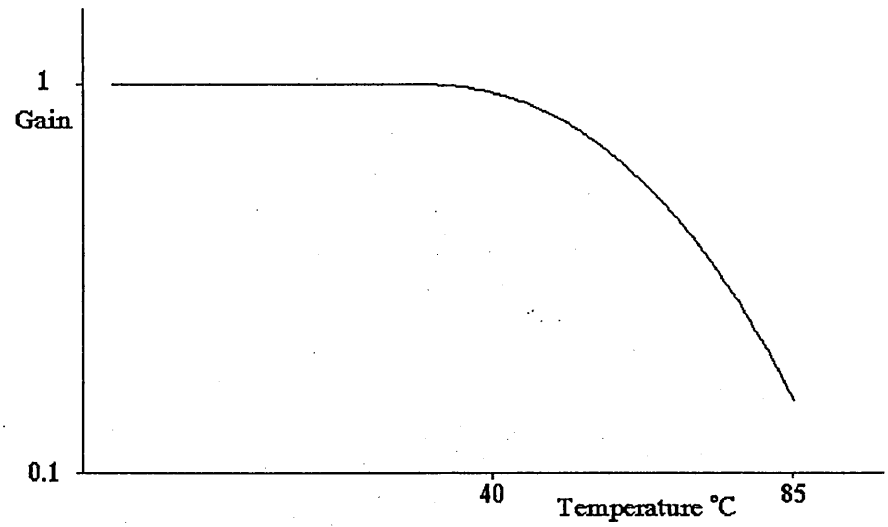

Figure 6.13. Generalised gain against temperature characteristic of temperature sensitive amplifier.

Originally the feedback combination had been a Res_s block but the optimisation process made the series resistor have no resistance so the simplified form of the feedback was adopted. Results obtained with all the variables included in the optimisation process showed that this new circuit is capable of achieving the required level of frequency compensation. Hence it was established that the use of the amplifier with temperature sensitive gain overcame the limiting factor of the restricted range of B values available for practical thermistors. The decision was made to take the thermistors out of the process and use values of parameters which represented real thermistors. A value for B of 4400 was used for all four thermistors because this was representative of the values obtained in the optimisation process throughout the investigation and because there were two thermistors which appeared in table 6.13 with this value, 47kΩ and 6.8kΩ.

6.7.11. Results and discussion for network number 5

Results obtained for this network with the thermistor parameters representing real thermistors are shown in table 6.12. These results show a maximum predicted error of less than ± 0.2ppm over the whole temperature range -40°C to +85°C.

Table 6.15.
Final set of results with thermistors included in the optimisation process.
(a) characteristic, (b) resistor values.

(a)

Temperature (°C)	Frequency deviation (ppm)
85	0.17
75	-0.19
65	-0.13
55	0.19
45	-0.01
35	-0.17
25	-0.18
15	-0.09
5	0.18
-15	0.06
-25	-0.18
-35	0.18
-40	-0.18

(b)

	Required value (Ω)
R1	3788
R2	793500
R3	725900
R4	3905
R5	56690
R6	9300
R7	1638
R8	2092
Th1	47000
Th2	6800
Th3	6800
Th4	47000

When these new results are compared with the results in table 6.12, which were obtained using theoretical thermistors, the new results are not as good over the middle portion of the temperature range but over the high portion of the temperature range, where the other networks have failed, the agreement is good. This confirms that the use of the amplifier with temperature sensitive gain produces the required modification to the thermistor characteristics even when

models of practical thermistors are used in the circuit. Hence the conclusion was drawn that a new temperature compensation circuit has been found based on NTC thermistors which is able to provide a higher level of temperature compensation for crystal oscillators using AT cut resonators and which operates from a low reference voltage. This higher level of stability is equal to, and possibly improves on, the level of stability that the alternative analogue compensation methods claim. It was decided to build up an oscillator and compensation network to test the new temperature compensation network in a practical TCXO.

A difficulty with the optimisation program which was encountered with the modelled components used to represent the compensation network was that the time taken for the program to run was sometimes many hours.

6.8. Experimental networks

6.8.1. Aim

The aim was to construct an oscillator and compensation network to determine how well the modelled network worked in a practical TCXO. At this time a problem was encountered. The thermistors that had been modelled in the second part of section 6.7 had a delivery time of 12 weeks. It was decided, in the interim period, to change the thermistor model to represent devices that were readily available, and to use the required thermistors later. Provided satisfactory results were obtained using models of the thermistors an experimental network could be built. As expected, these alternative thermistors did not give quite such good results as the original thermistors. However, they did give a predicted level of compensation that was within the required $\pm$0.5ppm, table 6.16.

Table 6.16.
Results of the optimisation using available thermistors.
(a) characteristic, (b) resistor values.

(a)

Temperature (°C)	Frequency deviation (ppm)
85	0.31
75	-0.31
65	-0.26
55	0.23
45	0.27
35	0.26
25	0.19
15	0.03
5	0.02
-15	-0.14
-25	-0.25
-35	0.23
-40	0.09

(b)

	Required value (Ω)
R1	2643
R2	499100
R3	21590
R4	15940
R5	333900
R6	25.5
R7	2807
R8	5387

6.8.2. First practical oscillator

The measurements taken during the characterisation which were used for the optimisation are shown in table 6.17.

Table 6.17.
Characterisation measurements.

Temperature (°C)	Th 1 (Ω)	Th 2 (Ω)	Th 3 (Ω)	Th 4 (Ω)	V_{tune} (V)	V_{ref} (V)
85	5542	567.5	571.9	5395	2.4070	4.002
75	7691	783.3	788.7	7502	2.6029	4.002
70	9167	924.0	930.6	8884	2.6517	4.004
65	10790	1090	1097	10520	2.6427	4.005
25	49380	4856	4897	48600	1.9738	4.014
0	149400	14570	14720	147700	1.6053	4.021
-10	249500	24290	24526	246600	1.5664	4.023
-15	329000	32000	32290	324200	1.5860	4.023
-40	1300000	130000	131800	1313000	2.1262	4.027

The number of measurement temperatures used for the optimisation of the real oscillator was fewer than when working with the models. It was hoped that the use of fewer characterisation temperatures would reduce the time taken to perform the optimisation part of the process. The samples chosen were the ends of the temperature range, the middle of the range with an emphasis at the two turning points. The result of the optimisation, table 6.18, was unexpected. One of the thermistors had the two resistors associated with it finish with zero resistance which took the thermistor out of the circuit.

Table 6.18.
Results of the optimisation using characterisation data.
(a) characteristic, (b) resistor values.

(a)

Temperature (°C)	Frequency deviation (ppm)
85	0.41
75	-0.18
70	-0.41
65	0.39
25	0.41
0	-0.40
-10	0.04
-15	0.32
-40	0.37

(b)

	Required value (Ω)
R1	1852
R2	372400
R3	0
R4	0
R5	187600
R6	9787
R7	2904
R8	6706

Either something had gone awry during the optimisation or there was a three thermistor network which gave the required level of compensation which had been missed during the earlier investigation. Certainly the maximum predicted error for the network was within the ± 0.5ppm.

The resistances that the optimisation program returns are not preferred values so the components for the network had to be made from combinations of resistors,

E96* series resistors were available in the laboratory. The resistors used are shown in table 6.19.

Table 6.19.
Resistor combinations used to make required values.

	Required value (Ω)	Combination (Ω)	Measured value (Ω)
R1	1850	1430+422	1850
R2	372000	93100×4	373000
R5	188000	93100×2+1400	188000
R6	9790	9310+280+196	9820
R7	2900	2800+105	2900
R8	6710	6490+215	6730

Two results of verifying the combination are presented in figures 6.14 and 6.15. The first has a settling time, between the chamber achieving the required temperature and the frequency measurement being made, of 5 minutes and the second has a settling time of 30 minutes.

---

* Over a decade, standard values for electronic components are determined by a power series given by $V(n) = 10^{\left(\frac{n}{C}\right)}$ where C is the component range and n is an integer in the range 0 to C-1. Instead of n taking on the value of C for the last component, n is set to 0 and a new decade is started. The usual values of C are 6, 12, 24, 48, 96 and 192. The values of V(n) are called *preferred values*

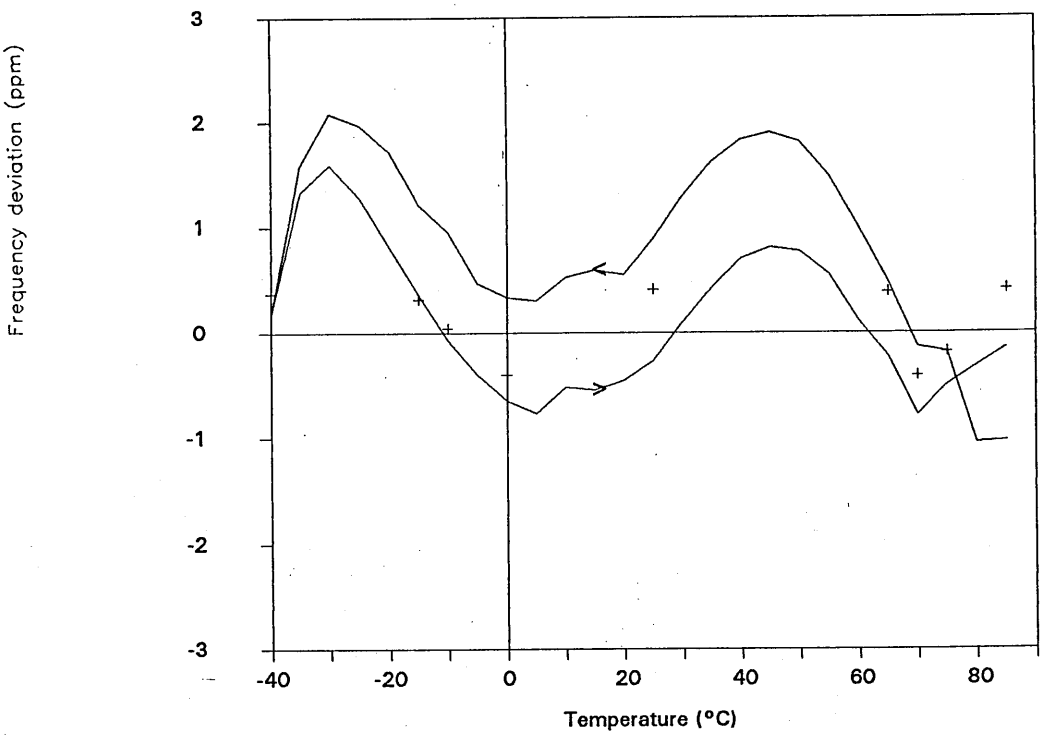

Figure 6.14. Verification results obtained using 5 minutes stabilisation time.

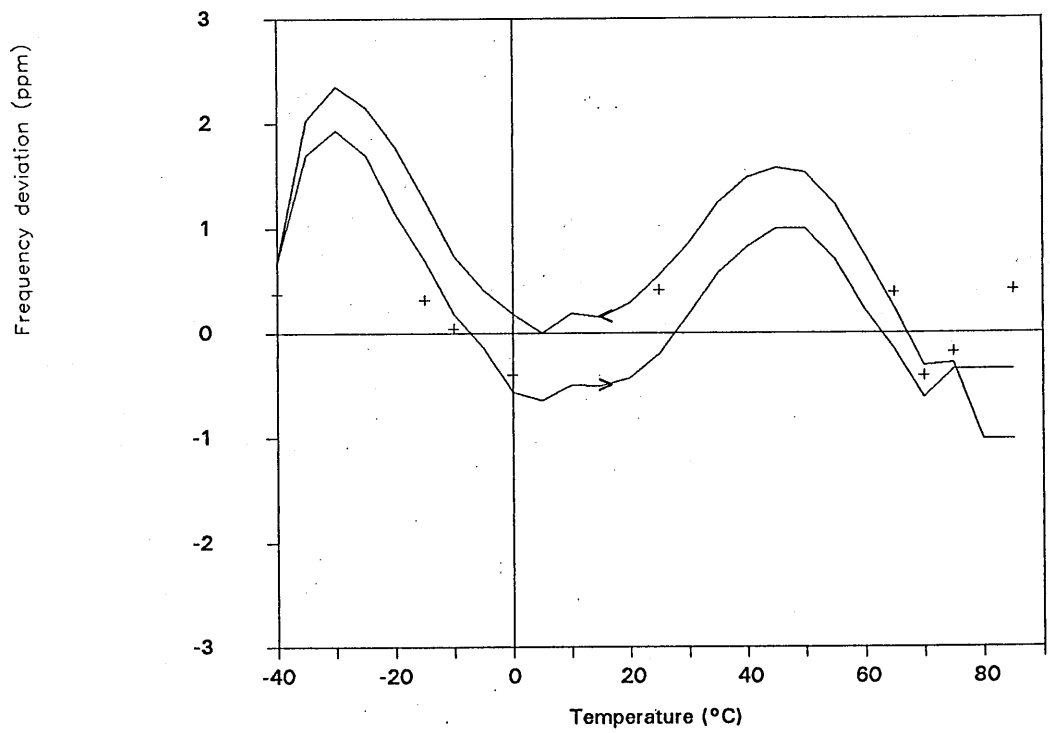

Figure 6.15. Verification results obtained using 30 minutes stabilisation time.

6.8.3. Results and discussion

There are three points that are to be noted: the level of compensation error, bandbreaks and the hysteresis.

Compensation error is much greater than expected. This shows that something had gone awry and that the network was not compensating the oscillator to the required level over the whole temperature range. This was caused by grouping the temperatures used in the optimisation around the turning points of the required tuning characteristic which acted as a weighting function for the optimisation program. The large compensation errors fell in the gaps. In future the temperatures for optimisation must be equally spaced or at least less bunched to ensure that this is not repeated. This result was not considered to be a major problem because its cause was understood and in future could be avoided.

Bandbreaks show in the verification results as deviations from the smooth curve. There are two in the crystal used for this oscillator, one around 10°C and another around 80°C. In temperature compensation of crystal oscillators the occurrence of bandbreaks is undesirable because they degrade the level of compensation that can be achieved because their effect cannot be included in the compensation process. Bandbreaks are a little more serious problem because they indicate that the crystal is being driven too hard and so the oscillator might need modification to reduce the drive to the crystal. The action taken to reduce the crystal drive level was described in section 4.6.

Hysteresis that appears in the verification is of the order of 1ppm for the first verification and 0.5ppm for the second so in part the hysteresis is attributable to the components achieving thermal equilibrium. At this stage the other causes were uncertain, but the crystal was the most likely source. This is the most serious

problem to have been revealed by this experiment and the one which it was decided to address next. With a level of hysteresis of 0.5ppm, or $\pm$0.25ppm, the level of stability that can be achieved by temperature compensation is reduced.

The required compensation voltage, shown in figure 6.16, and the output voltage of the compensation network, shown in figure 6.17, were measured for increasing and decreasing temperature.

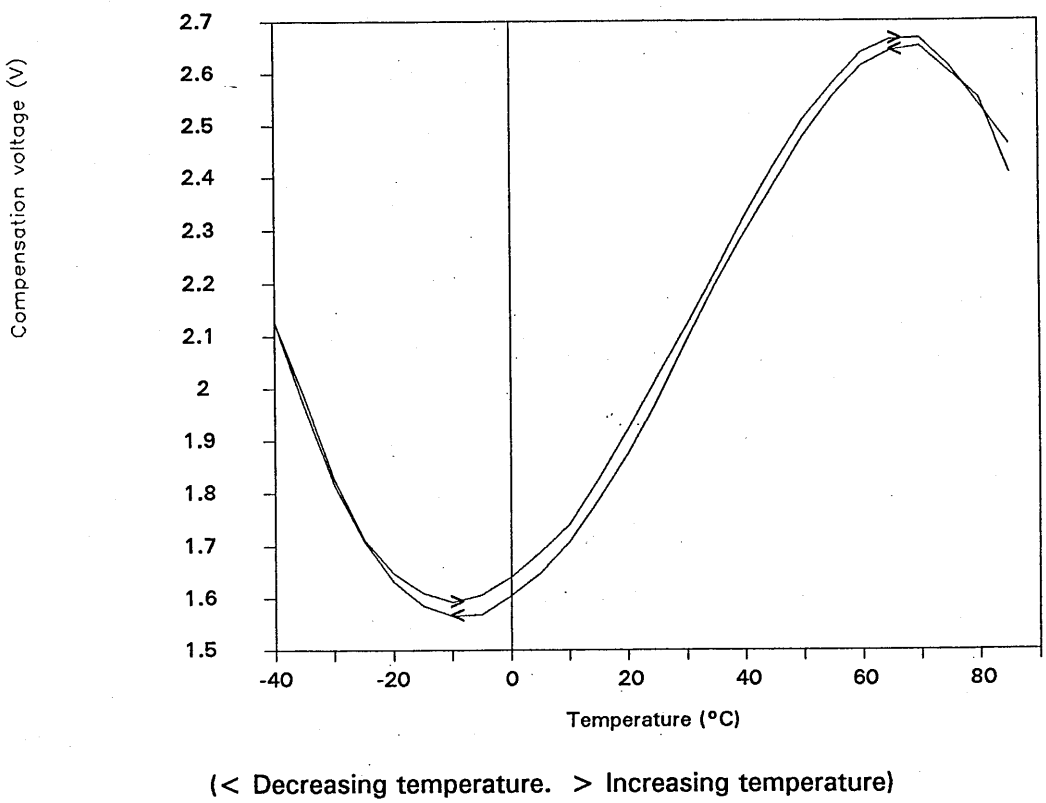

Figure 6.16. Temperature cycle of required compensation voltage.

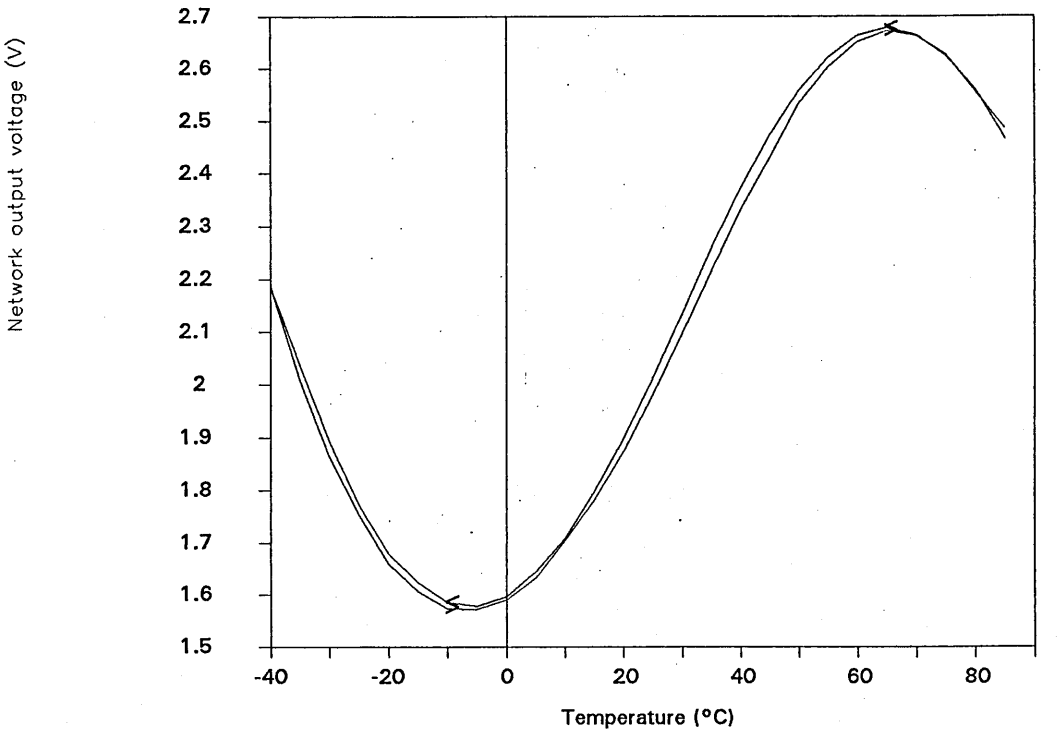

Figure 6.17. Temperature cycle of the compensation network output voltage.

Both graphs show hysteresis. It was considered that the hysteresis of the compensation network might be attributed to differences in the thermal environment between decreasing and increasing temperature because of the apparent shift along the temperature scale, see section 5.4. The hysteresis in the crystal tuning characteristic could not be explained at this stage and would need further investigation, which is described in section 4.6.

6.8.4. Second practical oscillator

Once it was considered that the problems with the crystals and the environmental chamber had been resolved, a second practical compensation network could be attempted. By this time the thermistors identified at the modelling stage were

available. The oscillator circuit used to drive the crystal is described in section 4.6. Measurements for the characterisation of the components were taken at 5°C intervals. Although this level of sampling would slow the optimisation program, it would ensure that the components would be well described. This second attempt was cut short because it was discovered that the bandbreak problem had not been adequately resolved (see section 4.6). Difficulties were being experienced with the optimisation of the network; compensation of $\pm$0.9ppm over the temperature range of -40°C to +85°C was readily achieved but it was with difficulty that compensation below $\pm$0.6 was achieved. The reason for this is apparent when the results of an optimisation is compared to figure 4.21. Over the temperature range +45°C to +85°C the two graphs are almost identical showing that over this temperature range the characteristic is dominated by the bandbreak. The optimisation process has spread the error over the whole temperature range in its attempt to reduce the error caused by the bandbreak.

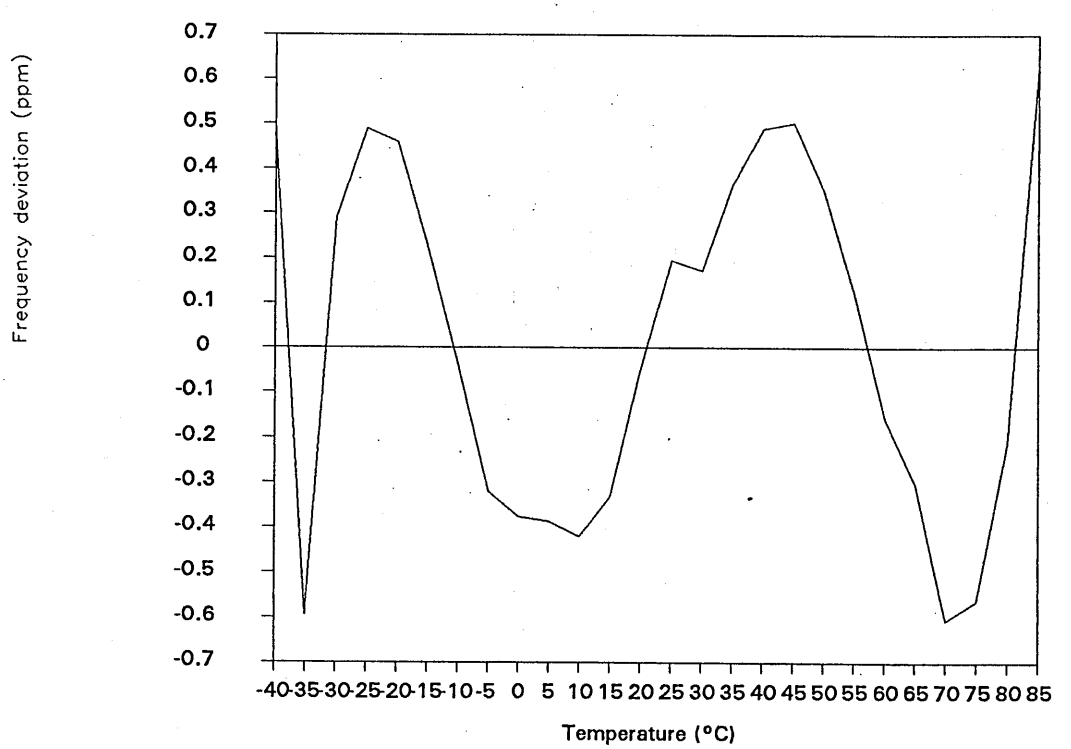

Figure 6.18. Results of the optimisation.

6.9. Conclusion

Networks of resistors and thermistors have been investigated by means of an optimisation computer program. During the investigation the factor limiting the level of temperature compensation for quartz crystal oscillators using AT cut resonators has been identified as being due to the available high stability thermistors not having a large enough B value. An original solution to this limit has been found by using an amplifier which has temperature sensitive gain. In this circuit arrangement a product of two exponential functions is formed, giving a new characteristic which has an effective B value formed by the sum of the B values of the two thermistors used. In theoretical studies the new network has achieved a level of compensation below ± 0.2ppm over the temperature range -40°C to +85°C. Theoretical studies on this compensation circuit have used real data to represent the required compensation and references voltages and mathematical models to represent the thermistors used in the compensation circuit. The level of frequency stabilities that have been obtained using this appraoch represent an advance for resistive temperature compensation circuits. Problems encountered whilst attempting to experimentally verify these results have been of a technical nature and these have been addressed. Hence future work will include experimental verification of the new temperature compensation circuit.

Commercially available thermistors have discrete values for their parameters. As part of the future work, it would be appropriate if the lattice angle of the crystal resonator were to be brought into the optimisation process. For this to be achieved either resonators with a range of angles would have to be characterised to provide the required compensation voltage data used in the optimisation process or an accurate model of the compensation process could be used to derive a representation of the required compensation voltage. Also the use of improved thermistor models will be investigated.

6.10. References

[1] Wilson J. S. (1983). An improved method of temperature compensation of crystal oscillators. *Proc 37th Annu. Freq. Control Symp.*, pp. 442-447.

[2] Harrison, A., Dowsett, J. and Sharpe, D. (1987). High frequency stable frequency sources for advanced systems. *Proc 41st Annu. Freq. Control Symp.*, pp. 539-543.

[3] Philips Components Ltd.. Private communication.

[4] Macklen, E. D. (1979). Thermistors, *Electrochemical Publications Ltd., Ayr*, pp 12-14.

[5] Fidler, J. K.. Private communication.

[6] Mullard Components Book 3, Part 1, f.

7. MATHEMATICAL ANALYSIS OF RESISTIVE TEMPERATURE COMPENSATION NETWORKS

7.1. Introduction

In this chapter mathematical analysis of the resistive temperature compensation networks is presented. This analysis has shown that the behaviour of the compensation networks can be modelled by imaginary components used in conventional electronic circuits. However, one of these models is realisable in a practical form and experiments have been performed with this model in the optimisation program with favourable results.

7.2. Thermistors

Negative temperature coefficient (NTC) thermistors are semiconductor devices that exhibit large changes of resistance as temperature changes. Changes in resistance of between 3% and 5% per °C are typical depending on the absolute temperature of the thermistor and its chemical composition. Theoretically the resistance of a NTC thermistor is characterised by

$$R = R_{\infty} e^{\frac{B}{T}} \tag{7.1}$$

where R is the resistance of the thermistor at absolute temperature T, R_{∞} is the resistance of the thermistor at infinite temperature ($\frac{1}{T} = 0$), which is usually represented by A, and B is a constant which is dependent of the composition of the device and is related to the energy needed to bring about conduction on the atomic level and Boltzmann's constant [1]. In practice B is not constant but increases slightly as temperature increases. Over the temperature range -40°C to +85°C typical increase is of the order of 5%.

Attempts to characterise the performance of thermistors so that the change in the value of B is accounted for have given rise to a variety of formulae. The one that has gained the most widespread acceptance is the Steinhart and Hart equation [2]. In the strictest sense the Steinhart and Hart equation was not originally used to improve (7.1); instead it was intended to improve the interpolation between calibration points for temperature measurement. For temperature measurement (7.1) is rearranged to

$$\frac{1}{T} = \frac{\ln R}{B} - \frac{\ln A}{B} \tag{7.2}$$

Equation (7.2) is usually rewritten with new constants which are, a little confusingly, also called A and B. This form is

$$\frac{1}{T} = A + B(\ln R) \tag{7.3}$$

Steinhart and Hart investigated fitting experimental data to a power series of ln R. They found that power series using odd powers gave the best results and for most purposes a series of just three terms gave very good results

$$\frac{1}{T} = A + B(\ln R) + C(\ln R)^3 \tag{7.4}$$

Although this series gives good results for interpolation, Steinhart and Hart found that it fails to give good results for extrapolation. They concluded that this does not represent a law for describing thermistor behaviour.

Many thermistor manufactures have recently started to quote the Steinhart and Hart equation in a rearranged form in order to give an improved expression for thermistor resistance over that obtained by using (7.1). However, when the network research was undertaken (7.1) was presented by the manufactures for the

resistance against temperature characteristic of the thermistors. From the results that have been obtained, this formula for thermistor resistance was adequate for determining the new network. Future work may require that the thermistors be represented by the Steinhart and Hart equation.

An alternative approach would be to apply a similar development to that used for the analysis of the higher order polynomials of the crystal as it is tuned during the compensation process. First consider the basic characteristic of the thermistor

$$R = Ae^{\frac{B}{T}} \tag{7.5}$$

If the components of the thermistor expression are temperature dependent then taking into account the linear terms gives

$$R = A(1+T_AT)e^{\frac{B(1+T_BT)}{T}} \tag{7.6}$$

where T_A is the temperature coefficient of A and T_B is the temperature coefficient of B. Rearranging gives

$$R = Ae^{T_B}(1+T_AT)e^{\frac{B}{T}} \tag{7.7}$$

The linear temperature coefficient of the B component gives a constant coefficient and the exponential part remains unchanged. This suggests that the descrepancies between the theoretical model and the observed characteristics might be accounted for by lumping the problem on to the A coefficient. The way to proceed here is to compare the characteristic obtained here with calibration data. This is an idea that developed during the latter stages of writing up so there has not been opportunity to check the literature in this direction to determine whether this approach has already been investigated. The literature to hand makes no mention of this approach. However, this literature is concerned with the use of thermistors as temperature sensors and not directly with the resistance against temperature

characteristic. Earlier it was stated that B increases slightly with temperature. This being the case it might be necessary to go to higher terms for the temperature coefficient of B.

$$R = A(1+T_A T)e^{\frac{B(1+T_{B1}T+T_{B2}T^2)}{T}} \qquad (7.8)$$

If an accurate model of the thermistor behaviour can be built with this approach, it might result is an expression which is mathematically more manageable than the Steinhart and Hart expression.

7.3. Principle of operation of resistive temperature compensation networks.

Temperature compensation circuits transform a constant reference voltage to the required compensation voltage over a predetermined temperature range. In a network of resistors and thermistors this is achieved by changing the gain of the network as a function of temperature. The voltage gain of the potential divider circuit is given by

$$\text{gain} = \frac{V_o}{V_i} = \frac{R_2}{R_1+R_2} \qquad (7.9)$$

The single resistive elements of the potential divider, R_1 and R_2, can be replaced by a combination of resistances in which case the gain is obtained by substituting the expression for the resistance of the combination into (7.9) and rearranging as appropriate. The use of a potential divider places a constraint on the reference voltage that can be used in a temperature compensated crystal oscillator because the reference voltage used has to be greater than the maximum required compensating voltage.

Inclusion of a thermistor in a potential divider circuit as one of the resistive components results in a circuit whose gain changes with temperature according to the action of the thermistor. When resistance R_1 in the potential divider circuit is replaced by a thermistor the gain of the circuit is given by

$$\frac{V_o}{V_i} = \frac{R_2}{Ae^{\frac{B}{T}} + R_2} \tag{7.10}$$

When R_2 is replaced by a thermistor the gain is given by

$$\frac{V_o}{V_i} = \frac{Ae^{\frac{B}{T}}}{R_1 + Ae^{\frac{B}{T}}} \tag{7.11}$$

These last two expressions show how a constant input voltage is transformed to a temperature dependent output voltage. The output voltage of the circuit either increases or decreases with temperature depending on the position of the thermistor within the circuit. This is the basis of resistive temperature sensitive networks used for temperature compensation.

7.4. Resistive circuit elements

A typical resistance against temperature characteristic of an NTC thermistor is shown in figure 7.1.

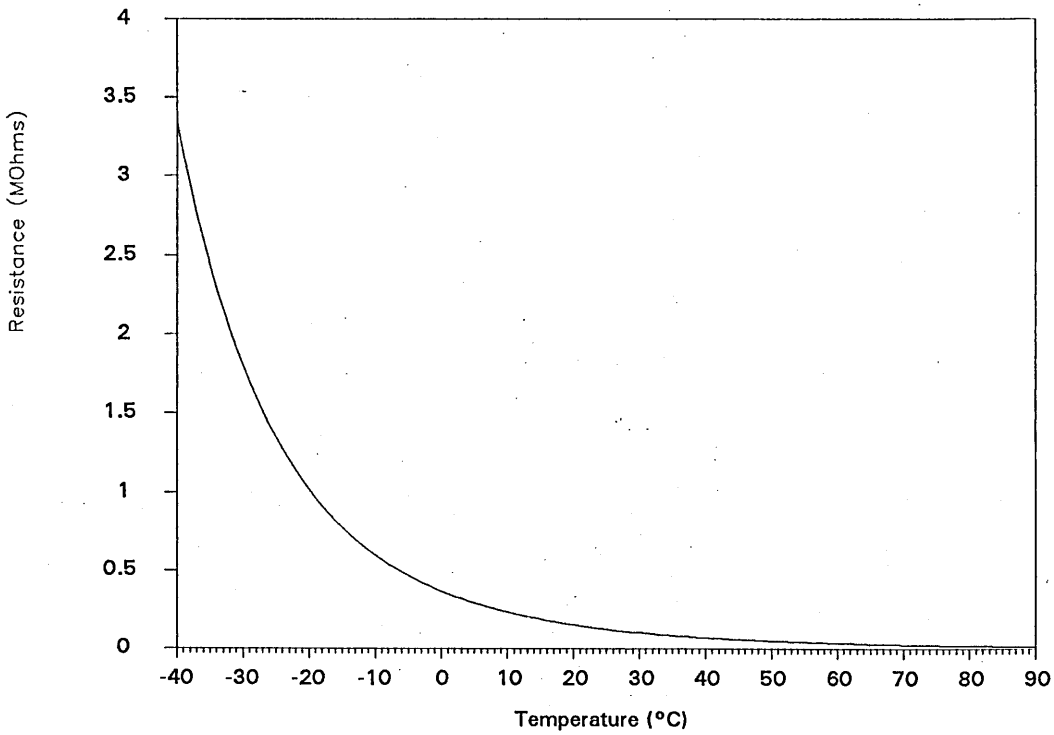

Figure 7.1. Typical thermistor resistance against temperature characteristic

When a resistor R_S is connected is series with a thermistor their combined resistance R is given by

$$R = Ae^{\frac{B}{T}} + R_S \qquad (7.12)$$

When the temperature, T, is low the resistance of the thermistor is much greater than the resistance R_S, hence the combined resistance $R \approx Ae^{\frac{B}{T}}$. When temperature is high, the resistance of the thermistor is much less than the resistance of R_S, hence the combined resistance $R \approx R_S$. A typical characteristic for a resistor in series with a thermistor is shown in figure 7.2.

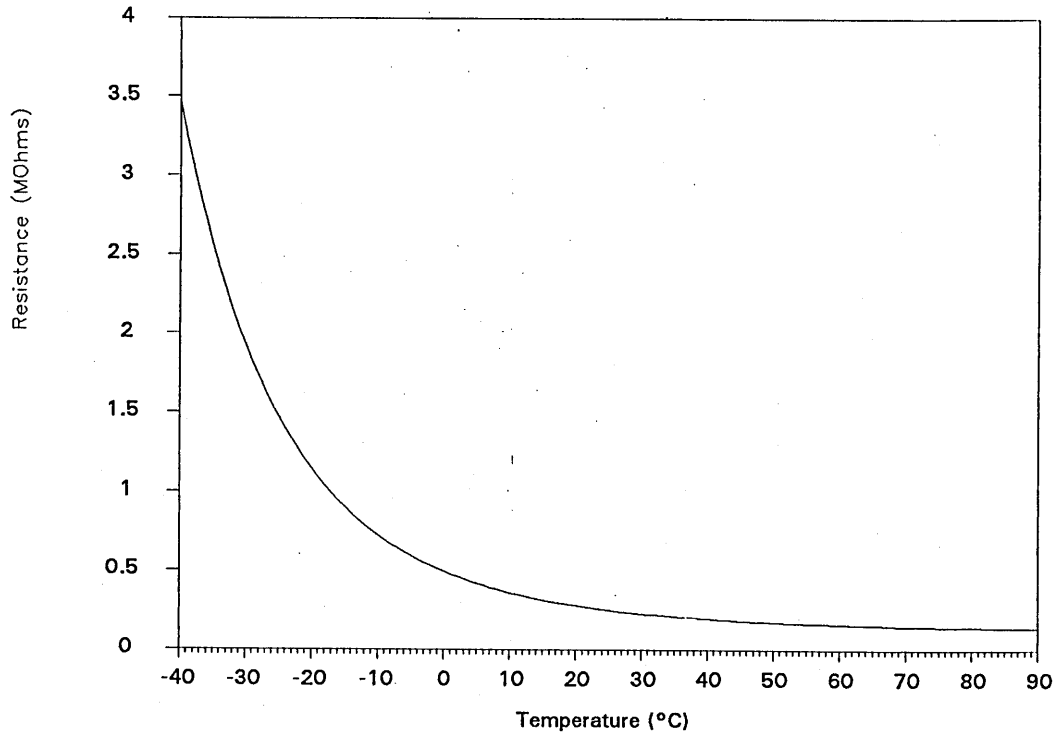

Figure 7.2. Thermistor with series resistor.

When a resistor R_p is connected in parallel with a thermistor the combined resistance R is described by

$$R = \frac{R_p A e^{\frac{B}{T}}}{R_p + A e^{\frac{B}{T}}} \tag{7.13}$$

For this arrangement, when temperature is low the resistance of the thermistor is large compared to the resistance of R_p, hence the combined resistance $R \approx R_p$. When temperature is high the resistance of the thermistor is small compared with the resistance of R_p, hence the combined resistance $R \approx A e^{\frac{B}{T}}$, see figure 7.3.

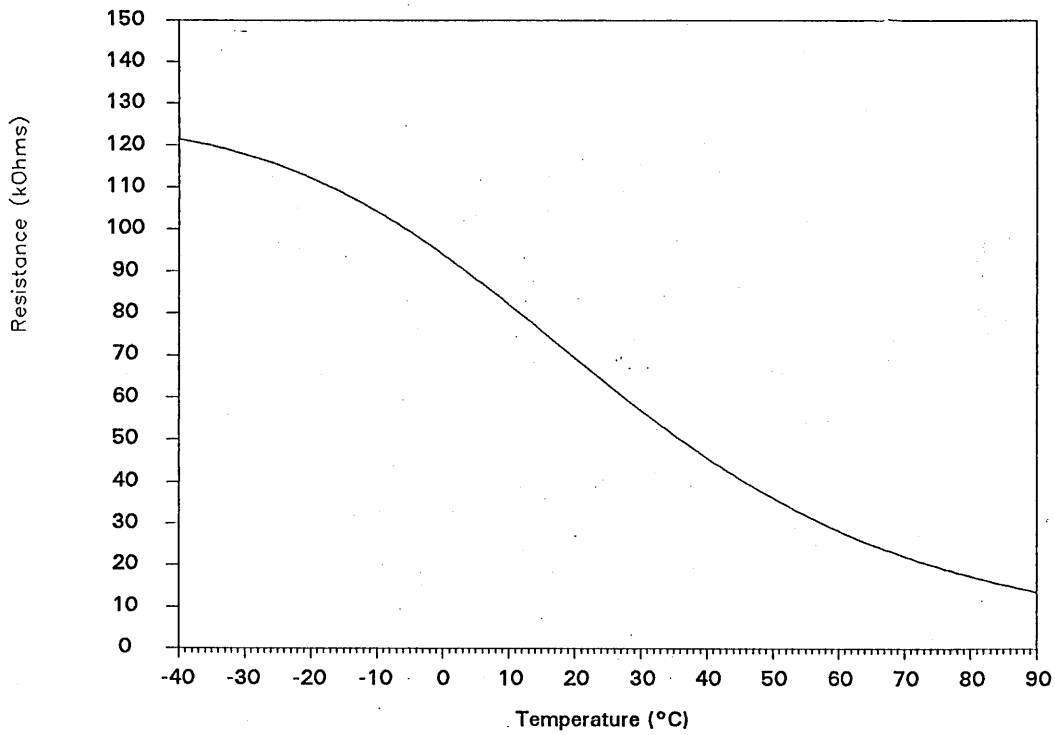

Figure 7.3. Thermistor with parallel resistor

For both these characteristics it has been assumed that the thermistor has A=1, B=3500 and the associated resistor R_s or R_p is equal to the thermistor resistance at 25°C (298°K).

If the resistor and thermistor combination is considered as a new circuit element, these results show that the new element can be made to appear to be temperature sensitive either above or below a certain temperature. This idea is extended in the next section.

7.5. Res combinations

By connecting a thermistor with a series resistor and a parallel resistor the temperature range that the circuit can be regarded as having a temperature sensitive resistance is limited for both low temperatures and high temperatures, as described

in the previous section. There are two ways of connecting a thermistor and two resistors. The two combinations are referred to in this thesis as Res_S, figure 7.4(a), and Res_P, figure 7.4(b). The subscripted letters refers to the resistor most directly associated with the thermistor.

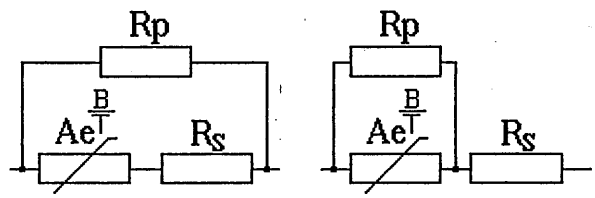

(Res_S) (Res_P)

Figure 7.4. The two basic Res combinations.

The resistance of the Res_S combination is given by

$$Res_S = \frac{R_p(Ae^{\frac{B}{T}} + R_s)}{Ae^{\frac{B}{T}} + R_s + R_p} \tag{7.14}$$

Resistance of the Res_P combination is given by

$$Res_P = \frac{R_p Ae^{\frac{B}{T}}}{R_p + Ae^{\frac{B}{T}}} + R_s \tag{7.15}$$

Rearranging gives

$$Res_P = \frac{(R_p + R_s)\left[Ae^{\frac{B}{T}} + \frac{R_p R_s}{R_p + R_s}\right]}{Ae^{\frac{B}{T}} + R_p} \tag{7.16}$$

The product term of the thermistor in the numerator has been treated as a common factor and taken outside the bracket in order to give the numerator and

denominator a similar form. The circuits which (7.14) and (7.16) describe have only one thermistor. However, in the expressions the thermistor appears twice which means that the operation of the circuits can be explained using two thermistors. This is explored later in greater detail.

7.6. Temperature sensitive potential dividers

The first temperature sensitive potential divider circuits to be considered have one of the resistances fixed and the other resistance is a Res combination. This gives rise to four different circuits. In this thesis only one of the circuit combinations will be considered in detail. However, similar results are obtained for all four potential dividers circuits.

The circuit being considered here is shown in figure 7.5. The circuit comprises a Res_S combination in the place of R_1 and R_2 is left as a fixed resistor.

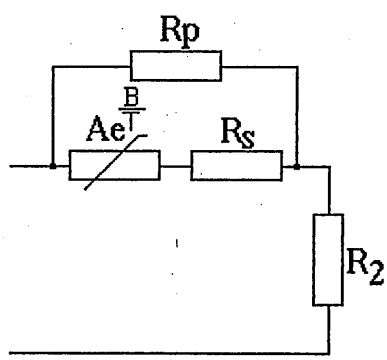

Figure 7.5. Circuit analysed in the text

Substituting Res_S (7.14) directly into (6.9) as R_1 gives

$$\text{gain} = \frac{V_o}{V_i} = \frac{R_2}{\left[\dfrac{(Ae^{\frac{B}{T}} + R_s)R_p}{Ae^{\frac{B}{T}} + R_s + R_p}\right] + R_2} \tag{7.17}$$

There are two ways of rearranging (7.17) which give rise to familiar expressions. These expressions describe the gain of common circuits. The first of these circuits is the potential divider circuit which is the same form as the original circuit. The second form is an expression which describes the gain of certain amplifiers. Based on the two circuit forms, mathematical models are built which have new components formed from the values of the components of the original circuit. Using these models a relatively simple explanation of the operation of the original circuit can be presented.

The first of the models to be presented here is that based on the potential divider. The gain of this model is given by

$$\frac{V_o}{V_i} = \frac{R_2\,(Ae^{\frac{B}{T}} + R_p + R_s)}{R_p(Ae^{\frac{B}{T}} + R_s) + R_2(Ae^{\frac{B}{T}} + R_p + R_s)} \tag{7.18}$$

This form shows that the original circuit can be modelled as a potential divider comprising a resistor and thermistor connected in series in both the R_1 and the R_2 positions. This model is shown in figure 7.6.

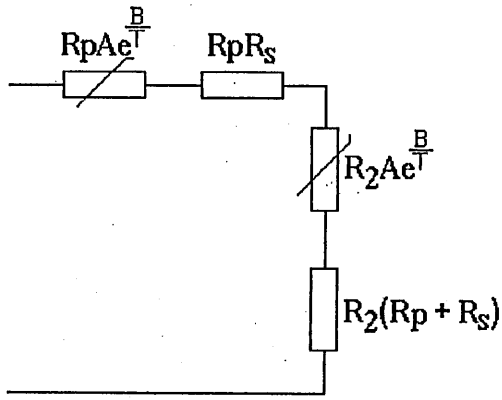

Figure 7.6. Simple network modelled as a potential divider comprising two thermistors and two series resistors.

The imaginary thermistors have identical exponential values. However the magnitude of the A coefficient of these imaginary thermistors is modified, being given by the original A coefficient multiplied by one of the fixed resistors of the original circuit.

In section 7.4. a description of the action of a thermistor in series with a resistor was presented based on their relative resistances. The basis of that explanation is extended here to describe the action of the potential divider circuit. When temperature is low the resistance of the imaginary thermistors is large, so that the resistance of the series resistors can be ignored, which gives

$$\frac{V_o}{V_i} = \frac{R_2 A e^{\frac{B}{T}}}{R_p A e^{\frac{B}{T}} + R_2 A e^{\frac{B}{T}}} = \frac{R_2}{R_p + R_2} \qquad (7.19)$$

as expected at low temperature. As temperature increases the resistance of the thermistors decrease until a point is reached where the series resistor of one of the branches is no longer small and so it can no longer be ignored. At that point (7.19) no longer holds. From (7.18) it is clear that the thermistor in series with the imaginary resistor whose value is $R_p + R_s$ will cease to dominate first. If the

transition between thermistor dominance and resistor dominance is quick then (7.18) becomes

$$\frac{V_o}{V_i} = \frac{R_2 (R_p + R_s)}{R_p A e^{\frac{B}{T}} + R_2(R_p + R_s)} \qquad (7.20)$$

As temperature increases further, the thermistor's resistance decreases so increasing the gain of the potential divider. Hence the output voltage increases. This continues until the resistance of the thermistor is no longer large compared with R_s. When the thermistor resistance is small compared with R_s the gain of the potential divider is solely dependent on the values of the imaginary series resistors. Now the gain is given by

$$\frac{V_o}{V_i} = \frac{R_2 (R_p + R_s)}{R_p R_s + R_2(R_p + R_s)} \qquad (7.21)$$

The model describes the action of the circuit by introducing two imaginary thermistors. The explanation divides into three parts. For two of these parts the thermistor forms no temperature sensitive part of the circuit and these are readily obtained from the original circuit. The usefulness of the model is the way in which it simplifies the circuit when the thermistor is in the active temperature range. The action of each thermistor is limited by the presence of a single series resistor. When the two brackets in the denominator of (7.18) are summed to form a single bracket the mathematical expression of the second model is identified which is

$$\frac{V_o}{V_i} = \frac{R_2 \quad (A e^{\frac{B}{T}} + R_p + R_s)}{(R_2 + R_p)\left[A e^{\frac{B}{T}} + R_s + \frac{R_2 R_p}{(R_2 + R_p)} \right]} \qquad (7.22)$$

The expression has been arranged so that the thermistor has no direct coefficient in either the numerator or the denominator. The thermistor coefficient of the numerator and denominator have been treated as a common factor in both cases. As in the potential divider model, there appear to be two imaginary thermistors formed whose action is limited by a resistance connected in series. Hence the description of the action of this model is similar to the previous description. However, this second form can be regarded as two separate gain elements. The first is a fixed gain given by a potential divider formed by R_p and R_2 and a temperature sensitive gain given by the ratio of the two imaginary thermistors and their associated imaginary series fixed resistances. Both of the thermistors in this model are identical to the thermistor in the original circuit whereas in the potential divider model the thermistors are modified by the other components in the circuit. This is the major difference between the two models. In order to form a circuit model of this mathematical expression an amplifier is needed, as in figure 7.7.

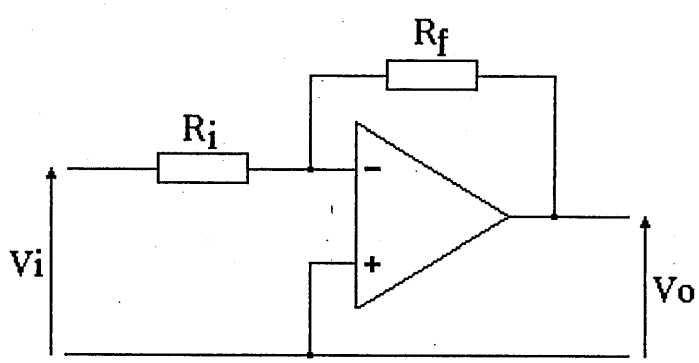

Figure 7.7. Amplifier circuit which forms the basis of the second model

The gain of this circuit is given by

$$\frac{V_o}{V_i} = \frac{-R_f}{R_i} \qquad (7.23)$$

With this model there is the slight problem of the negative gain of the amplifier. However, this merely means that a factor of -1 has to be introduced. One way of representing this is to make the input voltage negative which is shown in figure 7.8 which shows the amplifier based model of the circuit. Another way of introducing the factor of -1 is to use an amplifier of gain -1 which was the approach used in the experimental networks.

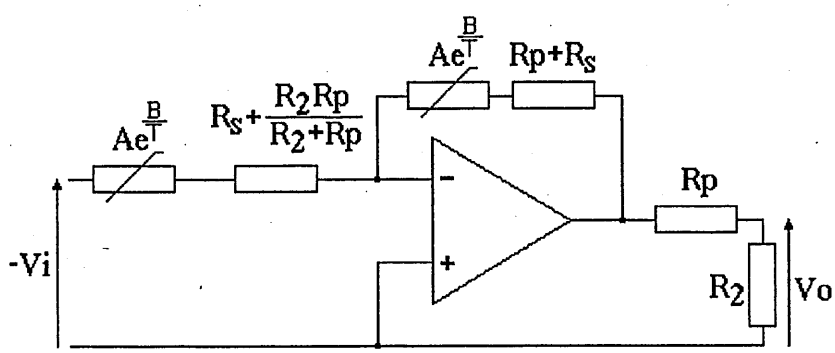

Figure 7.8. Circuit model based on the gain of an amplifier

If a Res_s block is put in the position of R_i of figure 7.7 the gain of the circuit is given by (7.24)

$$\frac{V_o}{V_i} = \frac{\mathbf{R_f}\left[\frac{B}{AeT} + \mathbf{R_p} + \mathbf{R_s}\right]}{\mathbf{R_p}\left[\frac{B}{AeT} + \mathbf{R_s}\right]} \qquad (7.24)$$

Bold characters are used to distinguish the resistors of this circuit from those of the potential divider circuit. When the form of (7.24) is compared with that of (7.22) the similarities are clear. Values can be determined so that this new circuit is functionally identical to the potential divider circuit that was the starting point. These values are given in table 7.1.

Table 7.1.
Comparison of the resistor values of the two circuits

Resistors of amplifier circuit	Resistors of potential divider circuit
$\mathbf{R_p}$	$\frac{R_p^2}{R_2+R_p}$
$\mathbf{R_s}$	$R_s+\frac{R_2R_p}{R_2+R_p}$
$\mathbf{R_f}$	$\frac{R_2R_p^2}{R_2+R_p}$

The results so far show that there are two models that can be used to describe the potential divider circuit, which was considered as the basic starting point for circuits to be used for temperature compensation networks in the crystal oscillator. These circuits aid in understanding how the simple network considered so far operates. Also from this work the relationship between a practical potential divider and a practical amplifier circuit is presented. The next thing to be considered is how the mathematics apply to a full temperature compensation network.

7.7. Application to temperature compensation networks

Having established the two basic forms that the mathematical expressions which describe the action of the compensation networks could be presented, attention moved to the first network to give results that were within $\pm$0.5ppm in the optimisation process, described in section 6.7. The network diagram is reproduced here for ease of reference, as figure 7.9.

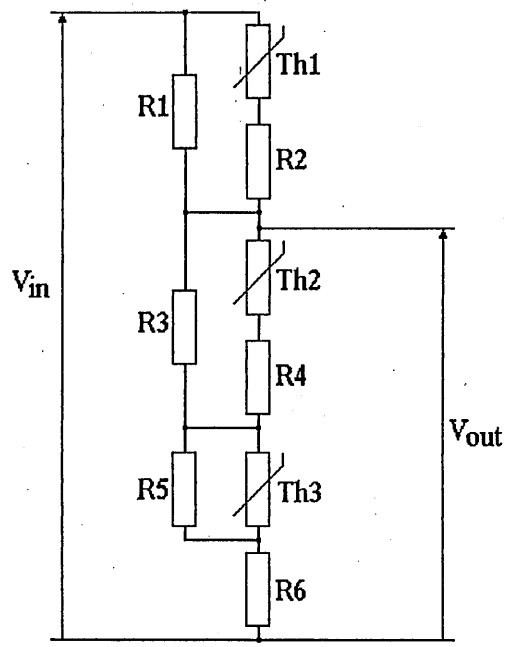

Figure 7.9. Circuit diagram of the first successful theoretical compensation network

In terms of the Res combinations the gain of this network is given by

$$\frac{V_o}{V_i} = \frac{Res_{s2} + Res_{p2}}{Res_{s1} + Res_{s2} + Res_{p2}} \tag{7.25}$$

Replacing the Res combinations by their associated components in the circuit gives

$$\frac{V_o}{V_i} = \frac{\dfrac{R_4 A_2 e^{\frac{B_2}{T}} + R_3 R_4}{A_2 e^{\frac{B_2}{T}} + R_3 + R_4} + \dfrac{(R_5 + R_6) A_3 e^{\frac{B_3}{T}} + R_5 R_6}{A_3 e^{\frac{B_3}{T}} + R_5}}{\dfrac{R_2 A_1 e^{\frac{B_1}{T}} + R_1 R_2}{A_1 e^{\frac{B_1}{T}} + R_1 + R_2} + \dfrac{R_4 A_2 e^{\frac{B_2}{T}} + R_3 R_4}{A_2 e^{\frac{B_2}{T}} + R_3 + R_4} + \dfrac{(R_5 + R_6) A_3 e^{\frac{B_3}{T}} + R_5 R_6}{A_3 e^{\frac{B_3}{T}} + R_5}} \tag{7.26}$$

Rearranging gives

$$\frac{V_o}{V_i} = \frac{\left[A_1 e^{\frac{B_1}{T}} + R_1 + R_2\right]\left[R_4 A_2 e^{\frac{B_2}{T}} + R_3 R_4\right]\left[A_3 e^{\frac{B_3}{T}} + R_5\right] + \left[A_1 e^{\frac{B_1}{T}} + R_1 + R_2\right]\left[A_2 e^{\frac{B_2}{T}} + R_3 + R_4\right]\left[(R_5 + R_6) A_3 e^{\frac{B_3}{T}} + R_5 R_6\right]}{\left[R_2 A_1 e^{\frac{B_1}{T}} + R_1 R_2\right]\left[A_2 e^{\frac{B_2}{T}} + R_3 + R_4\right]\left[A_3 e^{\frac{B_3}{T}} + R_5\right] + \left[A_1 e^{\frac{B_1}{T}} + R_1 + R_2\right]\left[R_4 A_2 e^{\frac{B_2}{T}} + R_3 R_4\right]\left[A_3 e^{\frac{B_3}{T}} + R_5\right] + \left[A_1 e^{\frac{B_1}{T}} + R_1 + R_2\right]\left[A_2 e^{\frac{B_2}{T}} + R_3 + R_4\right]\left[(R_5 + R_6) A_3 e^{\frac{B_3}{T}} + R_5 R_6\right]} \quad (7.27)$$

Mathematical expressions which describe the operation of this network are much more complicated than those obtained for the simple networks due to the larger number of components used to make the network. However, the models obtained in section 7.6, the potential divider model and the amplifier feedback model, can both be extracted from (7.27).

First, the potential divider model will be presented, then the amplifier feedback model. The expression for gain of the compensation network when it is modelled as an imaginary potential divider is given by

$$\left[\begin{array}{r}
(R_4+R_5+R_6)A_1A_2A_3e^{\left(\frac{B_1+B_2+B_3}{T}\right)} \\
+R_5(R_4+R_6)A_1A_2e^{\left(\frac{B_1+B_2}{T}\right)} \\
+(R_3(R_4+R_5+R_6)+(R_4(R_5+R_6)))A_1A_3e^{\left(\frac{B_1+B_3}{T}\right)} \\
+(R_1+R_2)(R_4+R_5+R_6)A_2A_3e^{\left(\frac{B_2+B_3}{T}\right)} \\
+(R_3R_5(R_4+R_6)+R_4R_5R_6)A_1e^{\frac{B_1}{T}} \\
+R_5(R_1+R_2)(R_4+R_6)A_2e^{\frac{B_2}{T}} \\
+(R_1+R_2)(R_3R_4+(R_3+R_4)(R_4+R_6))A_3e^{\frac{B_3}{T}} \\
+(R_1+R_2)(R_3R_5(R_4+R_6)+R_4R_5R_6)
\end{array}\right]$$

$$\frac{V_0}{V_i} = \frac{\left[\begin{array}{r}
(R_4+R_5+R_6)A_1A_2A_3e^{\left(\frac{B_1+B_2+B_3}{T}\right)} \\
+R_5(R_4+R_6)A_1A_2e^{\left(\frac{B_1+B_2}{T}\right)} \\
+(R_3(R_4+R_5+R_6)+(R_4(R_5+R_6)))A_1A_3e^{\left(\frac{B_1+B_3}{T}\right)} \\
+(R_1+R_2)(R_4+R_5+R_6)A_2A_3e^{\left(\frac{B_2+B_3}{T}\right)} \\
+(R_3R_5(R_4+R_6)+R_4R_5R_6)A_1e^{\frac{B_1}{T}} \\
+R_5(R_1+R_2)(R_4+R_6)A_2e^{\frac{B_2}{T}} \\
+(R_1+R_2)(R_3R_4+(R_3+R_4)(R_4+R_6))A_3e^{\frac{B_3}{T}} \\
+(R_1+R_2)(R_3R_5(R_4+R_6)+R_4R_5R_6)
\end{array}\right] + \left[\begin{array}{r}
R_2A_1A_2A_3e^{\left(\frac{B_1+B_2+B_3}{T}\right)} \\
+R_2R_5A_1A_2e^{\left(\frac{B_1+B_2}{T}\right)} \\
+R_2(R_3+R_4)A_1A_3e^{\left(\frac{B_1+B_3}{T}\right)} \\
+R_1R_2A_2A_3e^{\left(\frac{B_2+B_3}{T}\right)} \\
+R_2R_5(R_3+R_4)A_1e^{\frac{B_1}{T}} \\
+R_1R_2R_5A_2e^{\frac{B_2}{T}} \\
+R_1R_2(R_3+R_4)A_3e^{\frac{B_3}{T}} \\
+R_1R_2R_5(R_3+R_4)
\end{array}\right]}{} \quad (7.28)$$

This expression represents the gain of the circuit shown in figure 7.10.

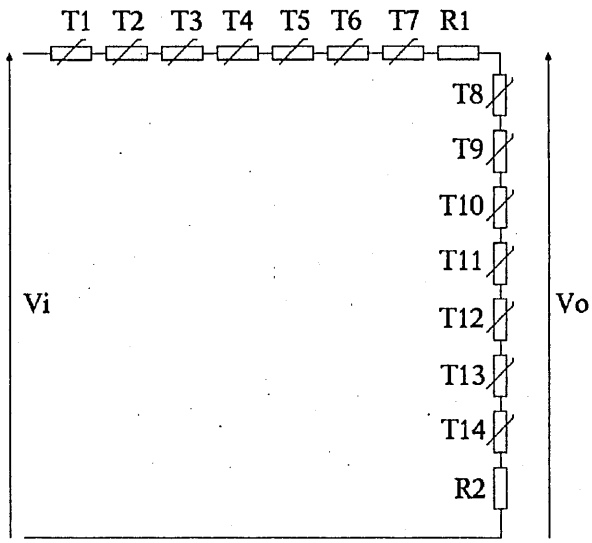

$$T1 = R_2A_1A_2A_3e^{\left(\frac{B_1+B_2+B_3}{T}\right)}$$

$$T2 = R_2R_5A_1A_2e^{\left(\frac{B_1+B_2}{T}\right)}$$

$$T3 = R_2(R_3+R_4)A_1A_3e^{\left(\frac{B_1+B_3}{T}\right)}$$

$$T4 = R_1R_2A_2A_3e^{\left(\frac{B_2+B_3}{T}\right)}$$

$$T5 = R_2R_5(R_3+R_4)A_1e^{\frac{B_1}{T}}$$

$$T6 = R_1R_2R_5A_2e^{\frac{B_2}{T}}$$

$$T7 = R_1R_2(R_3+R_4)A_3e^{\frac{B_3}{T}}$$

$$R1 = R_1R_2R_5(R_3+R_4)$$

$$T8 = (R_4+R_5+R_6)A_1A_2A_3e^{\left(\frac{B_1+B_2+B_3}{T}\right)}$$

$$T9 = R_5(R_4+R_6)A_1A_2e^{\left(\frac{B_1+B_2}{T}\right)}$$

$$T10 = (R_3(R_4+R_5+R_6)+(R_4(R_5+R_6)))A_1A_3e^{\left(\frac{B_1+B_3}{T}\right)}$$

$$T11 = (R_1+R_2)(R_4+R_5+R_6)A_2A_3e^{\left(\frac{B_2+B_3}{T}\right)}$$

$$T12 = (R_3R_5(R_4+R_6)+R_4R_5R_6)A_1e^{\frac{B_1}{T}}$$

$$T13 = R_5(R_1+R_2)(R_4+R_6)A_2e^{\frac{B_2}{T}}$$

$$T14 = (R_1+R_2)(R_3R_4+(R_3+R_4)(R_4+R_6))A_3e^{\frac{B_3}{T}}$$

$$R2 = (R_1+R_2)(R_3R_5(R_4+R_6)+R_4R_5R_6)$$

Figure 7.10. Potential divider model of the compensation circuit.

Gathering the terms to form the straight forward ratio expression gives:

$$\frac{V_0}{V_i} = \frac{\begin{array}{l}(R_4+R_5+R_6)A_1A_2A_3e^{\left(\frac{B_1+B_2+B_3}{T}\right)} + R_5(R_4+R_6)A_1A_2e^{\left(\frac{B_1+B_2}{T}\right)} \\ +(R_3(R_4+R_5+R_6)+(R_4(R_5+R_6)))A_1A_3e^{\left(\frac{B_1+B_3}{T}\right)} \\ +(R_1+R_2)(R_4+R_5+R_6)A_2A_3e^{\left(\frac{B_2+B_3}{T}\right)} \\ +(R_3R_5(R_4+R_6)+R_4R_5R_6)A_1e^{\frac{B_1}{T}} + R_5(R_1+R_2)(R_4+R_6)A_2e^{\frac{B_2}{T}} \\ +(R_1+R_2)(R_3R_4+(R_3+R_4)(R_4+R_6))A_3e^{\frac{B_3}{T}} \\ \\ +(R_1+R_2)(R_3R_5(R_4+R_6)+R_4R_5R_6)\end{array}}{\begin{array}{l}(R_2+R_4+R_5+R_6)A_1A_2A_3e^{\left(\frac{B_1+B_2+B_3}{T}\right)} + R_5(R_2+R_4+R_6)A_1A_2e^{\left(\frac{B_1+B_2}{T}\right)} \\ +(R_3R_4+(R_3+R_4)(R_2+R_5+R_6))A_1A_3e^{\left(\frac{B_1+B_3}{T}\right)} \\ +(R_1(R_2+R_4+R_5+R_6)+R_2(R_4+R_5+R_6)A_2A_3e^{\left(\frac{B_2+B_3}{T}\right)} \\ +(R_3R_5(R_2+R_4+R_6)+R_4R_5A_1e^{\frac{B_1}{T}} + R_5((R_1+R_2)(R_4+R_6)+R_1R_2)A_2e^{\frac{B_2}{T}} \\ +(R_1+R_2)(R_3R_4+(R_3+R_4)(R_4+R_6))A_3e^{\frac{B_3}{T}} \\ \\ +(R_1+R_2)(R_3R_5(R_4+R_6)+R_4R_5R_6)+R_1R_2R_5(R_3+R_4)\end{array}} \quad (7.29)$$

The circuit model for this is shown in figure 7.11.

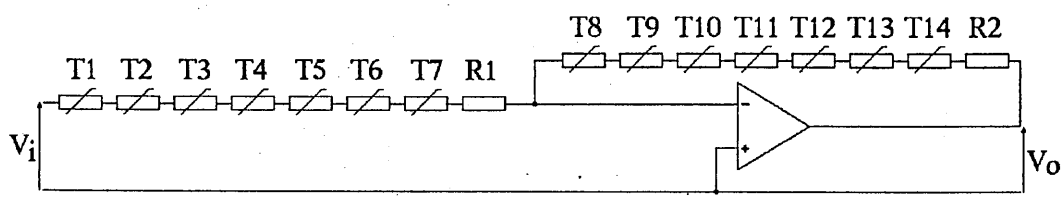

$$T1 = (R_2+R_4+R_5+R_6)A_1A_2A_3e^{(\frac{B_1+B_2+B_3}{T})}$$

$$T2 = R_5(R_2+R_4+R_6)A_1A_2e^{(\frac{B_1+B_2}{T})}$$

$$T3 = (R_3R_4+(R_3+R_4)(R_2+R_5+R_6))A_1A_3e^{(\frac{B_1+B_3}{T})}$$

$$T4 = (R_1(R_2+R_4+R_5+R_6)+R_2(R_4+R_5+R_6)A_2A_3e^{(\frac{B_2+B_3}{T})}$$

$$T5 = (R_3R_5(R_2+R_4+R_6)+R_4R_5A_1e^{\frac{B_1}{T}}$$

$$T6 = R_5((R_1+R_2)(R_4+R_6)+R_1R_2)A_2e^{\frac{B_2}{T}}$$

$$T7 = (R_1+R_2)(R_3R_4+(R_3+R_4)(R_4+R_6))A_3e^{\frac{B_3}{T}}$$

$$R1 = (R_1+R_2)(R_3R_5(R_4+R_6)+R_4R_5R_6)+R_1R_2R_5(R_3+R_4)$$

$$T8 = (R_4+R_5+R_6)A_1A_2A_3e^{(\frac{B_1+B_2+B_3}{T})}$$

$$T9 = R_5(R_4+R_6)A_1A_2e^{(\frac{B_1+B_2}{T})}$$

$$T10 = (R_3(R_4+R_5+R_6)+(R_4(R_5+R_6)))A_1A_3e^{(\frac{B_1+B_3}{T})}$$

$$T11 = (R_1+R_2)(R_4+R_5+R_6)A_2A_3e^{(\frac{B_2+B_3}{T})}$$

$$T12 = (R_3R_5(R_4+R_6)+R_4R_5R_6)A_1e^{\frac{B_1}{T}}$$

$$T13 = R_5(R_1+R_2)(R_4+R_6)A_2e^{\frac{B_2}{T}}$$

$$T14 = (R_1+R_2)(R_3R_4+(R_3+R_4)(R_4+R_6))A_3e^{\frac{B_3}{T}}$$

$$R2 = (R_1+R_2)(R_3R_5(R_4+R_6)+R_4R_5R_6)$$

Figure 7.11. Model of the compensation network based on an amplifier

These two forms do not, currently, appear to be very useful because the operation of the network cannot be readily be determined just by examining the expression. The action of the series resistors in cancelling the operation of each thermistor as

described in section 7.4 is not readily apparent for the full compensation circuit being considered here. The trivial cases, when the thermistors are large and when the thermistors are small, are readily identified for both of the models. However, this is not the case for the remainder of the terms in the expressions and the further development of this approach is the subject of future work.

7.8. Development of the mathematics of the second model

An attempt to factorise the numerator and denominator was made by forming a general expression with known factors and comparing coefficients. The factors taken were:

$$\left[\alpha A_1 e^{\frac{B_1}{T}} + \beta\right]\left[\gamma A_2 e^{\frac{B_2}{T}} + \delta\right]\left[\varepsilon A_3 e^{\frac{B_3}{T}} + \phi\right] \qquad (7.30)$$

Taking α, γ and ε as a common factor in their respective brackets gives

$$\alpha\gamma\varepsilon\left[A_1 e^{\frac{B_1}{T}} + \frac{\beta}{\alpha}\right]\left[A_2 e^{\frac{B_2}{T}} + \frac{\delta}{\gamma}\right]\left[A_3 e^{\frac{B_3}{T}} + \frac{\phi}{\varepsilon}\right] \qquad (7.31)$$

Here each bracket comprises an exponential term which is the mathematical model, used to describe the behaviour of the NTC thermistors, and a constant term which represents a fixed resistor. Hence each bracket represents a thermistor and a resistor connected in series.

Multiplying out (7.31) gives

$$\alpha\gamma\varepsilon\left(A_1A_2A_3e^{\left[\frac{B_1+B_2+B_3}{T}\right]}+\frac{\phi}{\varepsilon}A_1A_2e^{\left[\frac{B_1+B_2}{T}\right]}+\frac{\delta}{\gamma}A_1A_3e^{\left[\frac{B_1+B_3}{T}\right]}+\frac{\beta}{\alpha}A_2A_3e^{\left[\frac{B_2+B_3}{T}\right]}\right.$$

$$\left.+\frac{\delta\phi}{\gamma\varepsilon}A_1e^{\frac{B_1}{T}}+\frac{\beta\phi}{\alpha\varepsilon}A_2e^{\frac{B_2}{T}}+\frac{\beta\delta}{\alpha\gamma}A_3e^{\frac{B_3}{T}}+\frac{\beta\delta\phi}{\alpha\gamma\varepsilon}\right) \qquad (7.32)$$

In (7.32) the constant terms of the factors of (7.31) appear as coefficients. An attempt was made to determine whether the expression of (7.29) would factorise. For the numerator of (7.29) there are two forms presented; the first form is the coefficients of the expression (7.29) and the second form is the result obtained by multiplying out the brackets which have the constant terms taken from the expression.

Table 7.1. Comparison of numerator coefficients

	Coefficients from (7.29)	Products of (7.32)
$\alpha\gamma\varepsilon$	$R_4+R_5+R_6$	$R_4+R_5+R_6$
$\frac{\beta}{\alpha}$	R_1+R_2	R_1+R_2
$\frac{\delta}{\gamma}$	$R_3+\frac{R_4(R_5+R_6)}{R_4+R_5+R_6}$	$R_3+\frac{R_4(R_5+R_6)}{R_4+R_5+R_6}$
$\frac{\phi}{\varepsilon}$	$\frac{R_5(R_4+R_6)}{R_4+R_5+R_6}$	$\frac{R_5(R_4+R_6)}{R_4+R_5+R_6}$
$\frac{\beta\delta}{\alpha\gamma}$	$\frac{(R_1+R_2)(R_3R_4+(R_3+R_4)(R_5+R_6))}{R_4+R_5+R_6}$	$\frac{(R_1+R_2)(R_3R_4+(R_3+R_4)(R_5+R_6))}{R_4+R_5+R_6}$
$\frac{\beta\phi}{\alpha\varepsilon}$	$\frac{R_5(R_1+R_2)(R_4+R_6)}{R_4+R_5+R_6}$	$\frac{R_5(R_1+R_2)(R_4+R_6)}{R_4+R_5+R_6}$
$\frac{\delta\phi}{\gamma\varepsilon}$	$\frac{R_3R_5(R_4+R_6)+R_4R_5R_6}{R_4+R_5+R_6}$	$\frac{R_3R_5(R_4+R_6)+R_4R_5R_6}{R_4+R_5+R_6}+\left[\frac{R_4R_5}{R_4+R_5+R_6}\right]^2$
$\frac{\beta\delta\phi}{\alpha\gamma\varepsilon}$	$\frac{R_3R_5(R_4+R_6)+R_4R_5R_6}{R_4+R_5+R_6}\times(R_1+R_2)$	(above) $\times(R_1+R_2)$

A similar table is drawn up for the denominator. However for reasons of space the right hand column for the denominator is drawn up to show how the product differs from the coefficients of the expression.

Table 7.2. Comparison of denominator coefficients

	Coefficients from (7.29)	Differences from LH column
$\alpha\gamma\varepsilon$	$R_2+R_4+R_5+R_6$	
$\frac{\beta}{\alpha}$	$R_1+\frac{R_2(R_4+R_5+R_6)}{R_2+R_4+R_5+R_6}$	
$\frac{\delta}{\gamma}$	$\frac{(R_3R_4+(R_3+R_4)(R_2+R_5+R_6))}{R_2+R_4+R_5+R_6}$	
$\frac{\phi}{\varepsilon}$	$\frac{R_5(R_2+R_4+R_6)}{R_2+R_4+R_5+R_6}$	
$\frac{\beta\delta}{\alpha\gamma}$	$\frac{(R_1+R_2)(R_3R_4+(R_3+R_4)(R_5+R_6))}{R_2+R_4+R_5+R_6}$	$\left[\frac{R_2R_4}{R_2+R_4+R_5+R_6}\right]^2$
$\frac{\beta\phi}{\alpha\varepsilon}$	$\frac{R_5((R_1+R_2)(R_4+R_6)+R_1R_2)}{R_2+R_4+R_5+R_6}$	$\left[\frac{R_2R_5}{R_2+R_4+R_5+R_6}\right]^2$
$\frac{\delta\phi}{\gamma\varepsilon}$	$\frac{R_3R_5(R_2+R_4+R_6)+R_4R_5(R_2+R_6)}{R_2+R_4+R_5+R_6}$	$\left[\frac{R_4R_5}{R_2+R_4+R_5+R_6}\right]^2$
$\frac{\beta\delta\phi}{\alpha\gamma\varepsilon}$	$\frac{(R_1+R_2)(R_3R_5(R_4+R_6)+R_4R_5R_6)+R_1R_2R_5(R_3+R_4)}{R_2+R_4+R_5+R_6}$	see below (7.33)

The difference of the product term is

$$\frac{R_5^2(R_2^2(R_3+R_4)+R_4^2(R_1+R_2))}{(R_2+R_4+R_5+R_6)^2}+\frac{R_5(R_2+R_4+R_6)(R_2R_4)^2}{(R_2+R_4+R_5+R_6)^3} \qquad (7.33)$$

These results show that when the factorised form of the expression is multiplied out, the original expression is not obtained. However, the result that is obtained is quite close to the original and it is considered that further work on this form might explain the source of the cross products and whether they have a significant effect on the results.

Although currently the factorised form cannot be used with the potential divider network, it was considered that the factorised form of the expression might be implemented in a practical form based on the amplifier arrangement described in section 7.6. The generalised form for temperature compensation would be

$$\frac{V_o}{V_i} = \frac{\alpha\gamma\varepsilon\left[A_1 e^{\frac{B_1}{T}} + \frac{\beta}{\alpha}\right]\left[A_2 e^{\frac{B_2}{T}} + \frac{\delta}{\gamma}\right]\left[A_3 e^{\frac{B_3}{T}} + \frac{\phi}{\varepsilon}\right]}{acf\left[A_1 e^{\frac{B_1}{T}} + \frac{b}{a}\right]\left[A_2 e^{\frac{B_2}{T}} + \frac{d}{c}\right]\left[A_3 e^{\frac{B_3}{T}} + \frac{g}{f}\right]} \qquad (7.34)$$

This is a product expression of the simple network. For each of the thermistors there is a pair of bracketed terms, one in the numerator and one in the denominator. The gain characteristic for an amplifier with a thermistor Res_s block in the R_f position is given by

$$\frac{V_o}{V_i} = \frac{R_p\left[Ae^{\frac{B}{T}} + R_s\right]}{R_i\left[Ae^{\frac{B}{T}} + R_p + R_s\right]} \qquad (7.35)$$

And for the Res_p block in the R_f position the gain is given by

$$\frac{V_o}{V_i} = \frac{(R_p + R_s)\left[Ae^{\frac{B}{T}} + \frac{R_p R_s}{R_p + R_s}\right]}{R_i\left[Ae^{\frac{B}{T}} + R_p\right]} \qquad (7.36)$$

For both these arrangements each of the constant terms is determined by one resistor. In (7.35), for example, R_s is the constant term in the numerator bracket, R_p is added to R_s to give the constant term in the denominator and the constant gain is set by R_i in relationship with R_p. This contrasts with the operation of the potential divider form of the compensation network where each resistor does not act independently. A practical realisation of this compensation circuit is shown in figure 7.12 where R is a fixed resistor and Res1, Res2 and Res3 are Res combinations and each can be either Res_p or Res_s.

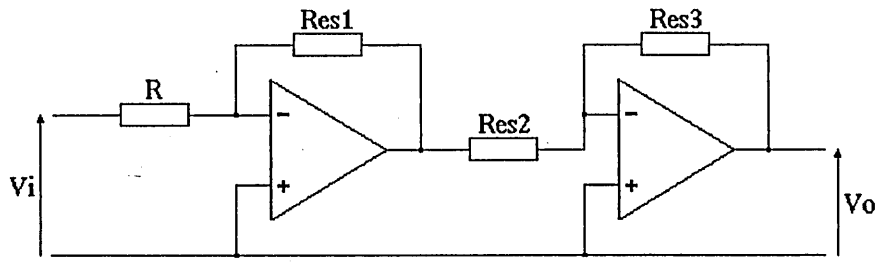

Figure 7.13. Practical realisation of the alternative compensation circuit

This arrangement has been tried in a three thermistor form in the optimiser using a modelled cubic function with good results, shown in figure 7.14.

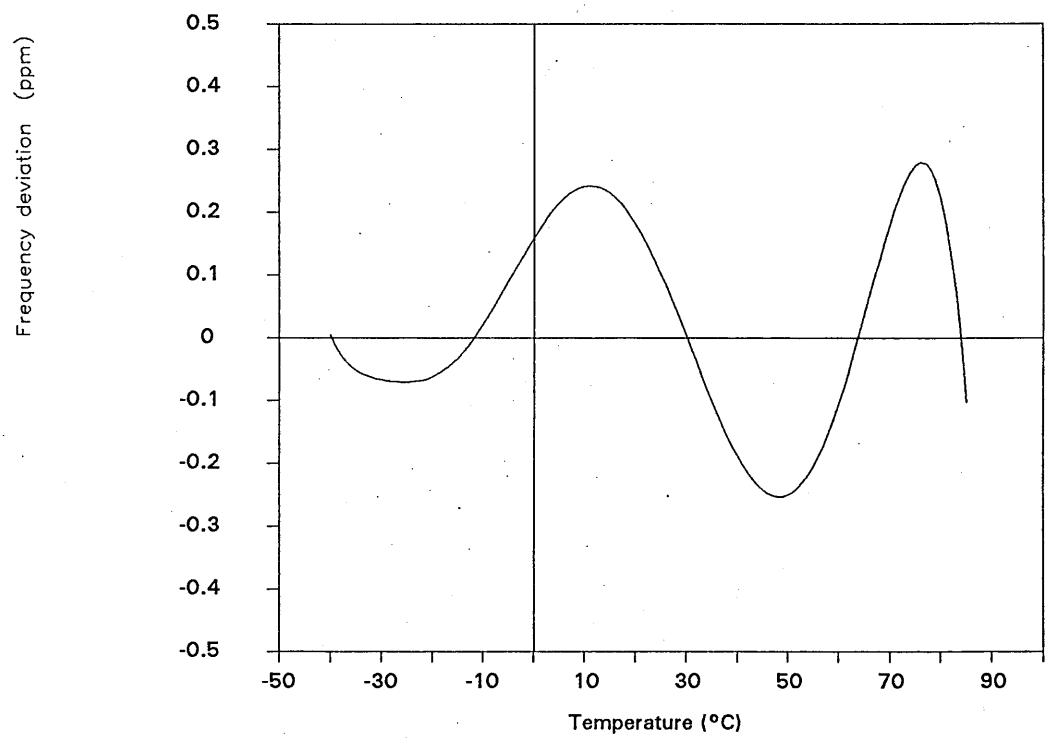

Figure 7.14. Three thermistor model matching a cubic characteristic corresponding to a 6'crystal angle.

An advantage of working with a compensation network of this form is that it is fairly trivial to determine starting values for the resistors in the optimisation process because the temperature range required of each thermistor is known. So the starting values of the resistors can be selected based on the resistance of each thermistor at the appropriate temperature.

7.9. References

[1] Macklen, E. D. (1979). Thermistors, *Electrochemical Publications Ltd., Ayr*, pp 29-36.

[2] Steinhart, J. S. and Hart, R. (1968). Calibration curves for thermistors. *Deep-Sea Research, vol. 15*, pp.497-503.

8. DIGITAL COMPENSATION

8.1. Introduction

An important field in modern methods of temperature compensation is the use of digital electronics techniques, and it was considered appropriate that some work be done in this area.

Indirect digital temperature compensated crystal oscillators (DTCXO's) employ digital electronics techniques to generate the compensation voltage applied to the varactor diode to offset the temperature induced frequency deviations. The technique is applied by forming a digital representation of the ambient temperature. This digital representation is used to determine the required digital representation of the compensation voltage for that temperature. Finally the digital compensation voltage is converted to the analogue voltage used to tune the oscillator, as in figure 8.1.

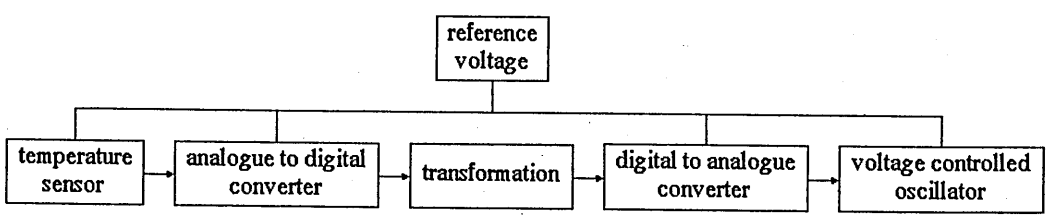

Figure 8.1. General arrangement of a digital temperature compensation circuit.

Digital temperature compensation is capable of achieving higher degrees of frequency stability than analogue temperature compensation because the digital techniques can be more closely matched to the required temperature to tuning voltage transformation. The research described in this chapter is concerned with ways of implimenting the transformation from digitised temperature to digitised compensation voltage.

8.2. Determination of digital resolution

In this section a method for determining the resolution of the digital representation of temperature and compensation voltage is presented. Suppose an oscillator is to operate over a temperature range T_1 to T_2. Call the temperature range T. The required compensation voltage range is V_1 to V_2. Call the voltage range V. If the temperature is represented by m bits and the tuning voltage by n bits then there are 2^m temperature levels and 2^n voltage levels represented. The values of m and n are determined by considering the crystal characteristic and the level of compensation required. The resolution of the compensation is given by

$$R = \frac{VP}{2^n} \tag{8.1}$$

where Rppm/bit is the tuning resolution of the DAC and Pppm/V is the tuning sensitivity. Hence the value for n is given by

$$n = \log_2\left\lceil\frac{VP}{R}\right\rceil \tag{8.2}$$

Reading from the crystal characteristic the maximum gradient for frequency deviation against temperature is determined. This gradient is used to determine the number of levels needed in the analogue to digital converter

$$2^m = \frac{GT}{L} \tag{8.3}$$

and hence the value for m

$$m = \log_2\left\lceil\frac{GT}{L}\right\rceil \tag{8.4}$$

where Gppm/K is the maximum gradient and Lppm is the required level of frequency deviation.

The values of m and n are the number of bits needed in the respective converters. Here a fraction of a bit has no meaning so m and n have to be taken as the next highest integer to ensure that there are sufficient levels represented in the converters. Frerking has taken this analysis further to optimise the size of memory device used in the digital circuit [1][2]. At a time when memory components were expensive this was an important exercise. However, memory costs have significantly reduced in the mean-time and reduction of memory size is no longer important.

8.3. Transformation from temperature to voltage

In this section the possible ways of performing the transformation from digitised temperature to digitised compensation voltage are discussed. There are two aspects to be considered; the method of transformation and the hardware implementation. In the analogue temperature compensation circuits considered in this thesis the compensation voltage is a continuous function derived from the exponential relationship between temperature and the resistance of the thermistors in the circuit. In a digital compensation circuit the function used has to be decided. There is no inherent relationship between the input of the ADC and the output of the DAC in a digital system. Such a relationship has to be imposed. Hence a variety of relationships have been reported in the literature.

The general method for characterising a temperature compensated crystal oscillator is to measure its components across the required temperature range, usually at equally spaced temperatures. With a digital temperature compensated crystal oscillator the limit of this is when the temperature increments correspond to the temperature change represented by each bit. Using this approach the compensation data is generated during characterisation and there is no separate customising stage

[3]. However this approach is difficult and very time consuming. The difficulty arises in obtaining precise temperature control over such a wide temperature range. If the temperature increments of the characterisation are greater than the temperature represented by one bit, the gaps that are left in the temperature range have to be filled. Hence a mathematical transformation has to be adopted. This has taken the form of linear interpolation between two adjacent measurements [4], or using the whole data set and performing a polynomial curve fit on the data [5]. Renard and Barnhill [6] compared these three methods of generating the compensation data and concluded that a seventh order curve fit to the data gave optimum results. Miyayama, Ikeda and Okano [7] compared linear interpolation and polynomial curve fitting on measurements made at 10°C intervals over a temperature range -30°C to +80°C. Their polynomial curve fitting results were consistent with the findings of others. However, their results for the linear interpolation appear not to meet the level that might be expected.

8.4. Temperature sensor

There have been many methods for producing the digital representation of temperature but they may be considered in two categories; those that use one crystal as both temperature transducer and compensated resonator and those that use a temperature transducer separate from the crystal. For the investigation described in this thesis a transducer external to the crystal was adopted. The AT cut resonator considered in this investigation is not suitable for use as the temperature transducer. Hence for the research presented in this thesis an external temperature sensor had to be used. The major disadvantage of this approach is that the transducer does not experience exactly the same temperature as the crystal when the thermal environment changes rapidly because the thermal response times of the components are different.

A platinum resistor was chosen as the temperature transducer here because these temperature sensitive resistors have very good long term stability and good linearity. Linearity is important because each bit of the analogue to digital converter must represent an equal change in temperature. The platinum resistor was built into a resistive bridge, shown in figure 8.2, as is usual for this type of device. The resistance values were chosen to make V_o zero at -45°C and the resistance change of the platinum resistor small compared to R_3. Hence the output of the bridge circuit is given by

$$V_o \approx \frac{R_4 V_i}{R_3} - V_{-45} \tag{8.5}$$

where R_4 is the platinum resistor and V_{-45} is the output of the potential divider formed by R_1 and R_2. Over the temperature range -45°C to +90°C the resistance of the platinum resistor changes by approximately 1% of R_3. Hence the approximation holds and the linearity is good. In general the values of R_1 and R_2 are chosen so that V_o is zero at the lowest temperature of the required operating temperature range.

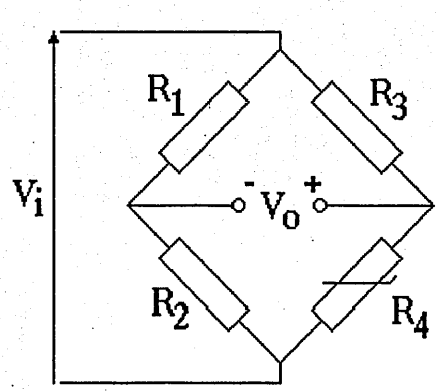

Figure 8.2. Circuit diagram of the temperature sensor bridge

The amplifier used with the bridge circuit is shown in figure 8.3. The temperature range that the temperature sensor will operate is determined by the input voltage range of the analogue to digital converter (ADC) and the gain of the amplifier. If the output of the bridge V_o is in the range 0 to V_{Tmax} and the input voltage range of the ADC is 0 to V_{Cmax} the required gain of the amplifier is given by

$$\text{gain} = \frac{V_{Cmax}}{V_{Tmax}} \tag{8.6}$$

In this arrangement changing the gain of the amplifier changes the operating temperature range of the sensor.

When the bridge and amplifier circuits are combined there is a possible simplification. A potential divider may be represented by a voltage source, equal to the output voltage of the unloaded potential divider, with a series resistance equal to the parallel combination of the two resistors used to form the potential divider. Hence it is possible to modify the amplifier circuit so that R_a is the effective source resistance of the fixed arm of the bridge. The resistor values are then chosen to give the same resistance as the original R_a whilst maintaining their ratio to leave the equivalent voltage source unchanged.

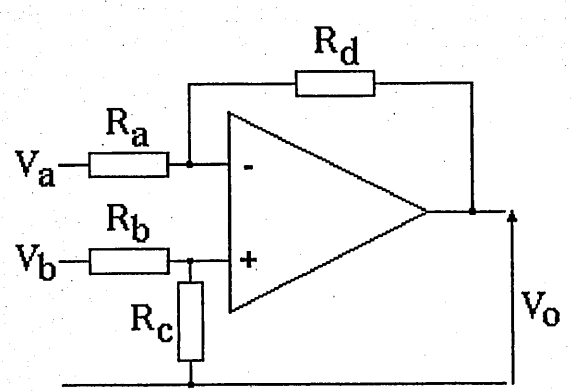

Figure 8.3. Differential amplifier circuit used to amplify the output of the resistance bridge circuit

In figure 8.4 the output voltage against temperature characteristic of the temperature sensor circuit is shown.

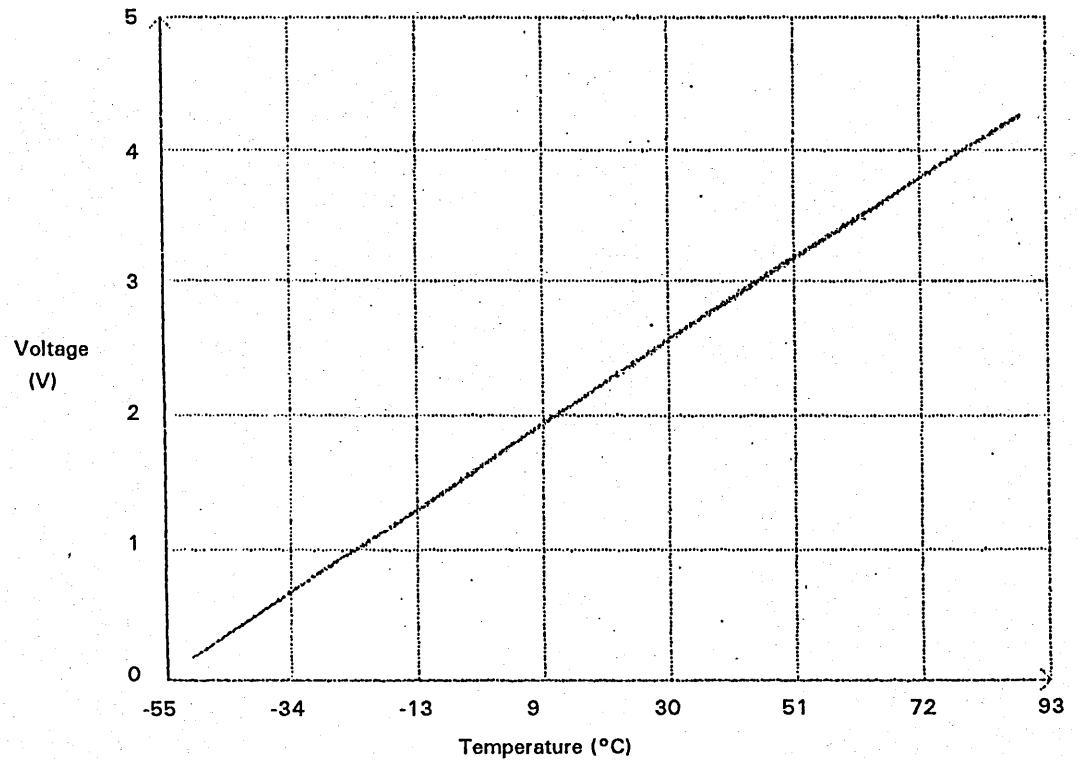

Figure 8.4. Voltage against temperature characteristic of the temperature sensor.

8.5. Polynomial temperature compensation

The objective for this experimental work was to observe the effectiveness of different orders of polynomial for temperature compensation of a crystal oscillator.

8.5.1. Method

The configuration of the apparatus used for the experiments was given in section 5.2. The output voltage of the temperature sensor was measured by the digital voltage meter and the tuning voltage was applied by the precision voltage source. This approach was adopted here so that the results for this work were not obscured

by digital quantisation. The drive circuit used here was the Buttler oscillator circuit described in section 4.6.

The oscillator and temperature sensor were characterised over the temperature range 90°C to -40°C in 5°C increments. An initial stabilisation time of 30 minutes was allowed at 90°C, but for the remaining temperatures a stabilisation time of 15 minutes was allowed. At each temperature the required tuning voltage was determined and the output of the temperature sensor was measured ten times separated in time by 10 seconds and averaged before being recorded to reduce the effects of the environmental chamber's limit cycle. These characterisation measurements were used in a least squares program to determine the coefficients for polynomials from third order to ninth order.

Verification for the polynomial compensation was performed over the same temperature range as characterisation. However, the temperature increment used was 1°C and the stabilisation time was 4 minutes. At each temperature the computer used the output of the temperature sensor to calculate the compensation voltage produced by each polynomial. Then, in turn, each voltage was applied to the oscillator and the corresponding frequency measured. Chamber temperature, temperature sensor output and frequency were recorded for each polynomial at every temperature.

It was considered important that the temperature régimes for the characterisation and the verification were different to ensure that the achievements were repeatable under a variety of conditions. This differs from the method of Renard and Barnhill who used identical thermal conditions for characterisation and verification. An anticipated difficulty was the loose thermal coupling between the crystal and the platinum resistor. However, this was deliberate in order to gain experience of the worst case conditions.

8.5.2. Discussion of results

Typical results for the 3rd, 6th, 7th and 8th order compensation are shown in figures 8.5 to 8.8. Figure 8.5 shows the frequency deviation against temperature when third order compensation is applied to the oscillator. There is a higher order error function other than the third order characteristic expected for an AT cut resonator. The peak magnitude of this error is approximately 0.5ppm which is $\frac{1}{20}$ of that for the uncompensated crystal. Differences between figures 8.6 and 8.7 and between 8.7 and 8.8 are difficult to determine from these figures so these differences are plotted in figures 8.9 and 8.10 with the predicted differences shown as crosses. The agreement between the predicted result and the experimental result in both cases is good. This agreement is better than the agreement between characterisation and verification of the compensation process. This shows that the tuning has remained consistant and that the change is due to changes within the oscillator. The nature of the differences apprear to be regular polynomial functions. The advantage gained in going from seventh order compensation to eighth order compensation is small which is consistant with Renard and Barnhill who concluded that the optimum order for polynomial compensation was seven. The cause of the discrepancy between the predicted results and the verification results is considered to be due to a combination of loose thermal coupling and ageing within the crystal and oscillator.

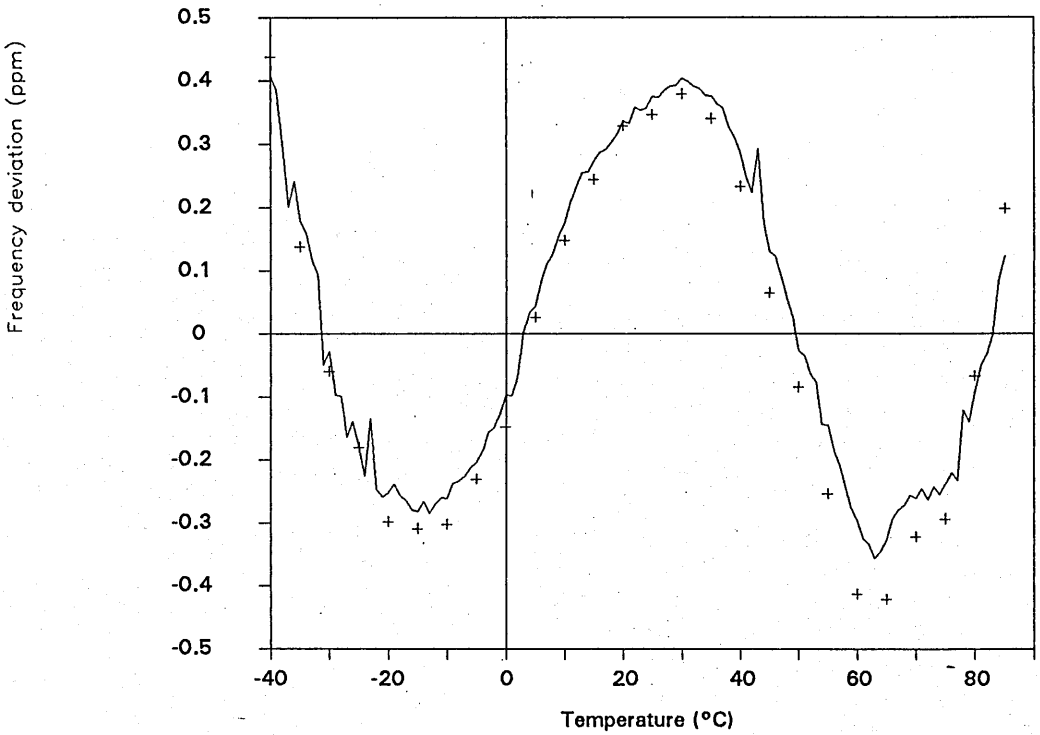

Figure 8.5. Third order compensation.

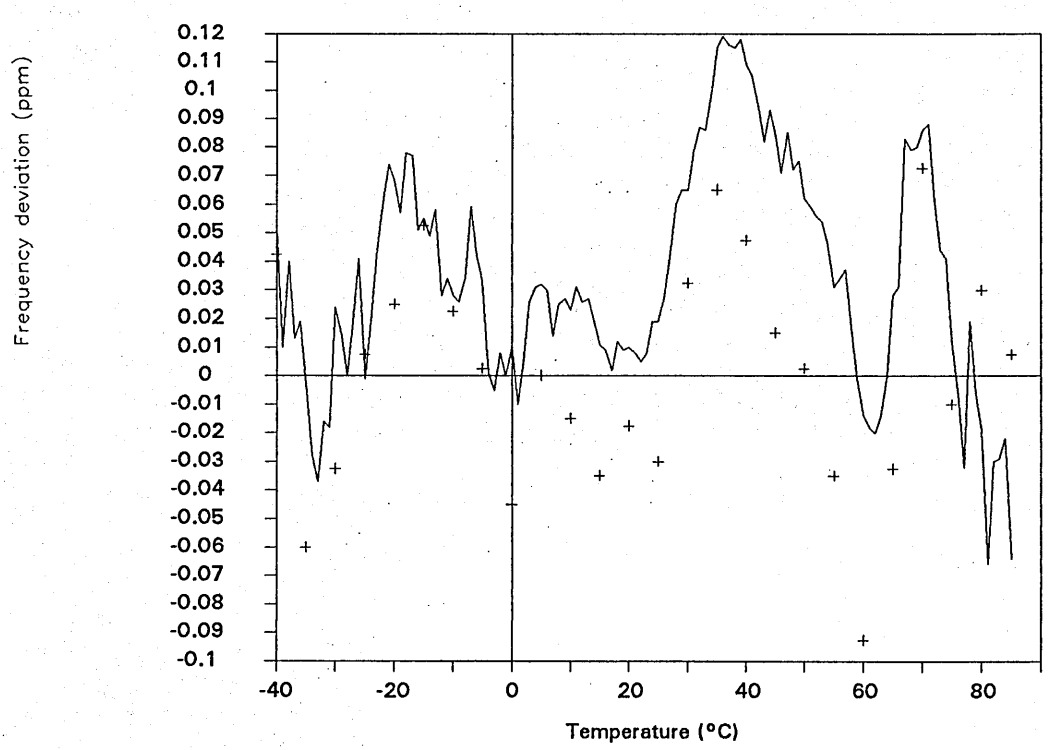

Figure 8.6. Sixth order compensation.

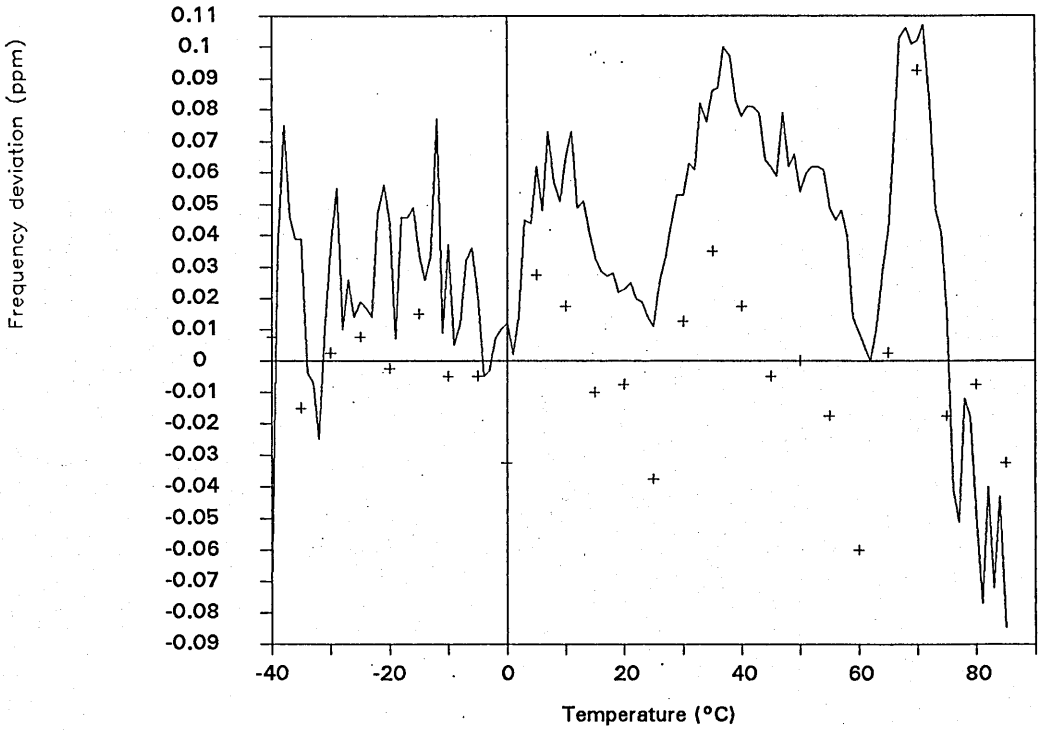

Figure 8.7. Seventh order compensation.

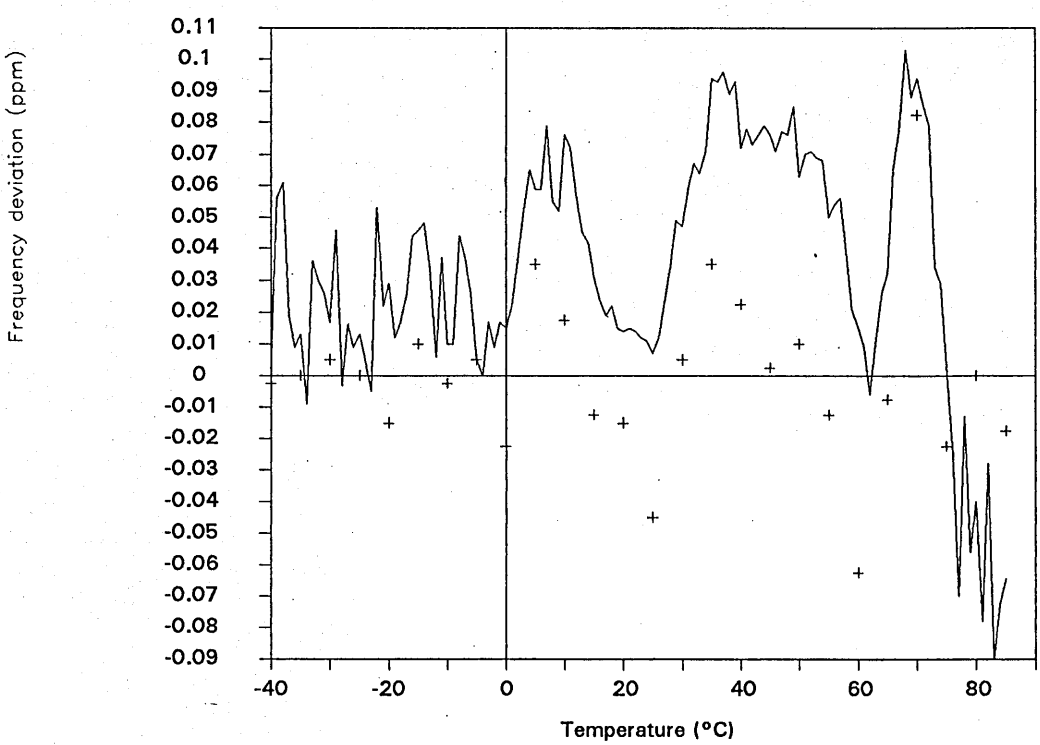

Figure 8.8. Eighth order compensation.

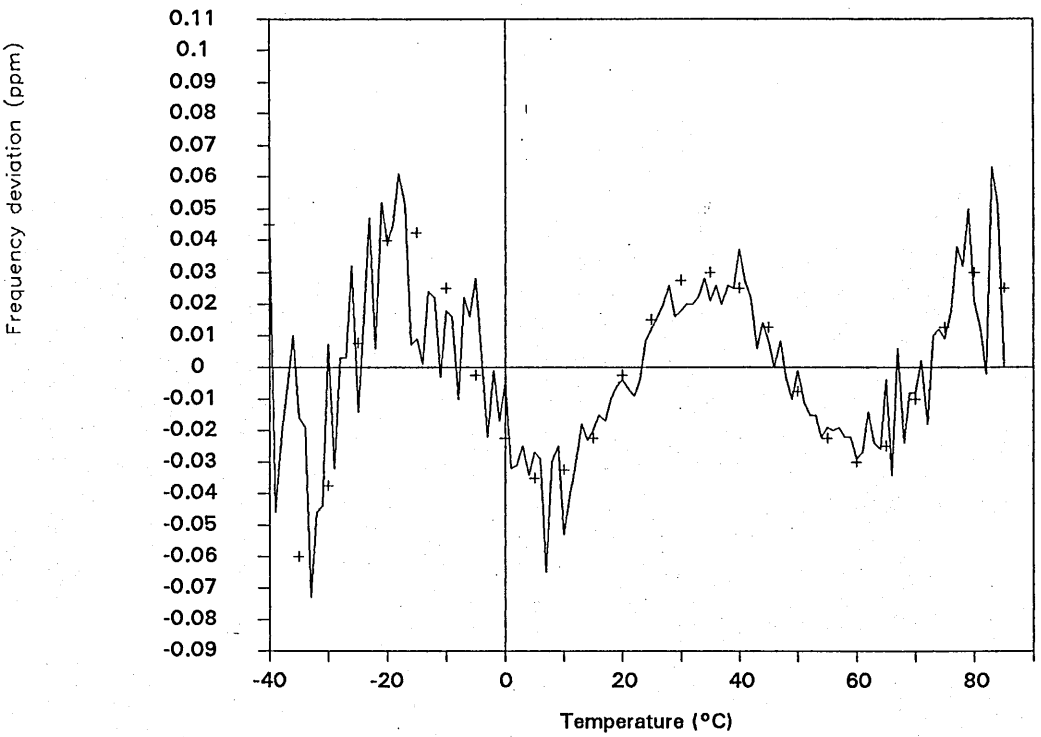

Figure 8.9. Difference between sixth order and seventh order ploynomial compensation.

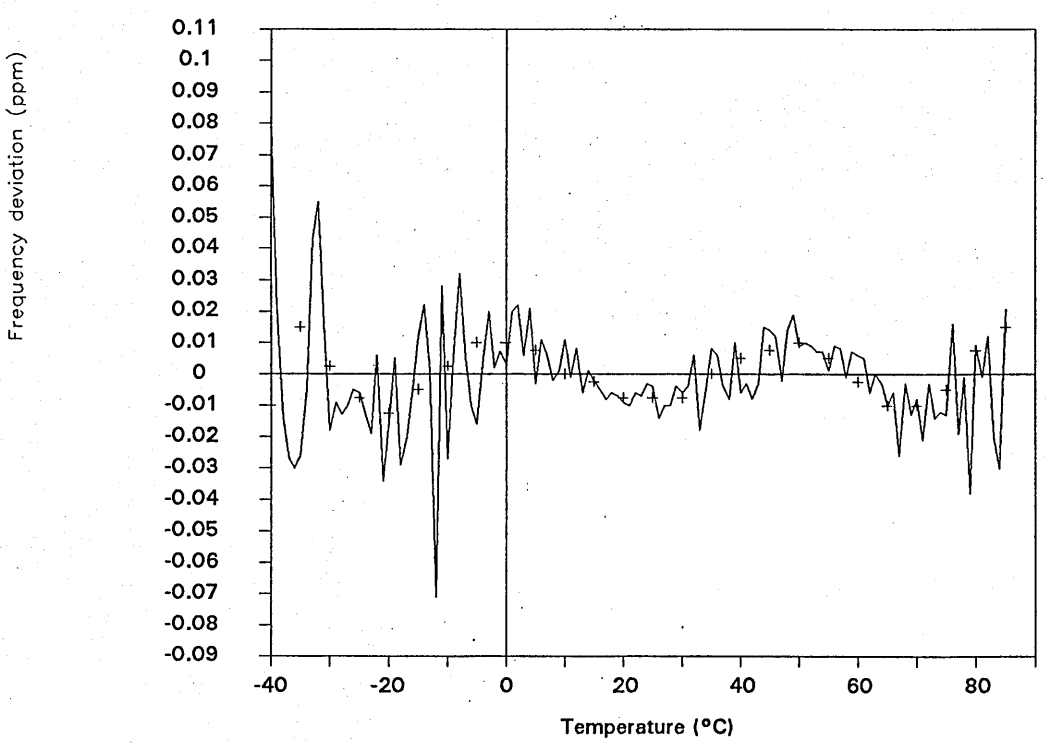

Figure 8.10. Difference between seventhth order and eighth order ploynomial compensation.

8.6. Lagrange interpolation as a means of generating the compensation data

Polynomials generated by least squares curve fitting programs are the most widely published means of generating the compensation data for DTCXO's. Linear interpolation has also been reported to a lesser degree. Linear interpolation has the disadvantage of trying to represent a higher order polynomial function by a series of straight lines. An improved expression for interpolation is the Lagrange interpolation formula which is a means of forming a higher order interpolation function. It was decided to investigate the use of Lagrange interpolation as a means of generating the compensation data.

The investigation into the use of Lagrange interpolation followed two avenues; a simulation was performed on a computer to determine the level of compensation that could be anticipated and an experimental compensation system was used to obtain practical results. Also presented is the Lagrange compensation applied to the data of the previous section.

The Lagrange interpolation formula is a means of generating a function which will pass through a set of known points. Two or more known points can be used. To generate the compensation data four points were used which gives

$$y(x) = \frac{(x-x_2)(x-x_3)(x-x_4)}{(x_1-x_2)(x_1-x_3)(x_1-x_4)} y_1 + \frac{(x-x_1)(x-x_3)(x-x_4)}{(x_2-x_1)(x_2-x_3)(x_2-x_4)} y_2 + \frac{(x-x_1)(x-x_2)(x-x_4)}{(x_3-x_1)(x_3-x_2)(x_3-x_4)} y_3 + \frac{(x-x_1)(x-x_2)(x-x_3)}{(x_4-x_1)(x_4-x_2)(x_4-x_3)} y_4 \qquad (8.7)$$

where y_1, y_2, y_3 and y_4 are known values at x_1, x_2, x_3 and x_4 and $y(x)$ is the interpolated value of y at x. This was applied by using digitised temperature as x and digitised compensation voltage as y.

The measurements made during the characterisation were used in the Lagrange interpolation formula to generate the data for compensation by taking the characterisation data in blocks of 4 data points. If the four data points are considered to be 1,2,3,4 the interpolation was performed for digitised temperatures between points 2 and 3. When all the points between 2 and 3 had been filled the data points used changed position; data for point 2 became data for point 1; data for point 3 became data for point 2; data for point 4 became data for point 3 and the next piece of unused data became data for point 4. At the extremes of temperature the interpolation was extended to generating the data between either 1 and 2 or 3 and 4 depending on whether at the cold end or hot end of the range.

8.6.1. Simulation of the digital compensation circuit.

A simulation of the compensation system was programmed into a computer software package to determine an expected level of compensation. The simulation assumed that the compensation voltage was represented by a polynomial in digitised temperature with roots at 0, 2048 and 4096:

$$V = \frac{-T(T-1028)(T-4096)}{3.30627\times10^{9}} \times 2^{n} \qquad (8.8)$$

where V is the compensation voltage and T is the temperature represented as an integer in the range 0 to 4095. 3.30627×10^{9} is the magnitude of the cubic at the turning points. By dividing by this value the range over the turning points is ±1. n is the number of bits represented in the digital to analogue converter.

Characterisation was simulated by calculating V for 14 values of T, separated by 315 bits. These simulated measurements were put into the Lagrange formula and compensation voltages for all temperatures were determined and compared with results obtained directly from (8.8).

8.6.2. Discussion of the results

A variety of combinations of real numbers and integers were tried to explore the effects of quantisation within the digital system. First the modelled characterisation data and the results of the Lagrange formula were real numbers. This is shown plotted in figure 8.11 and shows the limits of the resolution in the computer to be in the order of 10^{-14}.

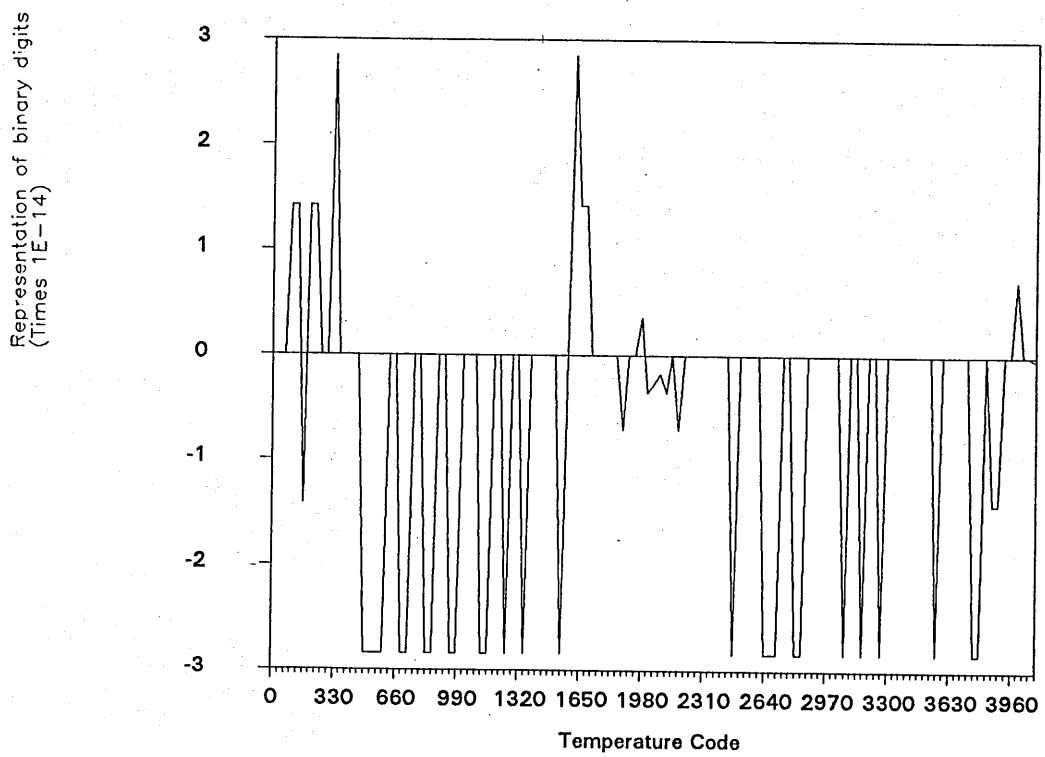

Figure 8.11. Results of both sets of data being real.

Having established that the Lagrange interpolation was working, next the modelled characterisation data was rounded to integer values which represents tuning the oscillator to a frequency error of $< \pm ½$ bit. The results obtained for this are a slow rolling curve which deviates by a maximum of ± 0.5, shown in figure 8.12. The abrupt changes in direction occur when the data points in the Lagrange formula changes.

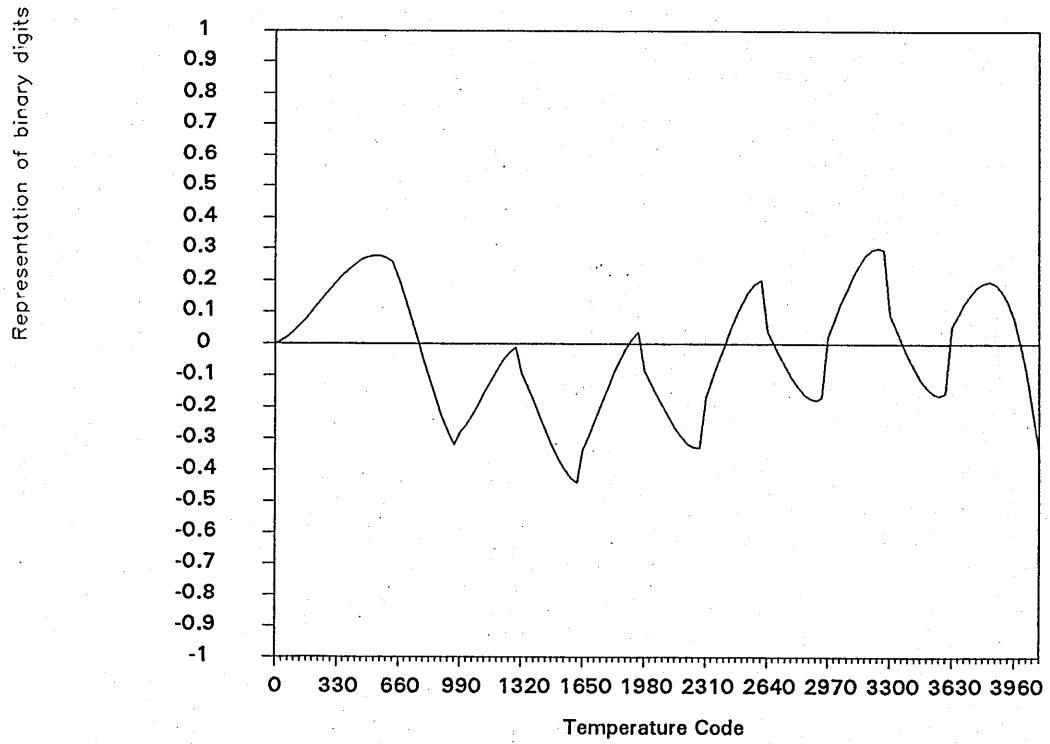

Figure 8.12. Modelled data with integer characterisation data and real compensation data.

The characterisation data was made to be real again and the results from the Lagrange formula were rounded to integer values. The results are shown in figure 8.13 and again deviate by a maximum of ± 0.5. However, this time the graph is very jagged.

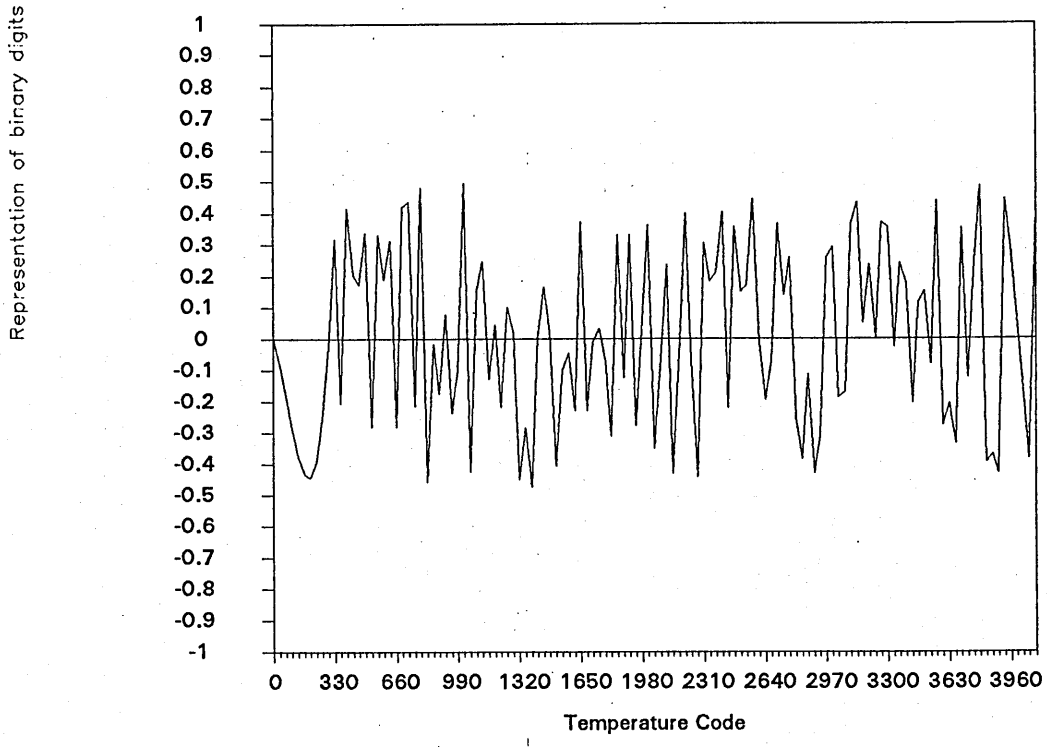

Figure 8.13. Modelled data with integer compensation data and integer characterisation data.

Finally both the simulated characterisation data and the results from the Lagrange interpolation formula were rounded to integers which gives a maximum deviation of ± 0.8 bit, shown in figure 8.14. However, most of the points still lie inside ± 0.5 bit. The results are similar regardless of the value of n. For the graphs presented here $n = 8$, consistent with the DAC being used in the practical experiments.

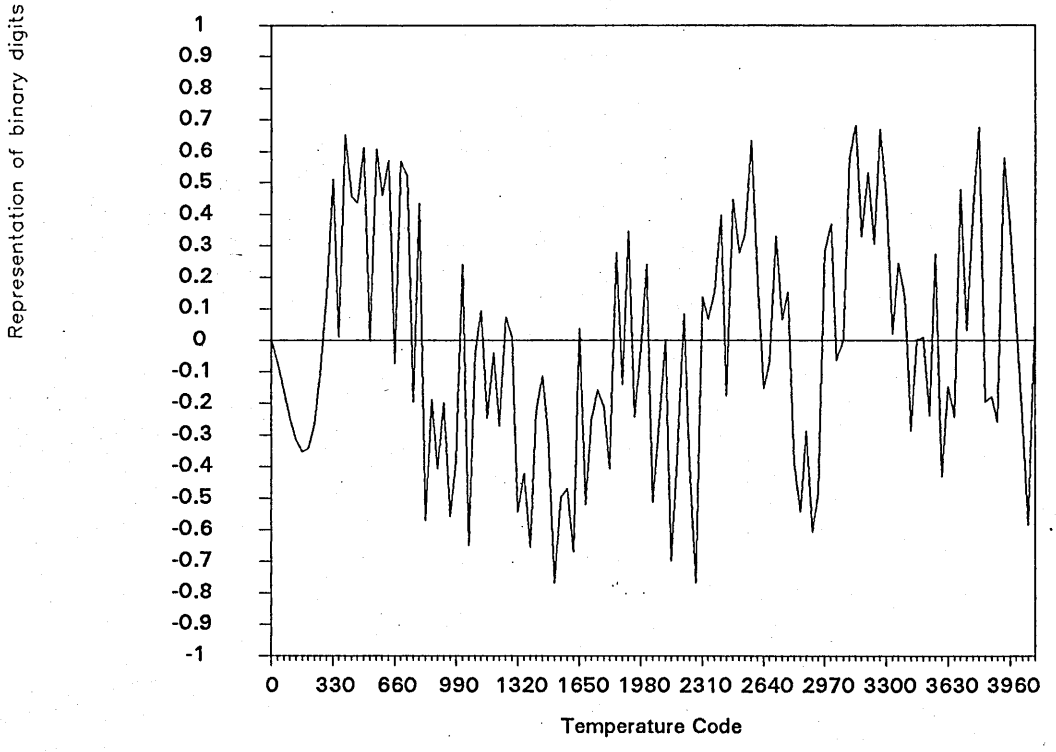

Figure 8.14. Modelled data with both sets of data as integers.

8.6.3. Experimental method

The temperature sensor and oscillator were characterised over the temperature range +87°C to -42°C. The temperature range was extended by 2°C to ensure that the verification would not fail at the extremes. Characterisation was by the average of 10 measurements taken at 10 second intervals at equally spaced temperatures over the +85°C to -40°C range. Verification was carried out in 0.05°C temperature increments in order to test the compensation scheme on just over half of the digitised temperature codes. The computer sent the required temperature to the environmental chamber then waited for the stabilisation time to elapse, usually between 1 and 10 seconds, before reading the temperature sensor, updating the compensation voltage and reading the oscillator frequency. During the verification there was no averaging of the measurements.

The apparatus was assembled as shown in section 5.22. A 12 bit analogue to digital converter (ADC) replaces the digital multimeter as the means of passing the temperature sensor output to the computer and an 8 bit digital to analogue converter (DAC) replaces the precision voltage source for tuning the oscillator. With this arrangement the two converters were mounted in the environmental chamber and experienced the same thermal conditions as the oscillator. In this arrangement of the apparatus the precision voltage source and the digital multimeter formed the interface between the computer and the environmental chamber. This arrangement was adopted because it gives greater resolution to the control of the chamber temperature. The level of resolution that is provided is much greater than the level to which the chamber can control it. This means that the ramp characteristic used in the verification could be smooth.

8.6.4. Discussion of results

For the verification process the 0.05°C temperature increment results in 2500 verification temperatures. Hence verification of this oscillator arrangement could be potentially time consuming. Initially the crystal and the temperature sensor had been mounted in free air as in the earlier experimental work. However, due to the large difference in thermal time constants and the relatively large temperature variation due to the limit cycle control system of the environmental chamber, the temperature sensor was not providing an accurate measure of the resonator temperature. This is shown in figure 8.15.

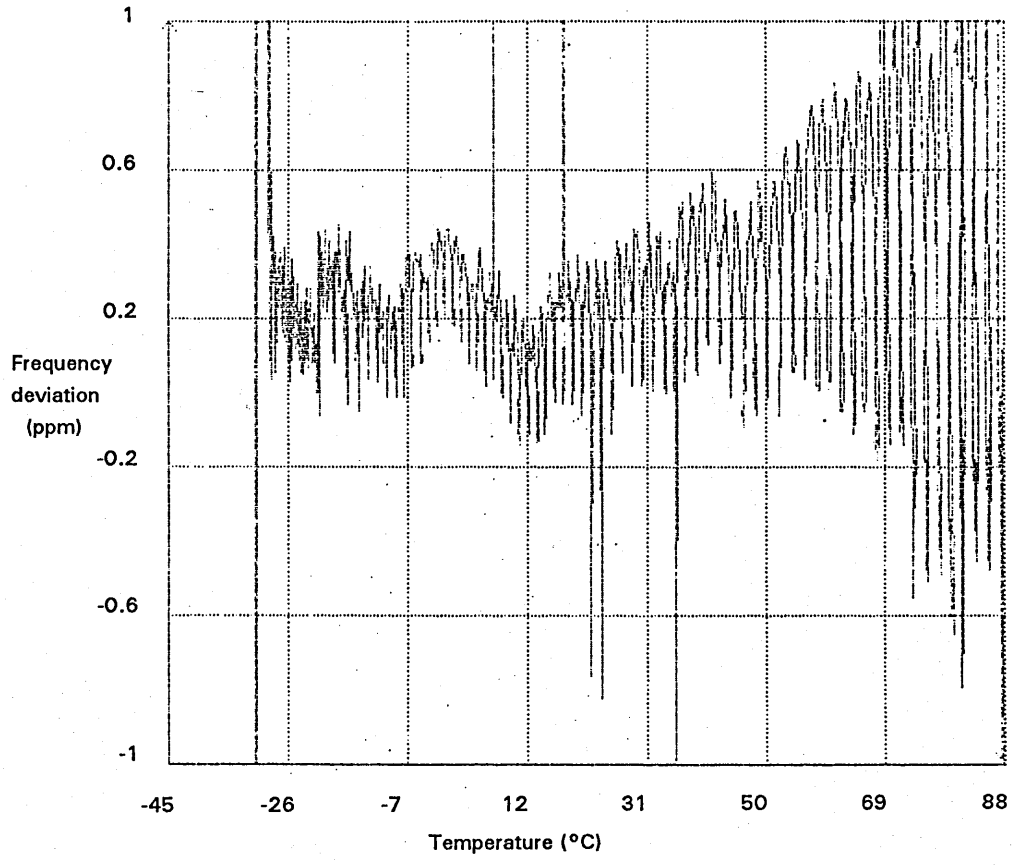

Figure 8.15. Verification results with crystal and platinum resistor in free air.

Closer thermal coupling was achieved between the resonator and temperature sensor by encapsulating the crystal holder and platinum resistor in silicone rubber to a thickness of approximately 3mm. Connecting a 0.1Hz low pass filter between the output of the temperature sensor and the ADC also improved the results although it is likely that the filter was removing electrical noise instead of significantly reducing any thermal effects. Subsequent measurement cycles showed that good matching between the sensor and the resonator was achieved by these modifications. The graph in figure 8.16 shows the results of a typical verification.

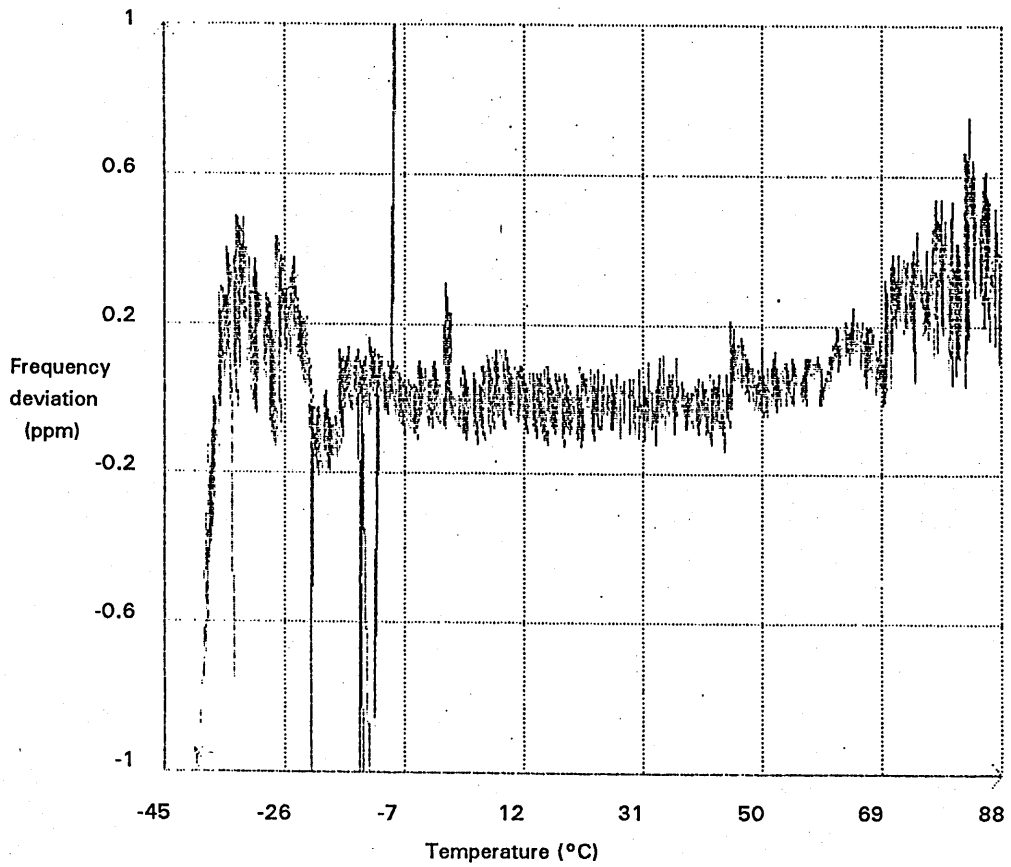

Figure 8.16. Typical verification results.

There are a number of points to be made about these results. First the general shape of the graph is not flat as it was in the simulated case of figure 8.14. At the cold temperatures there is a problem with the tuning range. The characterisation tuning voltage against temperature graph is shown in figure 8.17.

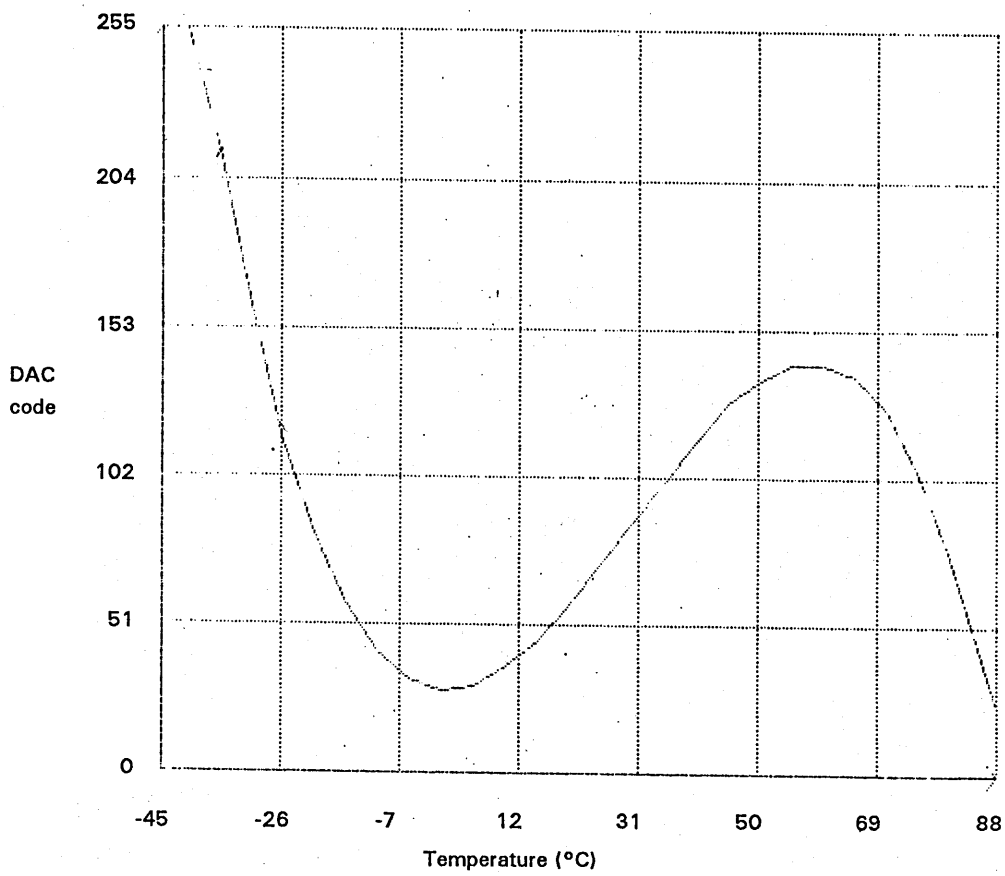

Figure 8.17. Compensation code against temperature

It is apparent that the DAC does not have sufficient range to tune the crystal on to the required frequency. This was caused by the crystal not being of the optimum cut. Unfortunately, at the time of doing this work a crystal with a better angle was not available and as only a small part of the temperature range is affected this is not a serious problem. The cause of the deviation from the expected characteristic at the high temperatures was difficult to identify. Initially it was considered that the problem might lie with the coupling between the temperature sensor and the crystal, despite the improvements made. However this was shown not to be the case by using different stabilisation times for the measurements during both characterisation and verification, the form of the graph remained unchanged. Detailed study of the temperature sensor digital output against temperature graph showed that the discrepancy in the frequency against temperature graph was related

to the temperature sensor. A detail of the frequency deviation against temperature graph is shown in figure 8.18 and the corresponding detail of the temperature sensor graph is shown in figure 8.19. Both graphs show a sudden change at around 70°C.

If the line approaching 70°C from below is extrapolated beyond 70°C then the recorded temperature code is low in comparison. When the measured temperature is low compared to the actual temperature above 70°C the applied compensation will cause the oscillator to generate a frequency that is too high, which is the case in figure 8.18. The cause is uncertain at the moment, but the effect is too large for a major code transition* within the ADC. Further, at the major code transitions there are no apparent problems. The cause of the problem is still under investigation. The difference between characterisation and verification implies that there has been a significant change in part of the system caused by the differences in the temperature characteristics. The effect is repeatable and has been observed many times.

---

* The major code transitions occur when the addition or subtraction of 1 causes all or nearly all the bits to change state, for example in an eight bit converter when the value represented changes from 127 to 128 which in binary is from 01111111 to 10000000.

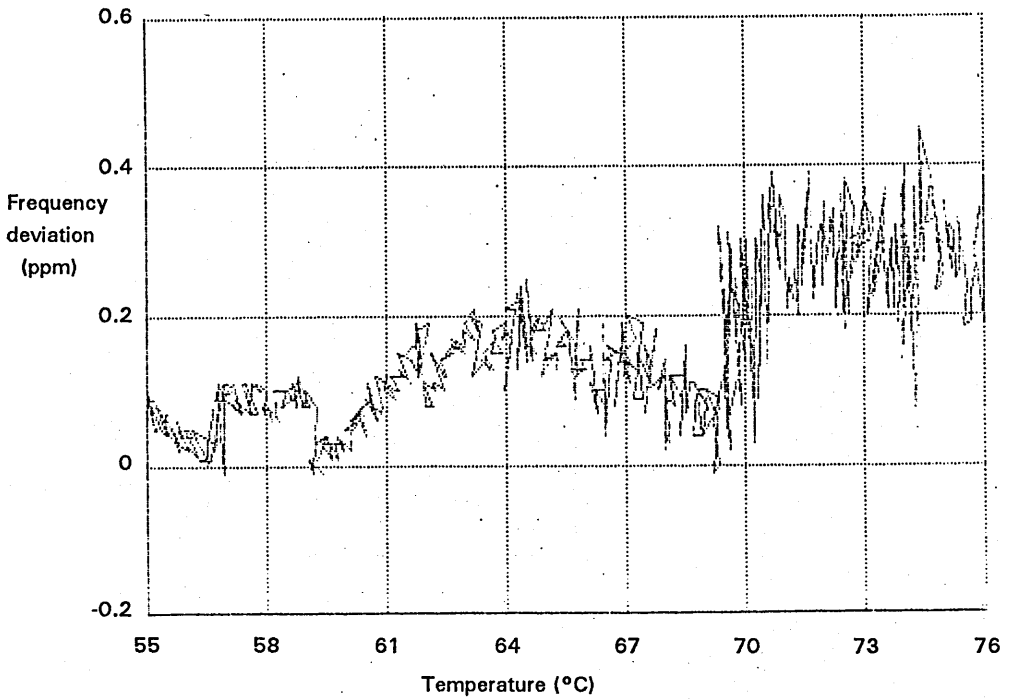

Figure 8.18. Detail of the frequency deviation against temperature characteristic about 70°C.

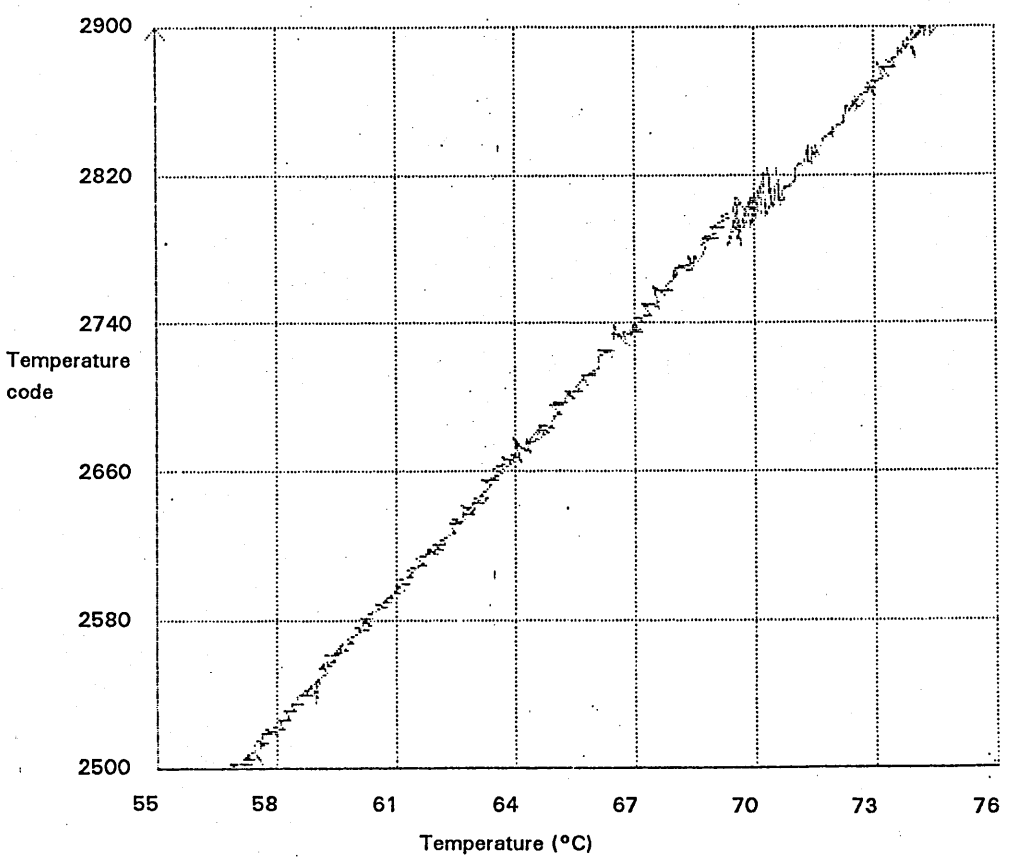

Figure 8.19. Detail of the temperature sensor characteristic about 70°C.

The middle portion of results shown in figure 8.20 is in agreement with the model. The tuning sensitivity of the DAC was a little less than 0.1ppm/bit and that is what is apparent for this part of the graph. Details of the frequency deviation against temperature and the output of the temperature sensor over the temperature range 15°C to 36°C are shown in figures 8.20 and 8.21. Occasionally it appears that the wrong compensation code has been generated because the recorded frequency error is greater than that represented by one bit. However, for the majority of the time the frequency deviation falls within a level representing $\pm$½ a bit, which is as predicted by the model. The close agreement between the model and the experimental results suggest that the thermal filtering that was added to the crystal and temperature sensor is effective in matching the thermal time constants of the two components. The occasional selection of the wrong code may be caused by electrical noise in the compensation circuit.

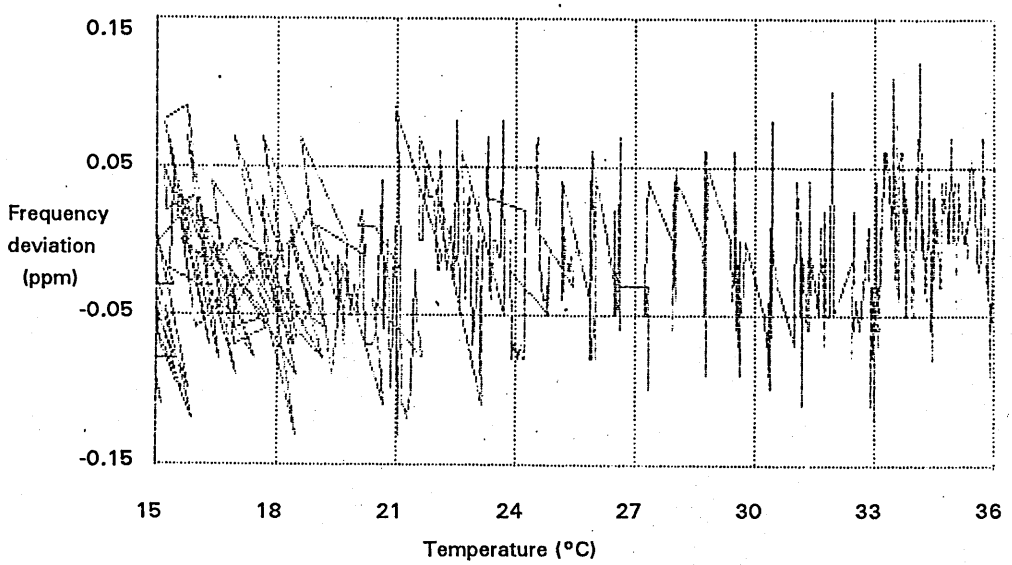

Figure 8.20. Detail of the frequency deviation against temperature characteristic about 25°C.

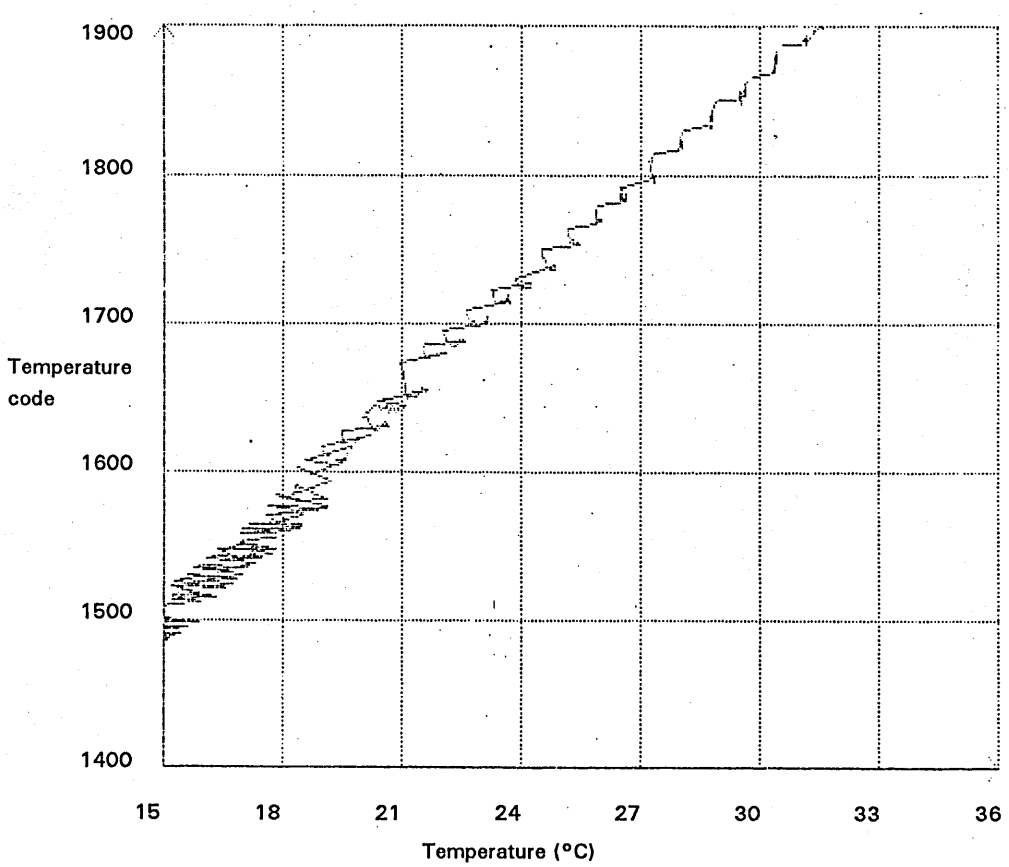

Figure 8.21. Detail of the temperature sensor characteristic about 25°C.

8.7. Comparison between Lagrange and least squares compensation

In this section data gathered during the least squares experiments is used to make a comparison between the two approaches.

8.7.1. Method

The characterisation data gathered during the experiments on least squares compensation was used in the Lagrange formula to generate an alterative set of compensation data. The difference between the seventh order compensation data and the Lagrange compensation data was subtracted from the seventh order verification data to indicate the level degree of compensation the Lagrange data might have achieved.

8.7.2. Discussion of results

The graph in figure 8.22 shows the difference between the seventh order compensation data and the Lagrange compensation data converted to predicted frequency deviation. As temperature increases the difference between the two sets of data increases in a manner that appears to be cyclic. The calculated Lagrange verification is plotted in figure 8.23. When compared with figure 8.7, which shows the seventh order polynomial verification, the frequency deviation for the Lagrange compensation is less jagged than the original seventh order verification and over most of the temperature range the Lagrange compensation has provided a superiour level of compensation. It is appears that the cyclic discrepancy between the two sets of data is introduced by the polynomial compensation techniqe. The cause of this is uncertain. For the Lagrange compensation it is meaningless to plot the predicted error using the compensation data because the compensation data passes through the characterisation points.

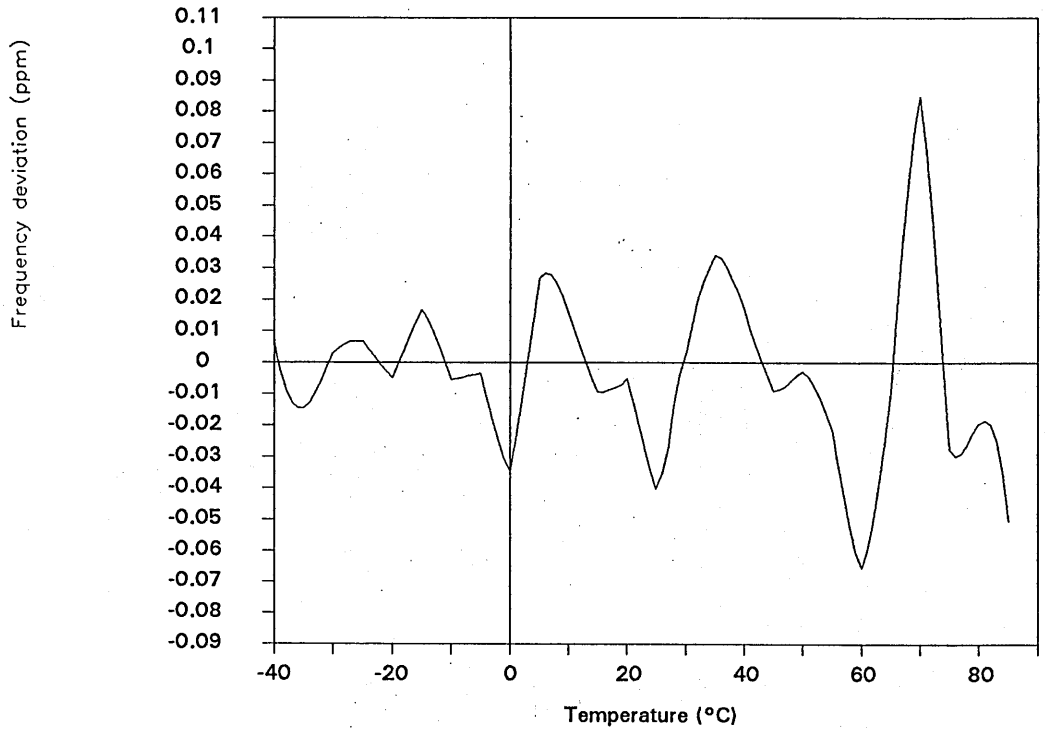

Figure 8.22. Difference between seventh order ploynomial compensation data and Lagrange compensation data.

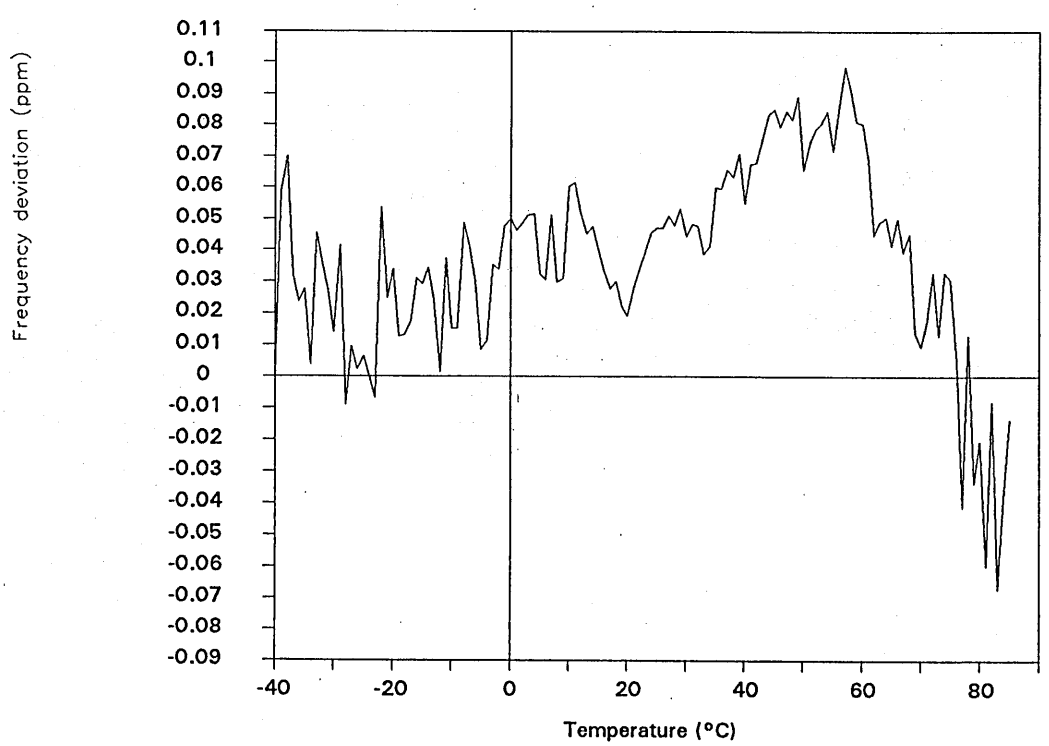

Figure 8.23. Predicted verification for Lagrange compensation.

8.8. Conclusions

Digital temperature compensated crystal oscillators, DTCXO's, use digital electronics techniques to perform the transformation from ambient temperature to the required compensation voltage. A digital temperature compensation circuit forms a digital representation of temperature and performs a digital transformation to determine the required digital representation of compensation voltage. In this type of digital circuit there is no inherent relationship between digitised temperature and digitised compensation voltage; the transformation has to be selected and added to the system. Two such transformations have been investigated in this thesis; least squares polynomial curve fitting and Lagrange interpolation. The results obtained with the least squares curve fitting technique are in agreement with others in this field in showing that an order higher than third order is required to accurately fit the tuning voltage characteristic.

The Lagrange interpolation investigation was undertaken in two parts; the system was modelled on a computer to determine the level of error to be expected from a practical compensation circuit and a practical compensation circuit was built to test the model. Several problems were encountered during the experimental work. These problems prevented the experimental results agreeing with the model over the whole temperature range. However, these problems are not evident over the whole temperature range and where the problems do not occur the agreement is very good. Comparison between the polynomial compensation and the Lagrange compensation showed that the Lagrage gave a marinally better fit to the required characteristic. This work establishes the Lagrange interpolation formula as a useful alternative for generating the compensation data for DTCXO's using a small number of characterisation temperatures.

8.9. References

[1] Frerking, M. E. (1979). Crystal Oscillator Design and Temperature Compensation, *Van Nostrand Reinhold Company Inc., New York.* pp. 152-157.

[2] Gerber, E. A. and Ballato, A. (editors) Frerking, M. E. (1985). Precision Frequency Control, vol. 2, *Academic Press Inc. (London) Ltd.*, pp. 99-111

[3] Scott, P. J. (1977). Design considerations for a digitally temperature compensated crystal oscillator. *Proc 31st Annu. Freq. Control Symp.*, pp. 407-411.

[4] Frerking, M. E., (1979). The application of microprocessors to communications equipment design. *Proc 33rd Annu. Freq. Control Symp.*, pp. 431-435.

[5] Onoe, M., Yamagishi, I. and Nariai H. (1978). Temperature compensation of crystal oscillator by microprocessor. *Proc Annu. Freq. Control Symp.*, pp. 398-402.

[6] Renard, A. M. and Barnhill, K. (1981). Digital temperature compensation of crystal oscillators. *Proc 35th Annu. Freq. Control Symp.*, pp. 455-457.

[7] Miyayama, T., Ikeda, Y. and Okano, S. (1988). A new digitally temperature compensated crystal oscillator for a mobile telephone system. *Proc 42nd Annu. Freq. Control Symp.*, pp. 327-333.

9. SUMMARY AND FUTURE WORK

9.1. Resistive network temperature compensation

At the start of the research temperature compensation circuits comprising resistors and thermistors were capable of achieving frequency stability of $\pm$1ppm over the temperature range -40°C to +85°C. Alternative analogue compensation methods had achieved stabilities $< \pm 0.5$ppm. During the course of the research the cause of the limitations in the resistive networks has been identified: thermistors with very high values of B are required to compensate over the high portion of the temperature range. Practical thermistors are only available with a limited range of B values, which does not extend to the values required for high stability TCXO's. To achieve the higher level of temperature compensation a thermistor with a B value significantly outside the available range is required. By forming a product of two thermistor characteristics an effective thermistor can be formed which has a B value equivalent to the sum of the B values of the two thermistors. An original solution has been found which employs an amplifier with temperature sensitive gain, set by a combination of resistors and a thermistor. The amplifier generates a product of two thermistor characteristics. This has resulted in a compensation network which, in theoretical simulation, has achieved frequency stability of $< \pm 0.2$ppm over the temperature range. Technical difficulties have meant that experimental verification of these results has not yet been achieved. These difficulties were associated with the crystal, the oscillator circuit and the environmental chamber. These have now been adequately addressed. Future work will involve experimental verification of the new compensation networks and the determination of tolerance bands that can be applied on the fixed resistors.

Practical thermistors are only available with a small number of discrete B values, whereas, for the purposes of optimisation, the crystal angle can be regarded as a continuous variable. The new mathematical expression describing the required compensation voltage can be used to extend the optimisation process, employed to identify one of the new compensation networks, to include the crystal angle. Hence the crystal angle selected will be the optimum for the available thermistors. The thermistor model used for this will include terms to account for the thermal dependence of the B value.

9.2. Mathematical analysis

The mathematical analysis of temperature compensation networks has identified a second network capable of achieving compensation to a level of $< \pm 0.5$ppm over a temperature range -40°C to +85°C. The gain of this network is represented by

$$\frac{V_o}{V_i} = \frac{\alpha\gamma\varepsilon\left[A_1 e^{\frac{B_1}{t}} + \frac{\beta}{\alpha}\right]\left[A_2 e^{\frac{B_2}{t}} + \frac{\delta}{\gamma}\right]\left[A_3 e^{\frac{B_3}{t}} + \frac{\phi}{\varepsilon}\right]}{acf\left[A_1 e^{\frac{B_1}{t}} + \frac{b}{a}\right]\left[A_2 e^{\frac{B_2}{t}} + \frac{d}{c}\right]\left[A_3 e^{\frac{B_3}{t}} + \frac{g}{f}\right]} \qquad (9.1)$$

The future development of this expression is to form a power series using Taylor's Theorem. In this form the expression for the compensation network would be in the same form as the crystal characteristic and could lead to expressions that gives the required resistor values by equating coefficients. In the first instance (9.1) will be expanded to a third order power series which will allow the theory to be developed on a cubic expression representing compensation voltage. However, to achieve a result which might be useful in high stability temperature compensated crystal oscillators, both the crystal characteristic and the compensation network will need to be expanded to higher order terms due to the recursive nature of the compensation process.

9.3. Lagrange interpolation

At the start of the research polynomial curving fitting and linear interpolation had been used to generate data used for digital temperature compensation. During this research it has been shown theoretically that the Lagrange interpolation formula can be used to generate the compensation data to the limits set by the analogue/digital interfaces. Initial experimental results over part of the temperature range are in agreement with the theoretical results. However, technical problems mean that verification over the whole temperature range has not been achieved. Future work here is to identify the cause of the problem and verify the results over the whole temperature range. Once these problems have been addressed the next area for investigation is to determine the minimum number of characterisation temperatures needed in order to maintain a level of stability which corresponds to ± 1 bit of the digital to analogue converter.